

**Functional Poly(ionic liquid) Materials based on
Poly(1,2,4-triazolium)s**

Dissertation

zur Erlangung des akademischen Grades

„Doktor rerum naturalium“

(Dr. rer. nat.)

in der Wissenschaftsdisziplin „Polymer- und Kolloidchemie“

eingereicht an der

Mathematisch-Naturwissenschaftlichen Fakultät

der Universität Potsdam

von

Weiyi Zhang

geboren am 07.12.1987 in Zunyi, China

Potsdam, Januar 2017

To my family,

Table of Contents

1. Introduction.....	4
1.1 Synthetic method of PILs.....	5
1.2 Physical properties and chemical structures of PILs.....	7
1.3 Applications and thermal behavior of PIL materials.....	10
Motivations.....	13
2. Synthesis of poly(1-vinyl-1,2,4-triazolium) poly(ionic liquid)s and their behavior in loading metal ions	15
2.1 Introduction.....	15
2.2 Experimental Section.....	16
2.3 Synthesis of poly(1-vinyl-1,2,4-triazolium) poly(ionic liquid)s.....	16
2.4 Characterization of poly(1-vinyl-1,2,4-triazolium) poly(ionic liquid)s.....	21
2.5 Metal ion absorption behavior of poly(1-vinyl-1,2,4-triazolium) poly(ionic liquid)s.....	27
2.6 Conclusions.....	28
3. Self-assembly in poly(1,2,4-triazolium) poly(ionic liquid) nanoparticles: One-step polymerization towards controllable internal morphologies.....	29
3.1 Introduction.....	29
3.2 Experimental Section.....	30
3.3 Dispersion polymerization of 1,2,4-triazolium type poly(ionic liquid) nanoparticles.....	30
3.4 Characterization of 1,2,4-triazolium type poly(ionic liquid) nanoparticles.....	31
3.5 Conclusions.....	47
4. Crosslinked 1,2,4-triazolium-type poly(ionic liquid) nanoparticles.....	48
4.1 Introduction.....	48
4.2 Experimental Section.....	48
4.3 Nanoparticle preparation.....	48
4.4 Characterization and discussion.....	51
4.5 Conclusions.....	60
5. Poly(1,2,4-triazolium) poly(ionic liquid) bearing triiodide anions: synthesis, basic properties and electrochemical behaviors.....	61
5.1 Introduction.....	61
5.2 Experimental Section.....	62
5.3 Results and discussion.....	62
5.4 Conclusions.....	70
6. Dispersed Palladium clusters stabilized by poly(1,2,4-triazolium) poly(ionic liquid) vesicle.....	71
6.1 Introduction.....	71

6.2	Experimental section	71
6.3	Results and discussion	71
6.4	Conclusions	81
7.	Summary.....	82
	Appendix.....	84
	A Materials and Methods	84
	B Experimental Part	87
	C Co-Authorship Statement	96
	D List of publications	97
	E List of abbreviations	98
	F Declaration	101
	G Acknowledgements.....	102
	H References.....	104

1. Introduction

In 1914, Paul Walden discovered a new organic salt (*i.e.* [EtNH₃][NO₃]) with an unusually low melting point of 12 °C, which he later referred to as an ionic liquid (IL).^[1] He defined this class of new materials as organic salts with a melting point below 100 °C.^[2] In fact, such materials have been even described in literature previously,^[3] but it is the term “ionic liquid” becomes the most popular since 1990s.^[4] ILs have been utilized in many areas owing to their interesting features and broad applications including catalysis, electrochemistry, analytical chemistry, energy conversion and storage, nanotechnology and many more.^[5]

Recently, the covalent incorporation of ILs into polymer architectures has become popular to combine the useful properties of ILs such as (electro-)chemical stability, non-flammability and high ion conductivity, with mechanical stability and good processability of polymers.^[6, 7] As early as in 1973, Salamone *et al.* introduced free radical polymerization of vinylimidazolium ionic liquid monomers;^[8] however it was only until the late 20th century that this approach was further refined and extended to new polymer systems. Ohno *et al.* used the term “poly(ionic liquid)” (PIL) for the first time to describe solid polymer electrolytes built up from ionic liquids with high ion conductivity.^[9] As promising materials in ion conduction in energy field, PILs match the rising research interest for energy storage and conversion, and ever since trigger the pursuit for investigation on their basic structural units, including permutation and combinations of various cations (*e.g.* imidazolium, pyridinium, alkylammonium, and alkylphosphonium) and anions (halides, polyatomic inorganics (BF₄⁻, PF₆⁻, AuCl₄⁻, FeCl₄⁻), *etc.*), and physical/chemical properties (glass transition temperature, solubility, *etc.*).^[10, 11] In 2005, Shen *et al.* employed three classical ionic liquid monomers ([1-(4-vinylbenzyl)-3-butylimidazolium tetrafluoroborate] (VBIT), [1-(4-vinylbenzyl)-3-butylimidazolium hexafluorophosphate] (VBIH), and [2-(1-butylimidazolium-3-yl)ethyl methacrylate tetrafluoroborate] (BIMT)) to produce polymers for CO₂ sorption and found that PILs showed higher capacity and faster rate in CO₂ sorption in comparison to their IL monomers.^[12] Recently Snow *et al.* designed and successfully synthesized PILs with extremely low glass transition temperature (T_g) that can flow in the bulk state at room temperature.^[13] Yuan *et al.* successfully used a similar low- T_g material as a reaction medium for catalysis and colloid particle synthesis.^[14] There are many examples where researchers have been pushing forward the frontier of PIL science and technology to design a versatile chemical toolbox for a broad range of materials applications.^[15-17] The incredible structural

versatility PILs possess has resulted in huge enthusiasm to investigate novel functions and compositions of PILs.

The IL species in PIL may either be incorporated into the backbone or appended along the side-chain. While there are plenty of examples for each case, the most common approaches for PIL synthesis, such as free radical polymerization, produce side-chain functionalized polymers. While PILs are a subclass of polyelectrolytes, their unique properties such as broad structural diversity, high (electro)chemical stability, low glass transition temperature and tunable solubility set them apart from conventional polyelectrolytes.^[6, 7, 10, 11] These properties are strongly related to the IL monomer units they are derived from, *i.e.* the contribution from the IL side. Unlike traditional polyelectrolytes that are only soluble in water or high polarity solvents, the solubility window of PILs can be tuned by simply changing their counterions,^[18] and thus expand their potential applications in energy field, such as metal battery, dye-sensitized solar cells, fuel cells and many more.^[15-17] PILs are easier to process into controllable shapes while keeping some of the properties inherited from their precursor ILs. Nevertheless, the application fields of PIL materials are currently far from full exploration, which motivates researchers to invent novel PIL design, discover their interesting properties and broaden the usage scope.

1.1 Synthetic method of PILs

Among all synthetic strategies towards PILs, two have become the most common. The first approach is post-modification of pre-existent polymers *via* quaternization or ion metathesis, and the second is direct polymerization of IL monomers.^[6, 7] There exist benefits and limitations in both pathways. Post-modification is a facile method in obtaining PILs when it is complicated to prepare desired PILs *via* direct polymerization of their ionic liquid monomers (ILMs). This method is available for polymers which bear certain functional groups, *e.g.* pyridinium. Figure 1a is an example of post-modification of poly(4-vinylpyridine). After the synthesis of neutral polymer, alkyl substitution reactants with good leaving group can be quaternized onto the N position. However, the major challenge of this reaction is its non-quantitative character, which always leads to copolymers with different ratio of charged and neutral part.

For direct polymerization of ILMs, PILs can have accurate cation/anion compositions and be of higher purity. Of the chain-growth approaches for polymerization, the most common ones are conventional free radical polymerization and “living” and/or controlled radical

polymerization,^[19] such as reversible addition–fragmentation chain-transfer polymerization (RAFT),^[20] atom transfer radical polymerization (ATRP)^[21] and cobalt mediated radical polymerization (CMRP).^[22] The disadvantage with these approaches is that not all ILs are easily polymerizable (especially large-sized anions are present), leading to synthetic issues and low molecular weight polymers. One solution to this issue is, as mentioned previously, the post-modification of an existent polymer to install the targeted ions along the polymer backbone. For example, the conventional free radical polymerization of 3-alkyl-1-vinyl-imidazolium bromide compound was picked as example (Figure 1b). However, post-polymerization anion exchange raises concerns due to its non-quantitative feature, which produces impure PILs and random copolymers bearing a mixture of two counter-ions. In this case, multiple times of ion metathesis process can be repeated to minimize the impurity.

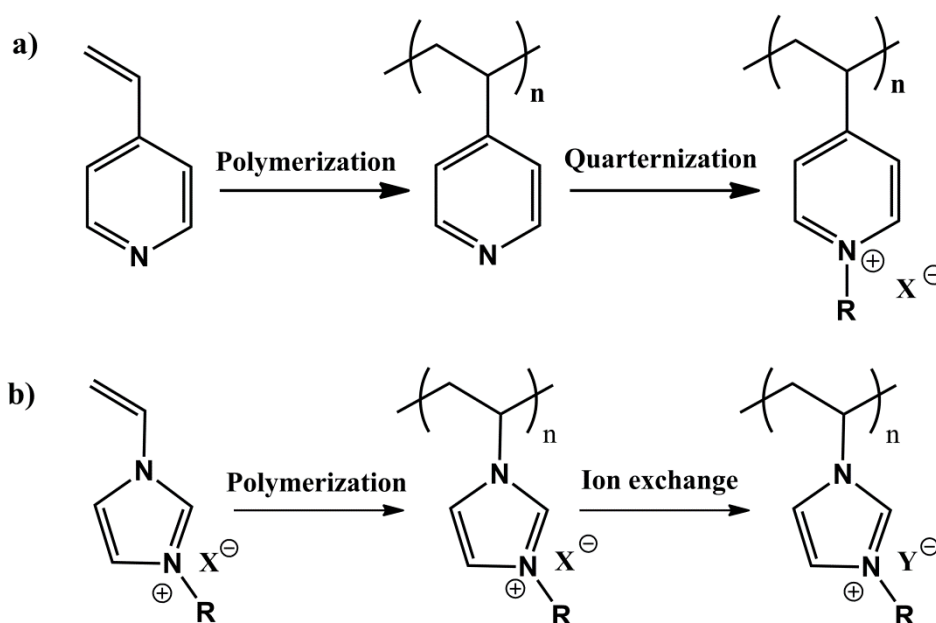


Figure 1. General synthetic routes to polycation type PILs *via* (a) post-modification (R-alkyl substitution, X⁻ halide anions, such as Br⁻) and (b) direct polymerization of ILMs

Since late 1990s, Ohno *et al.* applied free radical polymerization as a facile way to obtain many PILs,^[23] and this technique has become the most widely used in preparation of normal PILs. The main reason for its popularity lies in its high tolerance to impurities, humidity and versatile active functional groups, and simple synthesis.^[24] Among all ILMs used in conventional free radical polymerization, three types—vinyl, styrenic and (meth)acrylic ones were the most frequent precursors.^[6, 7] (Meth)acrylic type ILMs can be created by reaction of (meth)acryloyl chloride/anhydride with hydroxyl or carboxylic acid groups.^[25] Ragnogna *et al.* reported the synthesis of one phosphonium monomer possessing three methacrylate groups,

and its photopolymerization to generate highly cross-linked networks.^[26] Additionally, Firestone *et al.* reported one anionic PIL consisting of an acrylate-anion and imidazolium-type cation and is one of the fewer examples of an anionic PIL.^[27] One of the most commonly used chemical structures in PILs is imidazoliums possessing one *N*-vinyl polymerizable group due to its commercial availability. Starting from halide-containing imidazolium type monomers, Mecerreyes *et al.* synthesized several PILs *via* polymerization in chloroform, and followed by anion exchange to prepare PILs of different solubility.^[18] Dispersion polymerization of four imidazolium-type ILMs with long alkyl substituents in water resulted in PIL nanoparticles bearing alkyl chain length-dependent inner morphology.^[28] Alternatively, since 4-vinylbenzyl chloride is commercially available, styrenic group has been incorporated into lots of PIL synthesis.^[29]

When PILs with specific architectures or properties are targeted, other synthetic strategies such as ring-opening metathesis,^[30] “click” reactions,^[31] or even Michael addition reaction,^[32] can be used. While these approaches have merits from a fundamental aspect, these techniques are not the most convenient for accurate control over the length/molecular weight distribution, especially for block copolymer synthesis. Instead “living”/controlled radical polymerizations (CRP) including ATRP, RAFT and CMRP can be applied. For example, Matyjaszewski *et al.* achieved good control over molecular weight and polydispersity using styrenic type PILs by activators regenerated by electron transfer atom transfer radical polymerization (ARGET ATRP).^[33] Detrembleur *et al.* synthesized several imidazolium-based block copolymers *via* CMRP and studied their self-assembly behavior.^[34] *Via* controlled radical polymerizations, multi-block copolymers and even branched/hyper-branched ones can be possible options.^[35] Above all, multiple choices inside the toolbox of polymerization strategies are diverse and can make PILs into versatile, designable and multi-functional materials.

1.2 Physical properties and chemical structures of PILs

The nearly limitless number of chemical structures, anion/cation combinations, and polymer architecture leads to a large window of chemical and physical properties for PIL materials. The structure/property relationships in this regard are quite important and must be investigated for all new PILs. For example, the solubility of PILs such as poly(1-vinyl-3-alkyl imidazolium) can be adjusted by simply changing their counter-ions (Figure 2). Poly(1-vinyl-3-alkyl imidazolium) PILs with iodide, bromide, chloride or nitrate anions are soluble in polar protic solvents like water and methanol, while the trifluoromethanesulfonate (CF_3SO_3^-) anion may reduce solubility in water but retains solubility in methanol. More hydrophobic anions

such as tetrafluoroborate (BF_4^-), hexafluorophosphate (PF_6^-), and bis(trifluoromethane)sulfonamide ($\text{TFSI}^-/(\text{CF}_3\text{SO}_2)_2\text{N}^-$), result in PILs that are exclusively soluble in organic solvents. Ion metathesis is also a simple method for tuning other PIL properties.^[18] Upon exchanging the halide with TFSI^- , poly(1-vinyl-3-alkyl imidazolium) polymers will obtain higher thermal stability and lower glass transition temperatures, which can be attributed to variations of Columbic interactions and electrophilicity of fluorinated anions.^[18] The elongation of alkyl chains to some extent in poly(1-vinyl-3-alkyl imidazolium) polymers can lead to lower T_g and higher hydrophobicity for similar reasons.

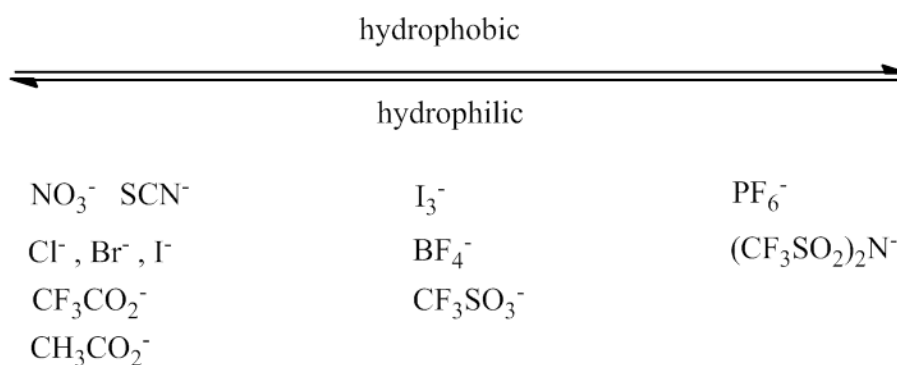
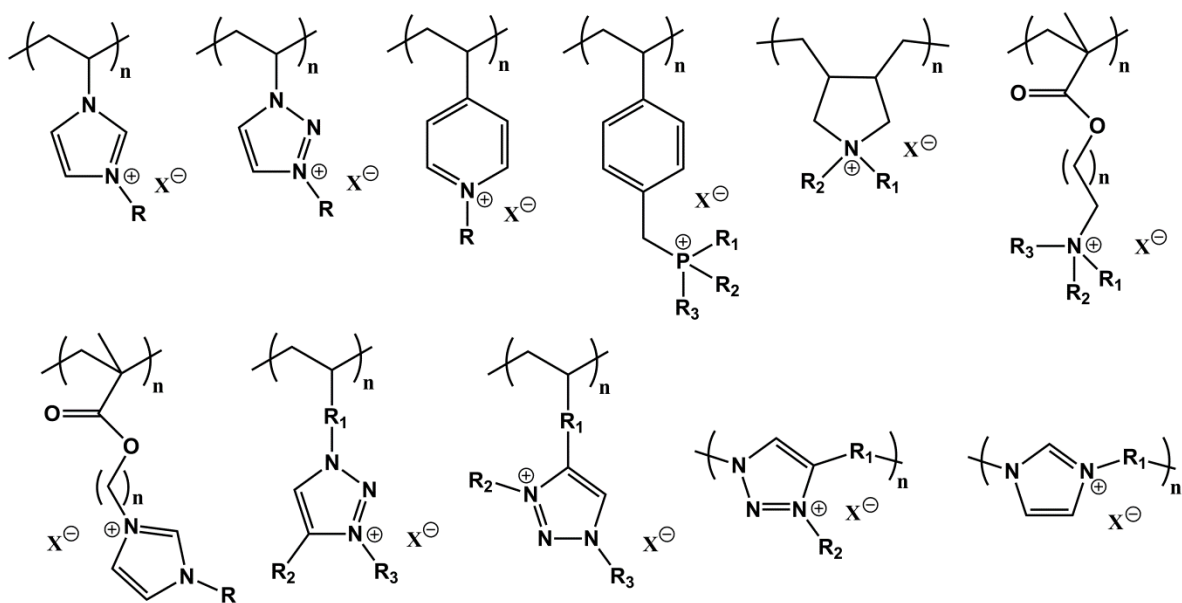
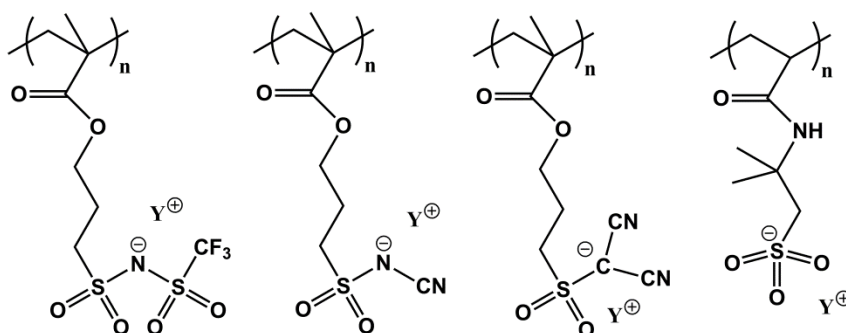


Figure 2. Common anions involved in ILMs and PILs.

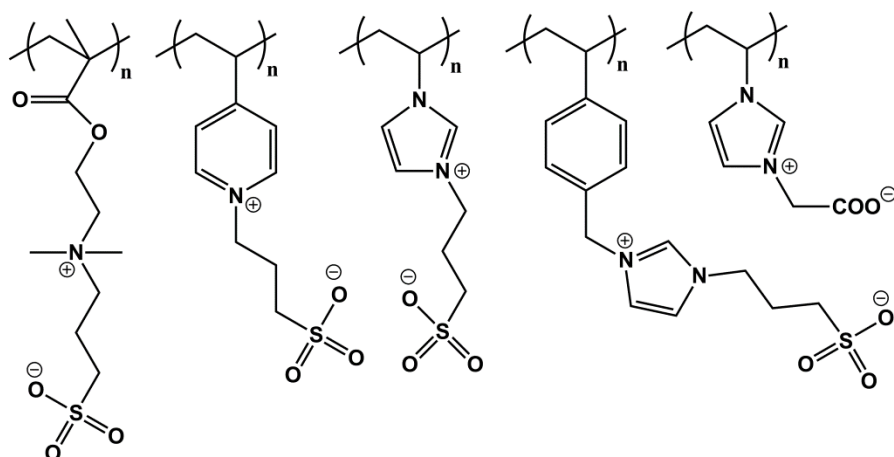
PILs can be categorized into three main groups in general: cationic, anionic and zwitterionic ones.^[6, 7] **Figure 3** displays representative examples. Among them, cationic PILs, especially imidazolium-based ones, are the most commonly used and studied. For example, imidazolium type PILs can be converted into polymeric carbene (**Figure 4**) and can be applied for CO_2 sorption and carbene catalysis.^[36] Taton *et al.* reported the synthesis of one imidazolium type poly(*N*-heterocyclic carbene) (poly(NHC)), and next its usage to build up poly(*N*-heterocyclic carbene- CO_2) adducts (poly(NHC- CO_2)) for catalysis in transesterification.^[37] In addition to polyimidazoliums, the database of cationic PILs contains plenty of other ionized functional groups, like phosphonium, pyridinium, pyrrolium, 1,2,3-triazolium and tetraalkylammonium species. Each cation group determines the very essential properties in its PILs, and only because of each unique chemical structure, vastly varied special properties can be developed in a specific PIL, thus leading us to broad applications.



Cationic PILs



Anionic PILs



Zwitterionic PILs

Figure 3. Examples of cationic, anionic and zwitterionic PILs (R-alkyl or other substitution, X-anions, Y-cations).

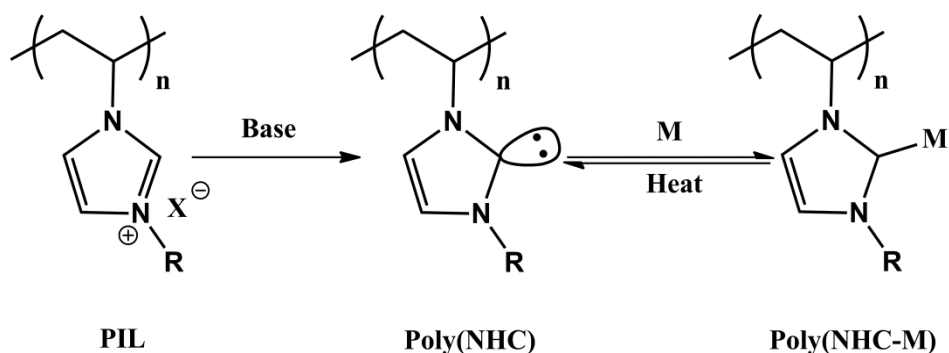


Figure 4. Formation process of poly(*N*-heterocyclic carbene) from a PIL and the poly(*N*-heterocyclic carbene-*M*) adducts. *M* can be CO₂ or other species.^[36]

Anionic PILs are far less explored than cationic ones mainly because of their more complicated synthesis (limited pool of monomer choices). Despite the few examples, anionic PILs exhibit interesting properties, such as extremely low T_g or uncommon viscoelastic behaviors derived from ionic assemblies.^[13] Anionic PILs with trifluoromethanesulfonamide, sulfate, phosphate, phosphoric, carboxylate polycations and some others have been synthesized and studied in literatures.^[38]

Zwitterionic ILMs are ILs with covalently connected cations and anions. Several PILs polymerized from such monomers have been reported,^[39] although zwitterionic monomers usually have relatively high melting point (> 100 °C). The representative structures of zwitterionic PILs are listed in **Figure 3**, including cations like imidazolium, pyridinium, tetraalkylammonium and anions like sulfate or carboxylate.

1.3 Applications and thermal behavior of PIL materials

The unceasing demands for versatile polymer materials that can be utilized in different specific conditions continuously drive scientists to explore novel functional polymers. PILs, as a newly emerging class of polymers, are unique in their construction style—theoretically any type of functional groups can be attached to their nucleophilic active sites (N, P, *etc.*), and this creates unlimited possibilities for their physical properties, thermal behaviors, electrochemical performances and most importantly application scopes. For instance, PILs with dicyanamide as anion can be high-yield carbon precursors,^[40] long alkyl chain substituted PILs are found to self-assemble in aqueous solutions during polymerization,^[28] just to name a few. Hence, PILs are considered as a multifunctional materials platform in a multitude of applications. Most of them have been reviewed by Green *et al.*,^[16] Mecerreyes *et*

al.^[11] and Yuan *et al.*^[7] thoroughly. Here we take several common application fields as examples to describe the advantages of PILs.

a) Porous materials

Due to their widespread applications, porous polymers are crucial for the fabrication of cosmetics, tail gas absorbers, gas storage, among many more.^[41] The combination of porous polymers and ILs creates new possibilities. For instance, Texter *et al.* synthesized a polymer gel with solvent-reversible poration.^[42] This crosslinked polymer gel is based on IL surfactants, which can be transformed into porous film upon anion exchange. Porous polymers can be produced from ILMs using a variety of synthetic methods and techniques. Dai *et al.* reported a type of IL-based cationic polymer network synthesized from thermal condensation of 1,3-biscyanomethylimidazolium type monomer.^[43] Upon annealing at 400 °C, a porous polymer with moderate specific surface area (481 m²/g) and anion-exchangeable property was obtained, which was used to adsorb perrhenate ions in aqueous solution. Other than condensation polymerization, porous polymers have also been manufactured from PILs directly. Yuan *et al.* successfully produced charged porous polymer powders by dropping a mixture solution of a hydrophobic PIL and poly(acrylic acid) (PAA) into NH₃-containing ethanol that triggers interpolyelectrolyte complexation.^[44] Following deprotonation of PAA by NH₃, electrostatic complexation took place between PIL and PAA, and resulted in instant phase separation which ended up with nanopores in the precipitate. Yuan *et al.* furthered this synthetic concept into porous membranes.^[45] Asymmetrical porous membranes were produced similarly by immersing a dried PIL/PAA blend film into aqueous NH₃ solution. The as-synthesized porous PIL membrane was applied as fast-response actuators, which are ultra-sensitive to lots of organic solvents like acetone, isopropanol and others.^[46] Porous polymers derived from ILMs or PILs are also useful in many other applications, such as CO₂ sorption, gas separation, catalysis, lithium batteries, *etc.*^[47] This field is currently attracting increasing activities and deserves further exploration.

b) Carbon materials

Carbon is a versatile material with almost omnipotential applications, *e.g.* in absorbent materials, catalysis and energy conversion/storages.^[48] Among all carbon precursors, ILs are an important class as a low-to-no vapor pressure liquid state reagent and a nitrogen-rich precursor, which can produce nitrogen-doped carbons of a high yield. Additionally, several TFSI-containing ILs carrying crosslinkable moieties (cyano- group, dicyanamide anion, *etc.*)

can be used to produce microporous carbon *via* self-templating mechanism.^[49] The potential of ILs in functional carbon production has been extended to PILs. PILs, which are composed of ILMs, inherit those unique properties and naturally become valuable carbon precursors. The first example of PIL carbonization can date back to 2010, when a highly graphitic and conductive carbon with mesoporous structure was produced after pyrolysis of an IL/PIL—metal salt mixture.^[50] Interestingly, PILs can also serve as multifunctional reagent in hydrothermal carbonization process. Wang and Yuan *et al.* reported a method to improve hydrothermal carbonization yield and nitrogen content *via* applying PILs as porogens, stabilizers and nitrogen resources in this process.^[51] PILs are also used as carbon sources in many other technological materials. For example, carbon nanobubbles made from colloidal PIL nanoparticles can stabilize carbon nanotubes in water;^[52] after electrospinning and carbonization, PILs can be carbonized into highly conductive carbon fibers.^[40]

c) Catalysis

PILs are especially talent in immobilizing metal species that have catalytic activity. Dai *et al.* reported several nanoporous ionic organic networks fabricated from a substitution reaction, in which AuCl_4^- was first incorporated inside and reduced by NaBH_4 .^[53] Ultrasmall gold nanoparticles with sizes around 1-2 nm were acquired. Based on such hybrid materials, a series of aerobic oxidation reactions of saturated alcohols were conducted, which resulted in exceptional catalytic activity. Yuan *et al.* produced “smart” hybrid reactor from colloidal PIL nanoparticles by coating the PIL nanoparticles with a mesoporous silica shell.^[54] It was found that when applying these nanoreactors in oxidation of aromatic alcohols under 1 mol% Pd, selectivity can reach 99% with high catalytic activity. Other than acting as catalyst supports, PILs can be catalysts themselves. For example, Taton *et al.* discussed one method to synthesize poly(N-heterocyclic carbene)s from their PIL precursors.^[37] In this literature, the imidazolium PIL with TFSI⁻ anion was first polymerized from bromide type IL monomer, followed by anion exchange with lithium TFSI. After treatment with a strong base at low temperature in THF, poly(NHC)s were produced. The poly(NHC)s showed reversible addition of CO_2 and formed air-stable thus easy-to-handle poly(NHC- CO_2) adducts. Both poly(NHC)s and poly(NHC- CO_2) adducts exhibited high activity in transesterification reactions and benzoin condensations, and poly(NHC- CO_2) adducts were found more tolerate to external conditions.

d) Microphase separation in PILs

Self-assembly is an important concept in chemistry and materials science because of two reasons: first, it is a key for researchers to understand similar behaviors we observed in biological field (folding of protein, base pairing of DNA, *etc.*); second, it offers us an alternative way to synthesize structures larger than molecules.^[55] So far, self-assembly behaviors of ILs have been explored by researchers thoroughly and used in different applications.^[56] For instance, Ohno *et al.* synthesized two ILs which can be self-organized into columnar structures.^[57] These special structures exhibited one-dimensional anisotropic ion conductive channels. Zhou *et al.* obtained mesoporous silica *via* applying self-assembled ILs as templates.^[58] Based on these, interesting phenomenon and utilization of self-assembly in materials derived from ILs as well as PILs can be expected. For instance, Weber *et al.* reported a series of PIL block-copolymers and studied the relationships between single ion conduction and the morphologies dependent on their microphase-separations.^[59] Tejero *et al.* synthesized a library of amphiphilic copolymers whose hierarchically self-assembled structures were obtained; their microstructures were studied *via* small- and wide-angle X-ray scattering.^[60] Additionally, Yuan *et al.* invented a new strategy to synthesize colloidal stable PIL nanoparticles in a one-step polymerization route, in which alkyl substitution dependent inner morphologies (multi-lamellar or unilamellar like) were formed.^[28, 61]

Motivations

In the world of chemistry, a subtle change in a molecule can induce drastic differences in specific properties and functions. For example, Vitamin C or L-ascorbic acid is a vital nutrient in human body and the lack of it will cause scurvy.^[62] However, the stereoisomerism of Vitamin C—erythorbic acid is unable to be absorbed by human body. Instead, this biological useless compound can function as antioxidant and is used in processing food worldwide.^[63] Another example can be the fatty acids. Despite their identical molecular formula, the *trans* and *cis* fatty acids have very different influence on their properties. Like elaidic acid, compared to its *cis* isomer, it has much higher melting point, and the diet of it can contribute to obesity and many other health problems, even when the *cis* one is a healthy food resources.^[64] It is clear that a small innovation on the chemical footprint may lead to huge impact in our physical world. This effect is also true in ILs and PILs. For instance, phosphonium ILs are more stable in basic environment than imidazolium ILs, therefore it can be made as a more stable hydroxide exchanger for fuel cells.^[65] Imidazolium ILs can be easily made into carbene compounds while pyridinium varieties not.^[36] The current state of PIL chemistry is diverse, growing and ripe for new discoveries and opportunities. In this context, compared to imidazolium or 1,2,3-triazolium ones, PILs from 1,2,4-triazolium have not yet

been explored, although a couple of polymers carrying 1,2,4-triazolium have been reported.^[32, 66] Previously imidazolium-based PILs have been systematically investigated on their structure-property-function relationship. Now we are motivated with a new type PIL—1,2,4-triazolium PIL. In comparison to imidazolium ones, we believe the one nitrogen difference in 1,2,4-triazolium PILs may vary some of their properties and applications. This thesis has its mission to explore 1,2,4-triazolium-based PILs, including their chemical synthesis, self-assembly behavior and solid properties, aiming to introduce to the PIL community a completely unknown class of PILs.

2. Synthesis of poly(1-vinyl-1,2,4-triazolium) poly(ionic liquid)s and their behavior in loading metal ions

2.1 Introduction

Although there exist countless structural possibilities of cation-anion pairs in PILs, to date the most commonly studied ones usually originate from the marriages of the cations selected from *N,N'*-dialkylimidazolium, *N*-alkylpyridinium, tetraalkylammonium, tetraalkylphosphonium, *N,N'*-dialkylpyrrolidinium or 1,2,3-triazolium, with anions chosen from halides (Cl⁻, Br⁻, I⁻), inorganic fluorides (BF₄⁻, PF₆⁻), or hydrophobic organics ((CF₃SO₂)₂N⁻, CF₃SO₃⁻).^[6, 67] Upon combination of cations and anions purposely, specific properties of PILs such as hydrophobicity/hydrophilicity and/or thermal stability can be adjusted and targeted.^[7, 11] For instance, solubility of poly(1-vinyl-3-alkyl imidazolium) polymers can be tuned by replacing the anions.^[18] Among many investigations in PILs, the imidazolium-based ones have been the most systematically studied as they exhibit the most common features of PILs. As a result, imidazolium-based PILs have been involved in numerous applications including gas adsorption, organic catalysis, morphosynthesis of inorganic/organic materials, membranes and many more.^[68, 69] Nevertheless, the seeking of novel polymer backbones, cations or anions remains a continuous effort in the community to enrich the structure toolbox and physical properties and functions. Recently, 1,2,3- and 1,2,4-triazolium-type ILs have caught increasing interests because of their exotic structure and potential applications as functional ILs for ionic reaction media and energetic materials.^[70] For example, Shreeve *et al.* reported several highly energetic ILs carrying 1,2,4-triazolium;^[71] Rovis *et al.* utilized 1,2,4-triazolium compounds as precursor of *N*-heterocyclic carbenes.^[72] However, despite organic compounds composed of 1,2,4-triazolium species have been intensively studied, 1,2,4-triazolium-based polymers are rarely investigated, not to mention the study of them through a PIL concept. So far, 1,2,3-triazolium containing polymers are the ones dominating the research on polytriazoliums. For instance, Drockenmuller *et al.* synthesized a number of PILs with superior ion conductivity derived from 1,2,3-triazolium.^[73] Literature survey shows that only Shreeve *et al.* and Miller *et al.* discussed 1,2,4-triazolium-based polymers and crosslinked PIL networks, respectively.^[32, 66] Besides, an initial study of a 1,2,4-triazolium-3-thiolate compound was reported by Altland *et al.* without discussion of its polymerization product.^[74] It is in our opinion that a group of functional polymers exists to be explored, where new knowledge and properties are expected to be discovered. Hence, it is highly motivated to

introduce 1,2,4-triazolium IL species into PILs, and here specifically a series of 1-vinyl-1,2,4-triazolium-based PILs bearing TFSI⁻ and PF₆⁻ as counter anions. These PILs were achieved either *via* a straightforward radical polymerization of the corresponding ILMs or through anion exchange of the corresponding polymer precursors bearing iodide anion. Other than their imidazolium/1,2,3-triazolium counterparts, poly(1-vinyl-1,2,4-triazolium)s exhibit a unique arrangement of nitrogen atoms in the cation ring, which results in enhanced coordination strength with transition metal ions.

2.2 Experimental Section

Materials, synthetic procedure, analytical instrumentation and additional experimental data are provided in Appendix.

2.3 Synthesis of poly(1-vinyl-1,2,4-triazolium) poly(ionic liquid)s

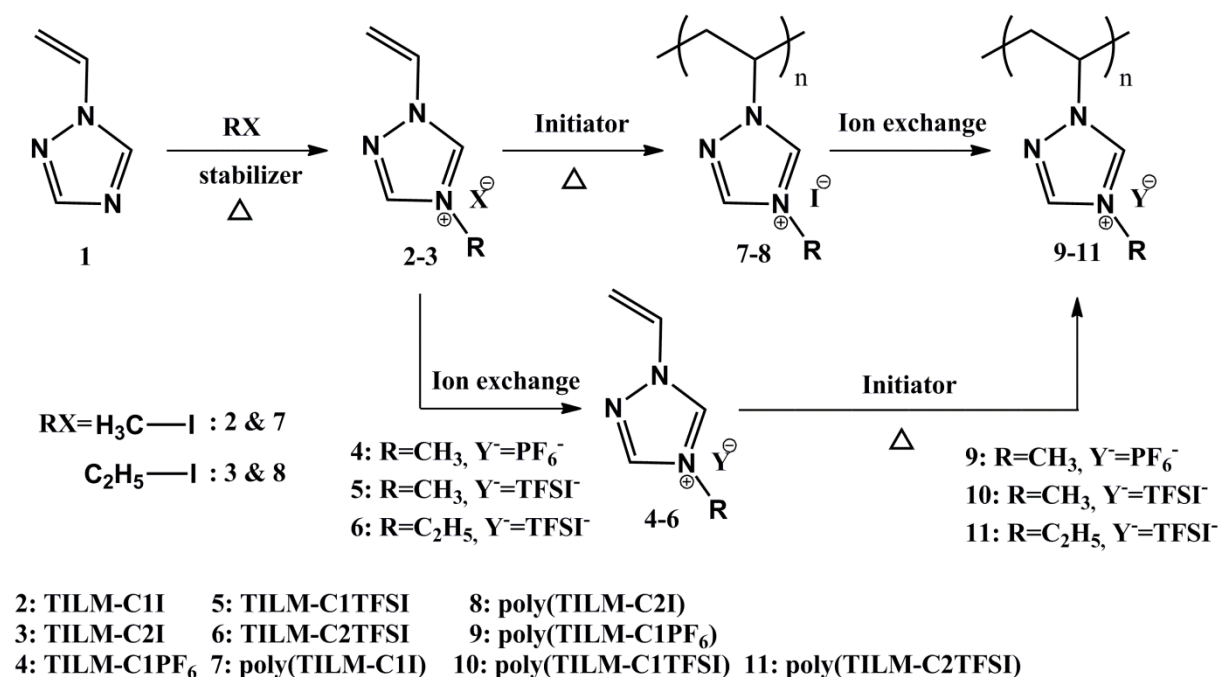


Figure 5. Synthetic route towards poly(4-alkyl-1-vinyl-1,2,4-triazolium) PILs through polymerization of ILMs and through anion exchange of iodide polymers. Corresponding monomers are termed as **TILM-C_nX**, ($n=1$ or 2 , $X=I, PF_6$ or $TFSI$), polymers as **poly(TILM-C_nX)**, ($n=1$ or 2 , $X=I, PF_6$ or $TFSI$).

As shown in **Figure 5**, poly(4-alkyl-1-vinyl-1,2,4-triazolium iodide)s with methyl (**7**: poly(TILM-C1I)) and ethyl (**8**: poly(TILM-C2I)) substituents were synthesized in two steps. Firstly, 4-alkyl-1-vinyl-1,2,4-triazolium iodide monomers **2** (TILM-C1I) and **3** (TILM-C2I)

were obtained by *N*-alkylation of 1-vinyl-1,2,4-triazole with iodomethane and iodoethane, respectively. Interestingly, the D-position nitrogen in the 1,2,4-triazolium ring is preferred for its *N*-alkylation reaction.

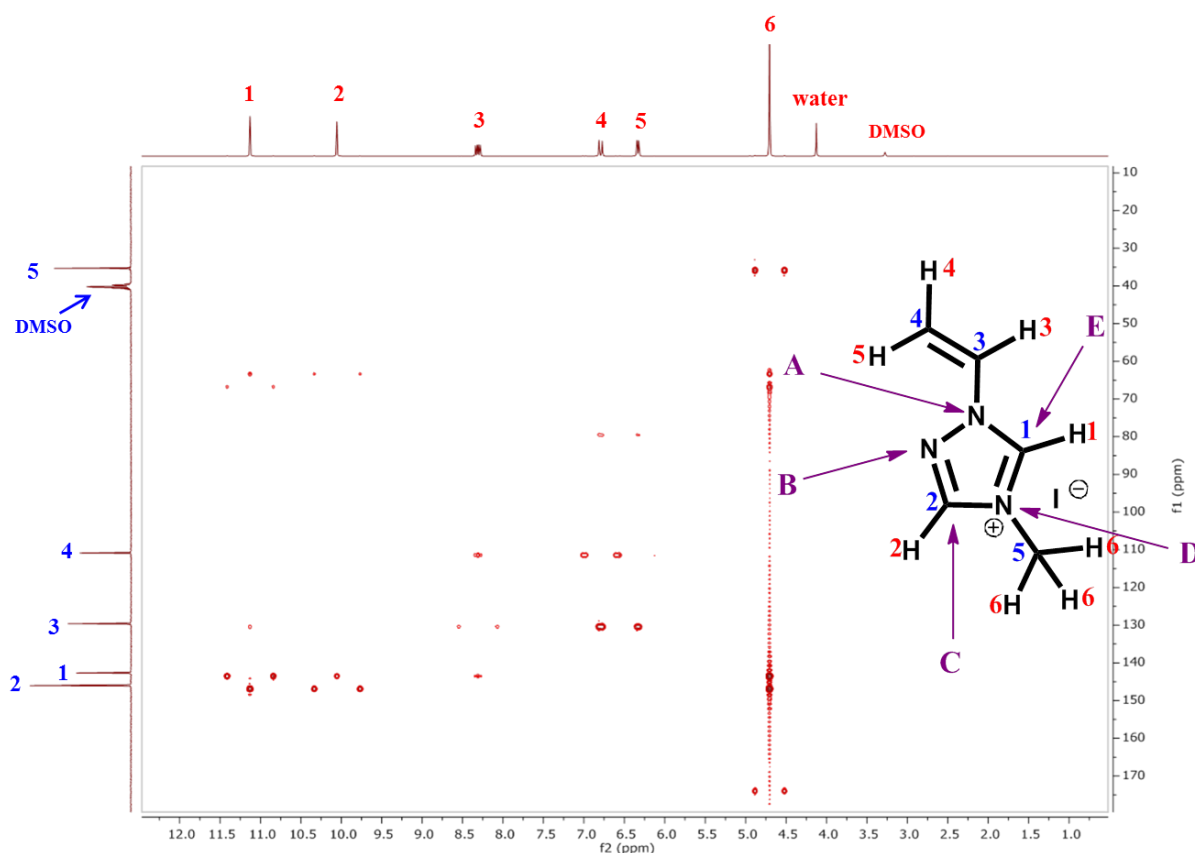


Figure 6. ^1H - ^{13}C HMBC spectrum of TILM-C1I and its corresponding structural analysis.

Experimentally in order to confirm the *N*-alkylation at D-position nitrogen in TILM-C1I, carbon heteronuclear multiple bond correlation (^1H - ^{13}C HMBC) (**Figure 6**) measurement of TILM-C1I was conducted. In **Figure 6** carbon 1 is found to be coupled with proton 2, 3 and 6, while carbon 2 was not coupled with proton 3, which indicates that carbon 1 is the one closer to the vinyl group. As for carbon 3, it is coupled with proton 1, 4 and 5, which defines its only possible position of the vinyl group as the carbon directly attached to nitrogen at A position; Considering that only two carbons can possibly interact with proton 3 configurationally, plus the fact that carbon 4 was only coupled with proton 3, we can conclude that carbon 4 should be assigned to the next carbon position in the vinyl group. Based on these analyses, the last signal as the methyl adduct can only be assigned to carbon 5. In other words, if carbon 5 was attached to B-position N, carbon 2 would be coupled with proton 6; while no evidence is observed, this possibility is excluded. Consequently, the B-position *N*-alkylation is not any more considered for 1-vinyl-1,2,4-triazolium compound. Hence, we confirmed the chemical structure of the iodide monomers as well as their D-position *N*-alkylation.

Table 1. Crystallographic data and structural refinement for TILM-C11.

Bond precision:	C-C = 0.0180 Å	Wavelength=0.71073	
Cell:	$a=5.0409(5)$	$b=25.591(4)$	$c=6.9793(8)$
	$\alpha=90$	$\beta=103.817(11)$	$\gamma=90$
Temperature:	293 K		
	Calculated	Reported	
Volume	874.29(19)	874.30(19)	
Space group	P 21/c	P 1 21/c 1	
Hall group	-P 2ybc	-P 2ybc	
Moiety formula	C5 H8 N3, I	C5 H8 N3, I	
Sum formula	C5 H8 I N3	C5 H8 I N3	
M_r	237.04	237.04	
$D_x, g\text{ cm}^{-3}$	1.801	1.801	
Z	4	4	
$M_u\text{ (mm}^{-1}\text{)}$	3.592	3.592	
F000	448.0	448.0	
F000'	446.22		
h, k, l_{max}	6, 30, 8	6, 30, 8	
N_{ref}	1601	1584	
$T_{\text{min}}, T_{\text{max}}$	0.386, 0.650	0.692, 1.000	
T_{min}'	0.305		
Correction method=	# Reported T Limits: $T_{\text{min}}=0.692$ $T_{\text{max}}=1.000$		
AbsCorr =	MULTI-SCAN		
Data completeness=	0.989	Theta(max)= 25.350	
R(reflections)=	0.0374(1217)	$wR_2(\text{reflections})= 0.0808(1584)$	
S =	1.062	$N_{\text{par}}= 83$	

An alternative way to verify the chemical structure of 1-vinyl-4-alkyl-1,2,4-triazolium iodide monomers is the single crystal analysis (**Figure 7**). As shown in **Table 1**, TILM-C11 crystallizes in the monoclinic group $P2_1/c$, with cell parameters of $a=5.0409(5)$ Å, $b=25.591(4)$ Å, $c=6.9793(8)$ Å and $\beta=103.817(11)^\circ$. Its *N*-alkylation position at D-position nitrogen is again confirmed, which is consistent with the analysis of ^1H - ^{13}C HMBC spectrum

mentioned above. **Figure 7** displays the packing model of TILM-C1I along three individual axes *a*, *b* and *c*, respectively. The preferential *N*-alkylation at D-position nitrogen in our opinion is a natural outcome of multiple factors, *i.e.* a higher electron density and a less sterical hindrance at D- than B-position nitrogen, as well as a favorable resonance structure in the *N*-alkylation product at D-position nitrogen.

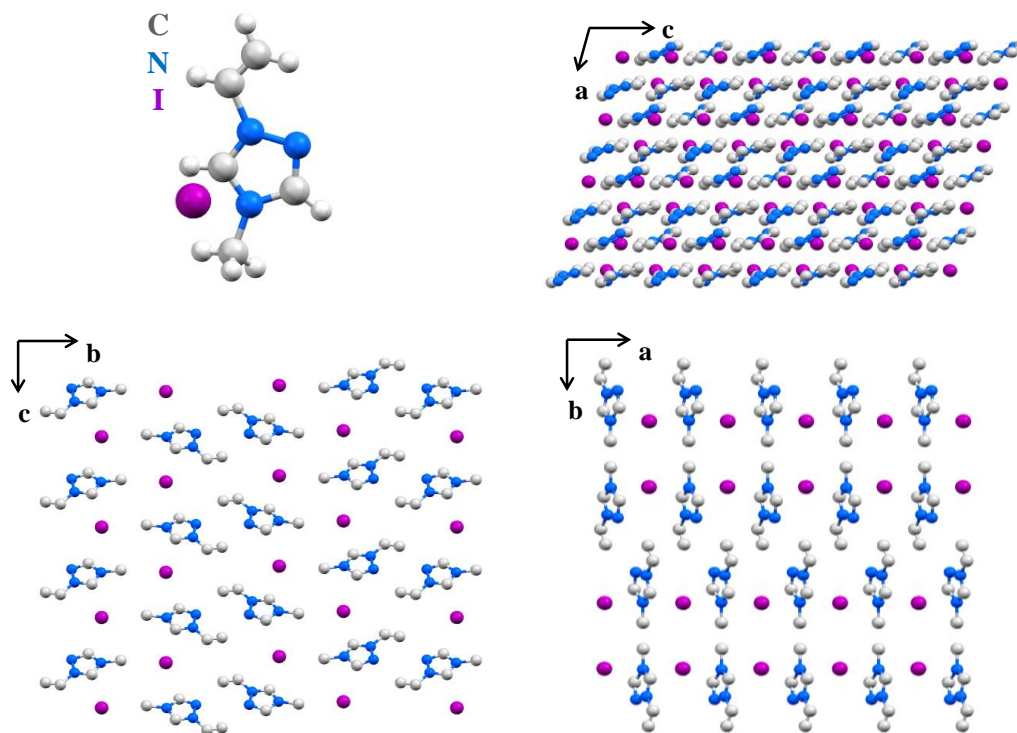


Figure 7. Single crystal structure and crystallographic packing model of TILM-C1I (CCDC 1436278 contains the supplementary crystallographic data for this article. These data can be found from the Cambridge Crystallographic Data Centre via www.ccdc.cam.ac.uk/data_request/cif.)

Once confirming the successful quaternization on D-position nitrogen with methyl/ethyl iodide, we next moved to the proton nuclear magnetic resonance (^1H NMR) and carbon nuclear magnetic resonance (^{13}C NMR) spectroscopy for TILM-C1I and TILM-C2I to further understand the influence of *N*-alkylation on chemical shifts (Appendix). In **Figure 8**, the ^1H NMR spectrum of 1-vinyl-1,2,4-triazole (**A**) was displayed as a reference to compare with its methylation product *i.e.* TILM-C1I (**B**). 1-Vinyl-1,2,4-triazole (**A**) clearly contains five protons, in which 3 are from the vinyl part (*c*, *d*, *e* at 7.33, 5.71 and 5.00 ppm, respectively) and 2 from 1,2,4-triazole part (*a* at 8.78 and *b* at 8.10 ppm). In TILM-C1I (**B**), all proton signals were shielded after methylation with methyl iodide and an additional peak *f'* (3.92 ppm) came up, which can be assigned to the protons in the methyl group adjacent to the *N*-

alkylated nitrogen. Upon calculating the integration ratio of f'/e' (or f'/a' , f'/b'), it was found that the integration ratio (3.0) matches the theoretic value of a full *N*-alkylation, and verified the quantitative methylation. By anion metathesis of TILM-C1I and TILM-C2I with target salts, 1,2,4-triazolium monomers with hydrophobic fluorinated anions of PF_6^- or TFSI^- (**4-6**: TILM-C1 PF_6 , TILM-C1TFSI and TILM-C2TFSI) were achieved. Their ^1H NMR spectra are similar to their iodide monomers.

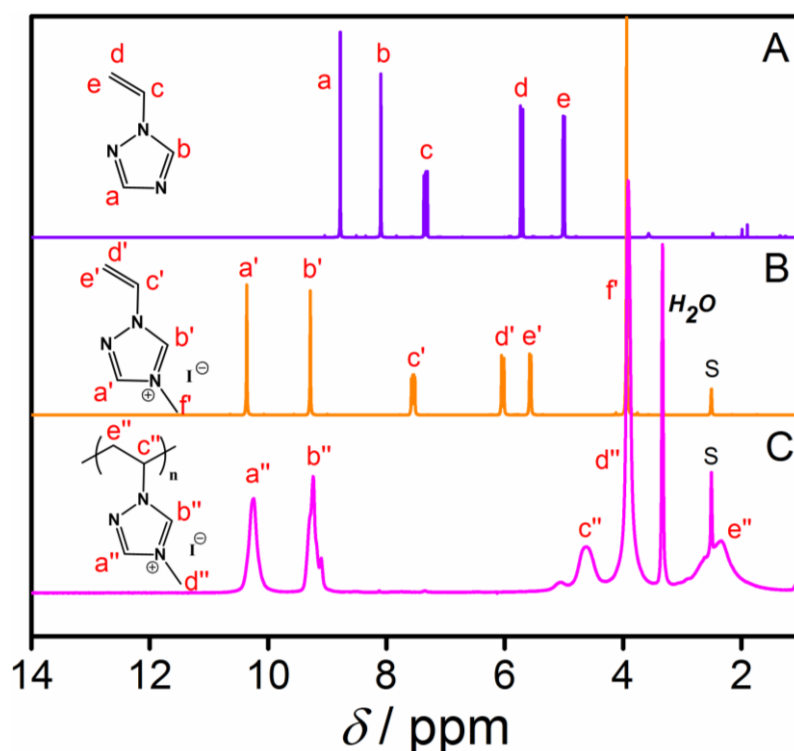


Figure 8. ^1H -NMR spectra of (A) 1-vinyl-1,2,4-triazole; (B) 4-methyl-1-vinyl-1,2,4-triazolium iodide (TILM-C1I); and (C) poly(4-methyl-1-vinyl-1,2,4-triazolium iodide) (poly(TILM-C1I)).

Poly(TILM-C1I) and poly(TILM-C2I) were synthesized from TILM-C1I and TILM-C2I, respectively, *via* free radical polymerization, which were purified by membrane dialysis with MWCO – 3,500 Da to remove residue impurities. ^1H NMR spectroscopy was applied to confirm the successful polymerization (Appendix). Here, ^1H NMR spectrum of poly(TILM-C1I) was illustrated in **Figure 8** (C). When polymers were formed, the proton peaks for vinyl group of TILM-C1I (c' , d' , e' at 7.55, 6.02 and 5.58 ppm, respectively) vanished, and new proton peaks (c'' at 4.60 and e'' at 2.34 ppm) from the backbone protons of the polymer appeared. This is a typical shielding behavior caused by disappearance of conjugation effects. Additionally, gel permeation chromatography (GPC) measurement was conducted for a further proof of successful polymerization. The measurement was carried out in an aqueous

solution of methanol using acetic acid as buffer. Both polymers displayed in the GPC trace a monomodal distribution and number-averaged apparent molecular weight of 47 and 55 kg/mol, respectively (**Table 2**). Following the similar procedure, poly(TILM-C1PF₆), poly(TILM-C1TFSI) and poly(TILM-C2TFSI) can be synthesized directly from their monomers (TILM-C1PF₆, TILM-C1TFSI and TILM-C2TFSI) as well. Notably, post-polymerization anion metathesis of poly(TILM-C1I) or poly(TILM-C2I) have been conducted as well to prepare these three polymers. However, according to previous literatures, post-modification of ionic polymers *via* anion exchange, though experimentally simple to perform, may induce the residue halide contaminant, which is unfavorable in some applications.

Table 2. Molecular weight and polydispersity index of poly(TILM-C1I) and poly(TILM-C2I) determined by GPC.

Polymer	M _n / g/mol	M _w / g/mol	PDI
poly(TILM-C1I)	47,300	89,900	1.90
poly(TILM-C2I)	55,600	105,000	1.88

2.4 Characterization of poly(1-vinyl-1,2,4-triazolium) poly(ionic liquid)s

As previously reported, the class of cation-anion pairs and interactions between them can decide the physical properties of ILs and their polymers. By simply changing the types of cations or anions, melting points, thermal stability as well as solubility of ILs and PILs can be adjusted. Differential scanning calorimetry (DSC) traces in **Figure 9** showed that TILM-C1I melted at 114.5 °C and remained stable up to 140 °C, after which thermal polymerization sets in with the appearance of a large exothermal peak. Notably, compared with the methyl substituted one, ethyl substituted TILM-C2I reaches a higher melting point at 145 °C. Interestingly, when replacing the anions of these monomers with larger hydrophobic fluorinated ones to reduce the cation-anion interaction, melting points of them are vastly changed. For instance, TILM-C1PF₆ melts at a much lower temperature of 72 °C.

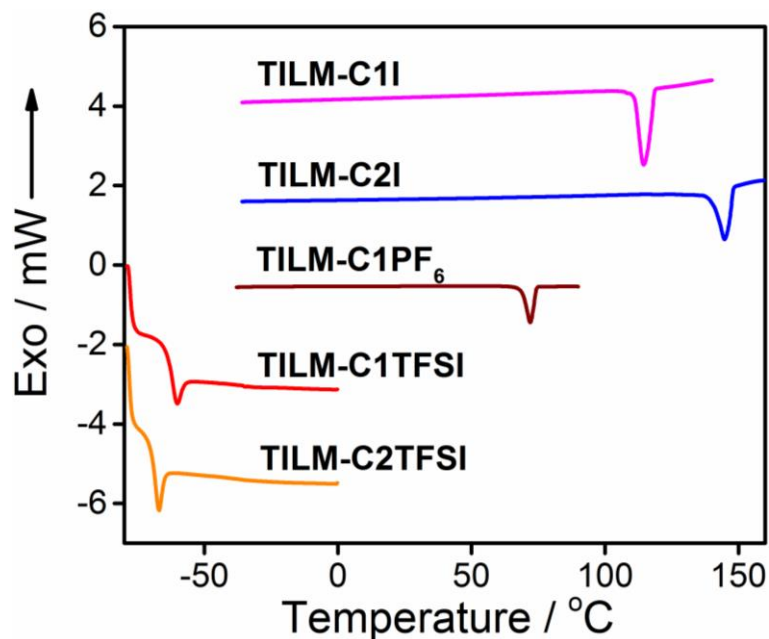


Figure 9. DSC curves of TILM-C1I (pink), TILM-C2I (blue), TILM-C1PF₆ (brown), TILM-C1TFSI (red) and TILM-C2TFSI (orange). Heating rate: 10 K/min under nitrogen. These are the heating curves in the second heating/cooling cycle.

Likewise, TILM-C1TFSI and TILM-C2TFSI display rather low T_g at -61 and -67 °C, respectively, thus being a viscous and sticky liquid at room temperature. Based on the classical definition of ILs by Paul Walden (with melting points below 100 °C),^[1] only TILM-C1PF₆, TILM-C1TFSI and TILM-C2TFSI are considered as ILs. Hence their polymers poly(TILM-C1PF₆), poly(TILM-C1TFSI) and poly(TILM-C2TFSI) are classified as PILs correspondingly, which are studied in detail next.

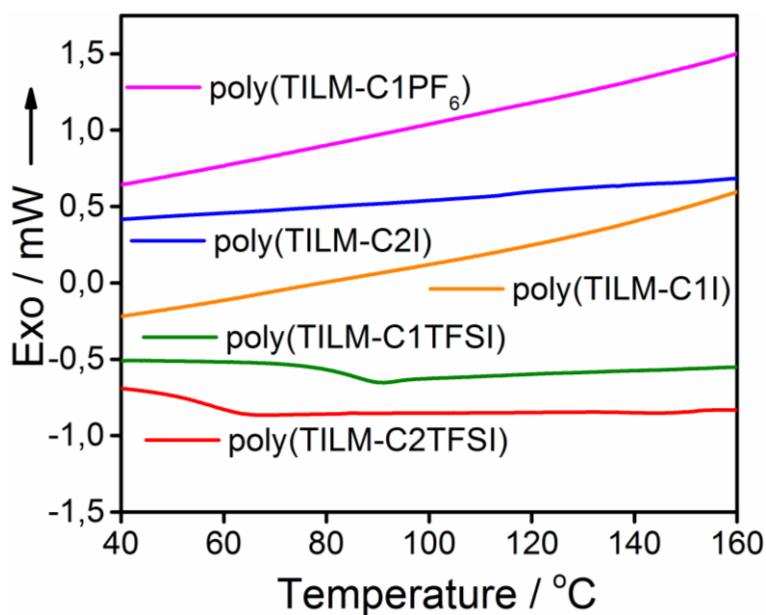


Figure 10. DSC curves of poly(TILM-C1I) (orange), poly(TILM-C2I) (blue), poly(TILM-C1PF₆) (pink), poly(TILM-C1TFSI) (olive) and poly(TILM-C2TFSI) (red). Heating rate: 10 K/min.

Figure 10 presents the DSC curves of all polymers. Poly(TILM-C1TFSI) and poly(TILM-C2TFSI) carrying TFSI⁻ anion show a T_g at 90 and 60 °C, respectively, while T_g in poly(TILM-C1PF₆) bearing PF₆⁻ anion and the iodide-containing poly(TILM-C1I) and poly(TILM-C2I) is absent up to 200 °C. This trend is consistent with the mechanism that the large sized TFSI⁻ anion can shift T_g to relatively low temperatures which can be detected by DSC, owing to its well-known plasticizing effect to increase the free volume. The thermal stability of PILs (poly(TILM-C1PF₆), poly(TILM-C1TFSI) and poly(TILM-C2TFSI)) as well as their precursors (poly(TILM-C1I) and poly(TILM-C2I)) was determined by thermogravimetric analysis (TGA, **Figure 11**) performed under N₂ flow. The decomposition temperature (defined as 5 wt% mass loss) of iodide-containing poly(TILM-C1I) and poly(TILM-C2I) are recorded to be 237 and 239 °C, respectively, both of which are lower than the PILs bearing fluorinated anions, which are 266 °C for poly(TILM-C1PF₆), 313 °C for poly(TILM-C1TFSI) and 283 °C for poly(TILM-C2TFSI), respectively. Since iodide is a stronger nucleophile than PF₆⁻ and TFSI⁻ and attacks the 1,2,4-triazolium/imidazolium ring at elevated temperature, the above-mentioned trend in thermal stability is indeed expected.^[75]

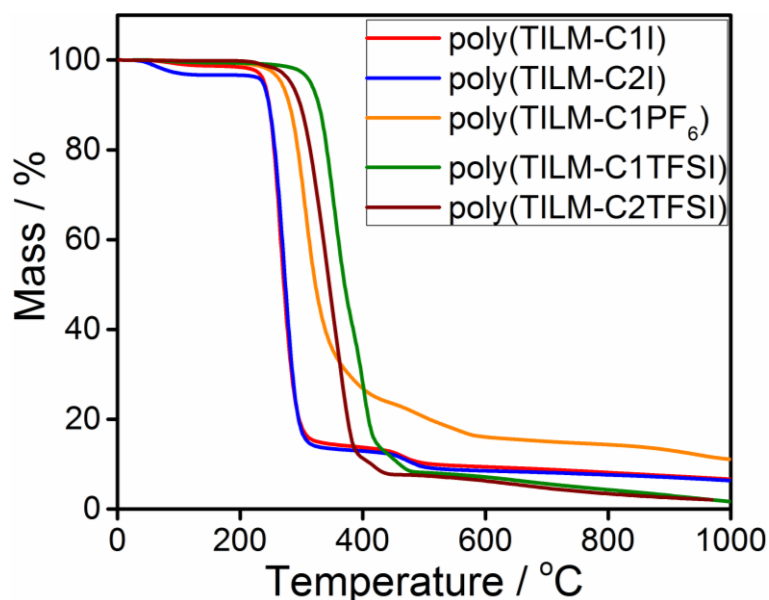


Figure 11. TGA curves of poly(4-alkyl-1-vinyl-1,2,4-triazolium)s. Heating rate: 10 K/min under nitrogen.

In order to prove the successful anion exchange for both monomers (TILM-C1I and TILM-C2I) and polymers (poly(TILM-C1I) and poly(TILM-C2I)) which cannot be verified by ¹H

NMR due to the silence of all these anions in ^1H NMR, ATR/FTIR spectroscopy (Attenuated total reflection/Fourier transform infrared spectroscopy) measurements were conducted to provide evidence (**Figure 12**). In the case of TILM-C1I and poly(TILM-C1I), since iodide anions are invisible in ATR/FTIR in the current measuring range, what we observed are the absorption bands of poly(4-alkyl-1-vinyl-1,2,4-triazolium) cation in the spectra. For monomers and polymers carrying TFSI $^-$ as anion, their IR spectra have been systematically studied in previous literatures.^[76] On account of that, in TILM-C1TFSI and poly(TILM-C1TFSI), three bands at 1177, 740, and 569 cm^{-1} can be clearly assigned to $\nu_a\text{CF}_3$, $\delta_s\text{CF}_3$, and $\delta_a\text{CF}_3$ of the TFSI $^-$ anion, respectively. Also four bands of stretching ($\nu_a\text{SO}_2$ at 1343 cm^{-1} , $\nu_s\text{SO}_2$ at 1133 cm^{-1}) and bending ($\delta_a\text{SO}_2$ at 611 cm^{-1} and shoulder $\delta_s\text{SO}_2$ at 600 cm^{-1}) of $=\text{SO}_2$ groups of TFSI $^-$ can be recognized.

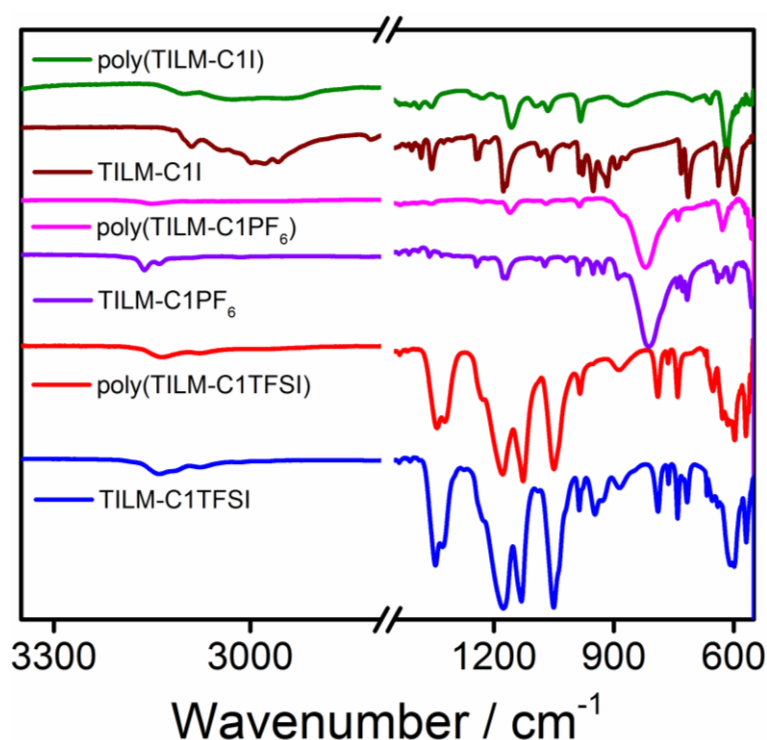


Figure 12. ATR/FTIR spectra of TILM-C1I (brown), TILM-C1PF $_6$ (purple) and TILM-C1TFSI (blue); poly(TILM-C1I) (green), poly(TILM-C1PF $_6$) (pink) and poly(TILM-C1TFSI) (red).

Furthermore, asymmetric (1051 cm^{-1}) and symmetric (764 cm^{-1}) stretching bands of S-N-S group, and symmetric stretching of C-S (790 cm^{-1}) were observed as expected, confirming the presence of TFSI $^-$ anion as well. For TILM-C1PF $_6$ and poly(TILM-C1PF $_6$) carrying PF $_6^-$ as anion, the broad band at 820 cm^{-1} can be assigned to the symmetric stretching of the PF $_6^-$ anion.^[77] Finally, the disappearance of stretching bands (vinyl C-H at 3100 cm^{-1}) when

monomers were polymerized, evidenced the successful polymerization. Therefore, ATR/FTIR spectra offered solid evidence of the anion exchange. It should be mentioned that the ATR/FTIR analysis here is only a qualitative measurement. To determine the purity of the monomers and polymers after anion exchange, titration was performed *via* using a silver nitrate reagent, which exhibits a quantitative anion exchange degree in the monomers (> 95%) and a high efficiency of anion exchange in the polymers (> 92%, **Table 3**).

Table 3. Iodide content and calculated anion exchange degree of monomers and polymers after anion metathesis (calculated from silver nitrate titration with Eosin Y as indicator).

Compound	Iodide content / wt%	Anion exchange degree / %
Monomer		
TILM-C1PF₆	0.60	98.8
TILM-C1TFSI	0 (no precipitate)	100
TILM-C2TFSI	0 (no precipitate)	100
Polymer		
poly(TILM-C1PF₆)	2.63	92.08
poly(TILM-C1TFSI)	1.50	95.53
poly(TILM-C2TFSI)	1.28	96.06

Altering the counter anions and alkyl chains of ILs and PILs can impact their solubility. **Table 4** summarizes the solubility of 1,2,4-triazolium-based monomers and polymers tested under ambient temperature at a concentration of 1.0 wt%. Independent of the anion type, all monomers and polymers were found insoluble in chloroform and toluene, and soluble in N,N-dimethylformamide (DMF) and dimethyl sulfoxide (DMSO). For other solvents tested, in general, when polymers or monomers bear iodide and short alkyl substitutes, they are soluble in water and polar organic solvents. Upon exchanging iodide to large fluorinated and

hydrophobic anions, the products become soluble only in organic solvents. For TILM-C1I, it can be dissolved in water, methanol and acetone. In the case of TILM-C2I, the alkyl length extends from methyl to ethyl, *i.e.* increasing slightly its hydrophobicity, thus it keeps the same solubility as TILM-C1I. When fluorinated, hydrophobic anions (PF_6^- or TFSI) were incorporated, the monomers can be dissolved in all tested polar organic solvents; one exception is TILM-C1 PF_6 carrying PF_6^- anion maintains its solubility in water, as PF_6^- is less hydrophobic than TFSI. Polymerization of monomers can alter solubility. For instance, iodide-containing poly(TILM-C1I) and poly(TILM-C2I) become only soluble in water and DMF/DMSO but not in methanol and acetone; poly(TILM-C1 PF_6) (bearing PF_6^-) even cannot be dissolved in any solvents other than DMF/DMSO. Interestingly, poly(TILM-C1TFSI) and poly(TILM-C2TFSI) (bearing TFSI) maintained the same solubility as their monomers.

Table 4. Solubility of 1,2,4-triazolium monomers and polymers in different solvents.

Compound	H ₂ O	MeOH/acetone/can	THF	CHCl ₃ /toluene	EtOAc	DMF/DMSO
TILM-C1I	+	+	-	-	-	+
TILM-C2I	+	+	-	-	-	+
TILM-C1 PF_6	+	+	+	-	+	+
TILM-C1TFSI	-	+	+	-	+	+
TILM-C2TFSI	-	+	+	-	-	+
poly(TILM-C1I)	+	-	-	-	-	+
poly(TILM-C2I)	+	-	-	-	-	+
poly(TILM-C1 PF_6)	-	-	-	-	-	+
poly(TILM-C1TFSI)	-	+	+	-	+	+
poly(TILM-C2TFSI)	-	+	+	-	-	+

(+) – soluble at 1.0 wt%; (-) - insoluble at 1.0 wt%

Poly(TILM-C2TFSI) (bearing TFSI) was further compared with poly(1-vinyl-3-ethylimidazolium TFSI) (termed as poly(ImILM-C2TFSI)), which has a chemical structure of high similarity, except in the cation ring - one carbon atom in the imidazolium ring was replaced by nitrogen. We found that poly(TILM-C2TFSI) exhibits a general similar solubility to poly(ImILM-C2TFSI) except in methanol, in which poly(TILM-C2TFSI) is soluble but poly(ImILM-C2TFSI) not.^[68] Doubtlessly, the single atom change in the 5-member cation ring from imidazolium to 1,2,4-triazolium does bring new physical properties and will be discussed more in the following.

2.5 Metal ion absorption behavior of poly(1-vinyl-1,2,4-triazolium) poly(ionic liquids)

PILs are able to bind transition metal ions *via* coordination, which is of significant value in numerous practical applications, such as catalysis, metal-carbene compounds, selective sorption, metal ion scavenging, just to name a few. A high capacity of metal ion loading by PILs is important for some applications. For example, imidazolium-based microporous PILs that were able to load as much as 25 wt% of CuCl_2 , presented an exceptional efficiency in catalyzing aerobic oxidation of hydrocarbons.^[44] This finding inspired us to investigate the adsorptive capability of poly(1-vinyl-1,2,4-triazolium) PILs towards transition metal ions because of the extra lone electron pair in D-position nitrogen for coordination with metal species.

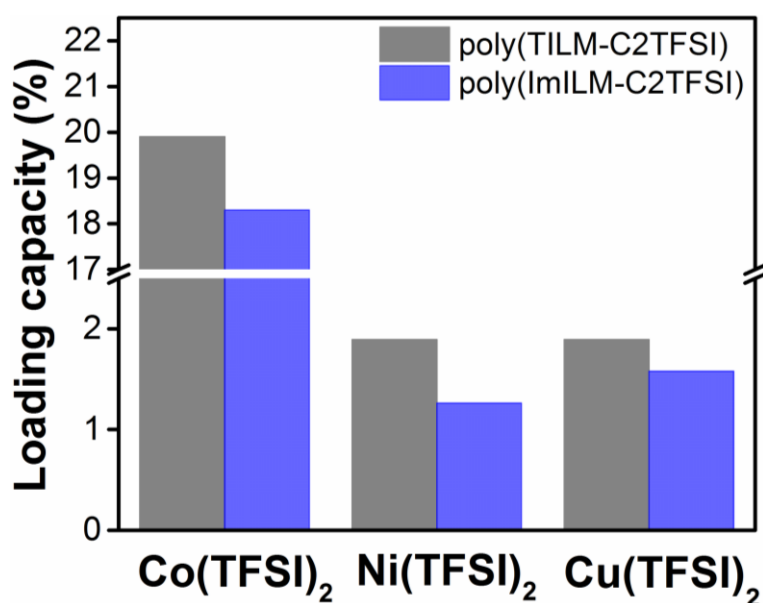


Figure 13. Loading of Co/Ni/Cu ions in poly(TILM-C2TFSI) (gray) and poly(ImILM-C2TFSI) (blue) at a fixed mixing molar ratio of metal/monomer unit ~ 2 . The y axis, loading capacity denotes the molar percentage of the loaded metal ions with regard to the monomer unit.

Here, poly(ImILM-C2TFSI) as one of the most popularly studied PILs, was used as reference to compare with poly(TILM-C2TFSI) due to their structural similarity. Three metal salts, *i.e.* $\text{Co}(\text{TFSI})_2$, $\text{Ni}(\text{TFSI})_2$, and $\text{Cu}(\text{TFSI})_2$, which feature the same anion TFSI^- as poly(TILM-C2TFSI) to skip the anion factor, were tested. Experimentally poly(TILM-C2TFSI) and poly(ImILM-C2TFSI) were mixed individually with $\text{Co}(\text{TFSI})_2$, $\text{Ni}(\text{TFSI})_2$, or $\text{Cu}(\text{TFSI})_2$ in

DMF. The metal salts were used in excess with molar ratio of (Co, Ni, or Cu)/imidazolium or 1,2,4-triazolium. After stirring overnight, samples were exhaustively dialyzed to remove free metal salts. The final polymer/metal complex products were dried under high vacuum (1×10^{-3} mbar) at 100 °C for 24 h. The residue solid was examined by elemental analysis to determine the metal content, which is shown in **Figure 13**.

Based on the histograms in **Figure 13**, two trends can be seen: first, irrelevant to the type of metal ions, poly(TILM-C2TFSI) presents a higher loading capacity than poly(ImILM-C2TFSI), here specifically 10%, 50% and 20% more in molar ratio in the case of Co(II), Ni(II) and Cu(II), respectively. As reported previously, 1,2,4-triazolium ions normally possess stronger acidity for the E-position proton than their imidazolium analogues,^[78] and this proton deprotonates easier in DMF, a weak or neutral Lewis base, thus coordinating stronger with transition metal ions. Nevertheless, no experimental proof to this deprotonation process has been provided to this polymeric system so far, which needs further exploration in the future. Besides, the higher loading capacity of Co(II) than Cu (II) and Ni(II) in both poly(TILM-C2TFSI) and poly(ImILM-C2TFSI) might stem from their coordination structures, in which Co(II) is known to build up an octahedral ligand field, while Cu(II) and Ni(II) prefer square planar or tetrahedron configuration. Hence it can be concluded that poly(1-vinyl-1,2,4-triazolium) PILs undergo stronger coordination with transition metal ions than polyvinylimidazolium PILs. It is additionally observed that Co(II) ions complex much stronger than Ni(II) and Cu(II), independent of the type of the PILs tested here. Thus, the metal immobilization in PILs is ion-specific.

2.6 Conclusions

In conclusion, we synthesized and characterized a series of 4-alkyl-1-vinyl-1,2,4-triazolium-based ILs and PILs. A systematic exploration of their synthetic routes and physicochemical properties has been conducted. Similar to common ILs, the melting points/glass transition temperatures as well as the solubility of 1,2,4-triazolium monomers/polymers can be tailored by selecting different anions. Interestingly, the 1,2,4-triazolium PILs are different from their imidazolium analogues in immobilizing transition metal ions, which makes this group of PILs appealing in, *e.g.* catalysis, sorption and scavenging. Compared with imidazolium counterparts, the replacement of one carbon atom by nitrogen in the 1,2,4-triazolium PIL does lead to visible different properties, such as stronger acidity and hydrophilicity. Moreover, the high content of nitrogen in the 1,2,4-triazolium ring may be suitable precursors for nitrogen-doped carbons.

3. Self-assembly in poly(1,2,4-triazolium) poly(ionic liquid) nanoparticles: One-step polymerization towards controllable internal morphologies

3.1 Introduction

How to precisely control the outer shape of soft matters in particle form is well-investigated in literature,^[79] while the more delicate manipulation of internal morphologies is still far from comprehensive understanding in polymer nanoparticles. It is clear that both the surface and the inner morphology are crucial for polymer nanostructures to define their properties and functions, and need to be strictly controlled when specific application is targeted.^[80] A good many of techniques and methods such as “soft patchy” nanoparticles or polymer block co-micelles have been so far used in realizing such design, and these efforts dominantly have been given to manipulation of shapes, dimensions and/or surface functionalities of nanoparticles.^[81] The careful organization of the nanoparticle interior remains seldom addressed with only few examples. Müller *et al.* reported a method about hierarchical self-assembly of polymer nanoparticles built up from miktoarm star terpolymer triggered by counterion transformation.^[82] Via an emulsion process Hawker *et al.* demonstrated self-assembly of diblock copolymer particles, the morphology of which is governed by external surfactants.^[83] These pathways rely on modulating the interactions between solvent and polymer nanoparticles. Overall it is fair to say that the capability to tailor both the overall shape and the fine interior represents a high-level of control over characteristics of polymer (nano)particles, which are important for their specific functions and applications such as catalyst supports^[84] or drug delivery.^[85] Although some achievements in polymer microparticles have been designed with defined shape and interior structure, synthetic techniques are missing in polymer science for particles with size of less than 50 nm. This size scale is approaching the size of some single macromolecules, such as bottle brushes and single-strain DNAs.

Self-assembly is also a popular topic in PIL research. For instance, Weber *et al.* reported a series of PIL-based block-copolymers with microphase separations recently.^[59] Additionally, previously our group reported onion-like PIL nanoparticles and their elongated form “nanoworms” via aqueous dispersion polymerization of vinylimidazolium-based ILMs with long alkyl chains (dodecyl, tetradecyl, hexadecyl and octadecyl chains).^[28] In this chapter, we

will identify and analyze an abnormal morphological variation between an onion-like and a striped ellipsoid-like morphology discovered in 1-vinyl-1,2,4-triazolium-type PIL nanoparticles that are extremely small (nanoparticle diameters below 50 nm and domain size below 5 nm), structurally complex, yet synthetically facile *via* a one-step polymerization. For the first time, morphological transition intermediates in these PIL nanoparticles were visualized due to their favorable stability, which enlighten us with more detailed information about the whole structural variation process. Additionally, it is shown that even a tiny change in the chemical structure of the IL monomers, here specifically by replacing a carbon atom in the imidazolium ring with nitrogen, can trigger significant changes of both internal and external morphology and dispersion behavior. Besides, with the assistance of cryogenic electron tomography (cryo-ET) technique, it becomes possible for us to recognize two unique structure models in “onion-like” and “striped ellipsoid-like” structural configurations. This new advance offers polymer scientists a useful tool to precisely engineer polymer nanostructures.

3.2 Experimental Section

Materials, synthesis routes, characterization techniques and additional experimental data are provided in Appendix.

3.3 Dispersion polymerization of 1,2,4-triazolium type poly(ionic liquid) nanoparticles

PIL nanoparticles studied here were prepared *via* a one-pot dispersion polymerization. Four 1,2,4-triazolium-based ionic liquid monomers (TILMs) with different alkyl chain length and anion type are used, *i.e.* 4-dodecyl-1-vinyl-1,2,4-triazolium iodide (TILM-C12I), 4-dodecyl-1-vinyl-1,2,4-triazolium bromide (TILM-C12Br) and its longer alkyl chain derivatives TILM-C14Br and TILM-C16Br, respectively (**Figure 14&15**). The monomer concentration in the polymerization was fixed at 20 g/L (51.1 mM) in aqueous solutions (70 °C, 24 h), and water-soluble nonionic 2,2'-azobis[2-methyl-N-(2-hydroxyethyl)propionamide] (VA086) was used as initiator. These PIL nanoparticles were formed in the absence of any externally added stabilizer since the ILMs themselves are efficient dispersants during polymerization. *Via* dynamic light scattering (DLS) the hydrodynamic diameter (D_h) of the primary nanoparticles was determined to be 20, 21, 27 and 29 nm for poly(TILM-C12I), poly(TILM-C12Br), poly(TILM-C14Br) and poly(TILM-C16Br), respectively, bearing a standard size deviation of 0.20 ± 0.03 (**Figure 16**).

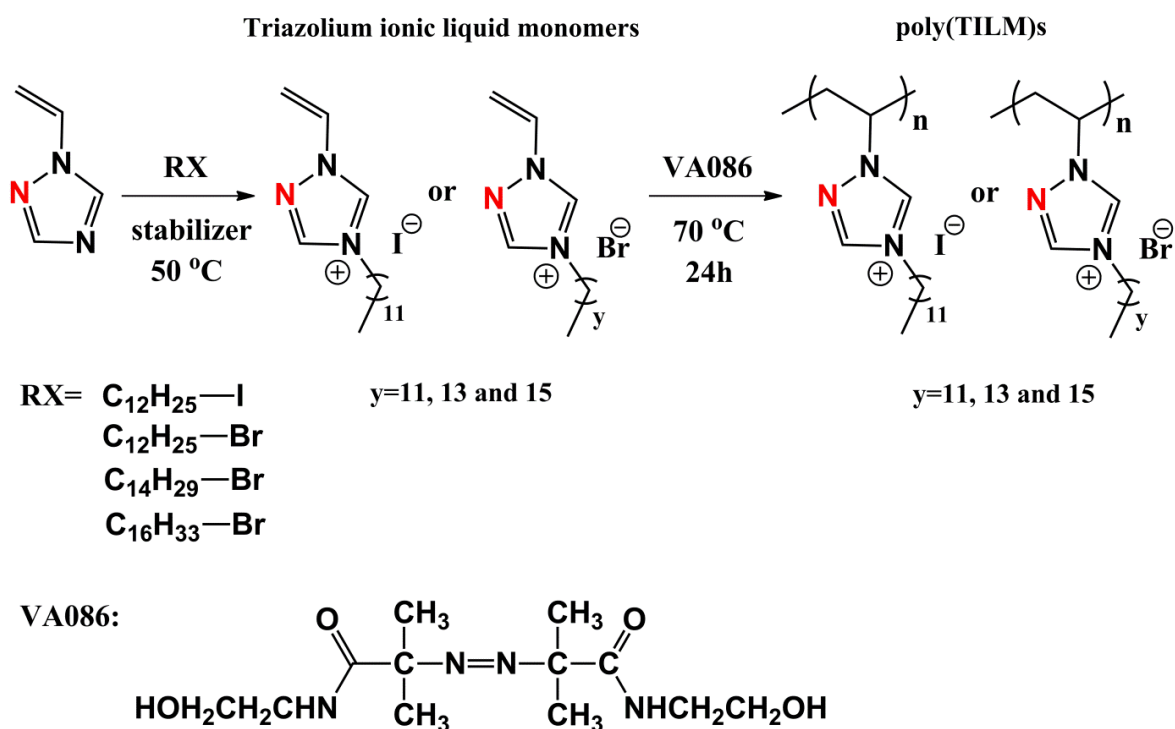


Figure 14. Chemical structure and synthetic route to 1,2,4-triazolium-based poly(ionic liquid) (TPIL) nanoparticles *via* dispersion polymerization. **VA086** is water-soluble thermal initiator.

3.4 Characterization of 1,2,4-triazolium type poly(ionic liquid) nanoparticles

Polymerization of 1,2,4-triazolium-type IL, in comparison to the imidazolium-type PIL nanoparticles, requires a lower monomer concentration to form individual nanoparticles rather than their aggregates. It is possibly due to stronger interactions between 1,2,4-triazolium derivatives. In our previous study^[28] in imidazolium PIL nanoparticles, the self-assembly of PIL nanoparticles begins with pre-assembled mesophases composed of surfactant-like ILMs bearing ionic moieties and long alkyl chain nanodomains. It can be speculated that similar mechanism controls morphology formation in the present system. The phase separation process is a natural outcome of the incompatibility between hydrophobic alkyl chains and the polar ion pairs localized in the polymer backbone region, similar to mesostructures in polyelectrolyte-surfactant complexes.

In the transmission electron microscopy (TEM) images (**Figure 16**) of poly(TILM-C12I) and poly(TILM-C12Br), dark particles of an ellipsoid shape were observed, while for poly(TILM-C16Br) only (quasi-)spherical shape particles were found. Poly(TILM-C14Br) comprises both

ellipsoids and (quasi-)spherical shapes. A particle-based structure was also observed *via* scanning electron microscopy (SEM) characterization in **Figure 17**. The particle sizes from TEM characterization agrees well with that from DLS results. These primary characterizations triggered our interest in what the nature of their inner organization is. In TEM, due to solvent evaporation during the sample preparation, no firm conclusion can be made on their interior that appears homogeneous. Cryogenic electron microscopy (cryo-EM) measurements were conducted next to visualize the true solution structures.

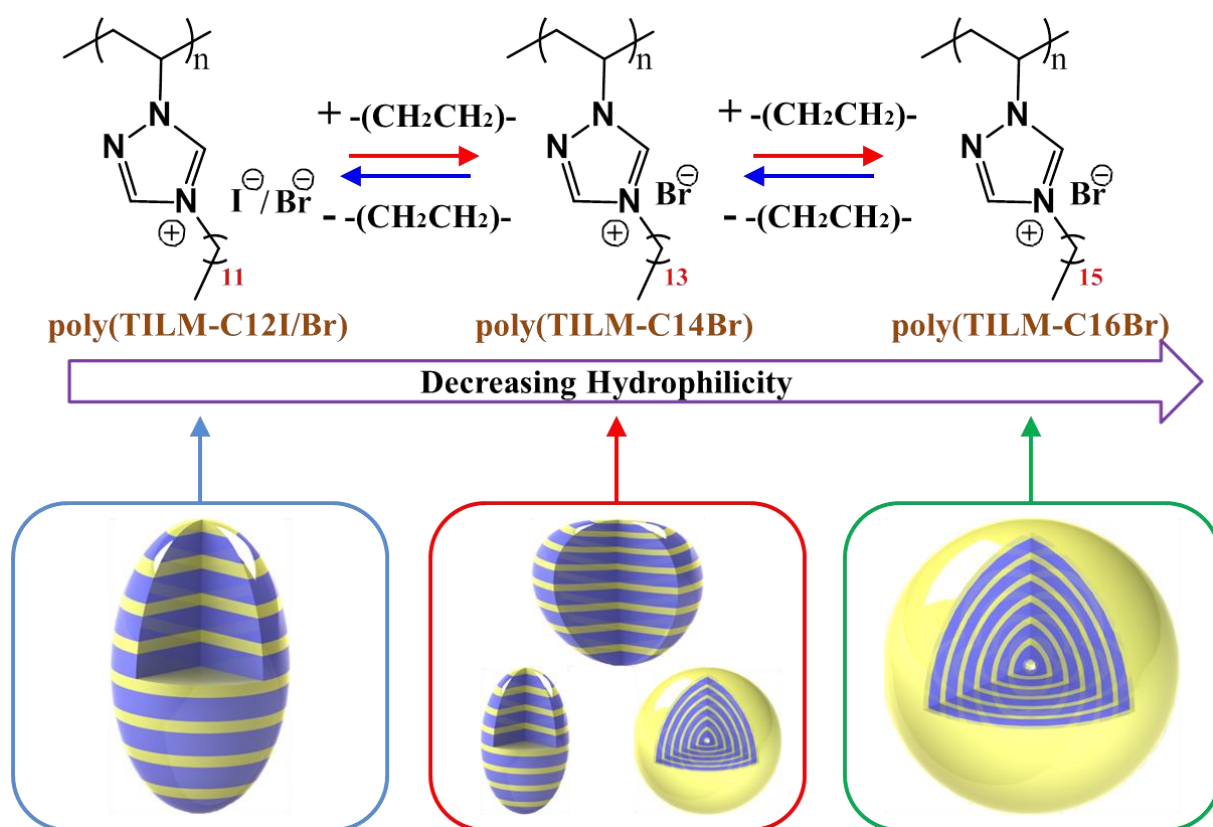


Figure 15. Chemical structures of the investigated poly(ionic liquid)s and the corresponding cartoons of nanoparticle morphologies.

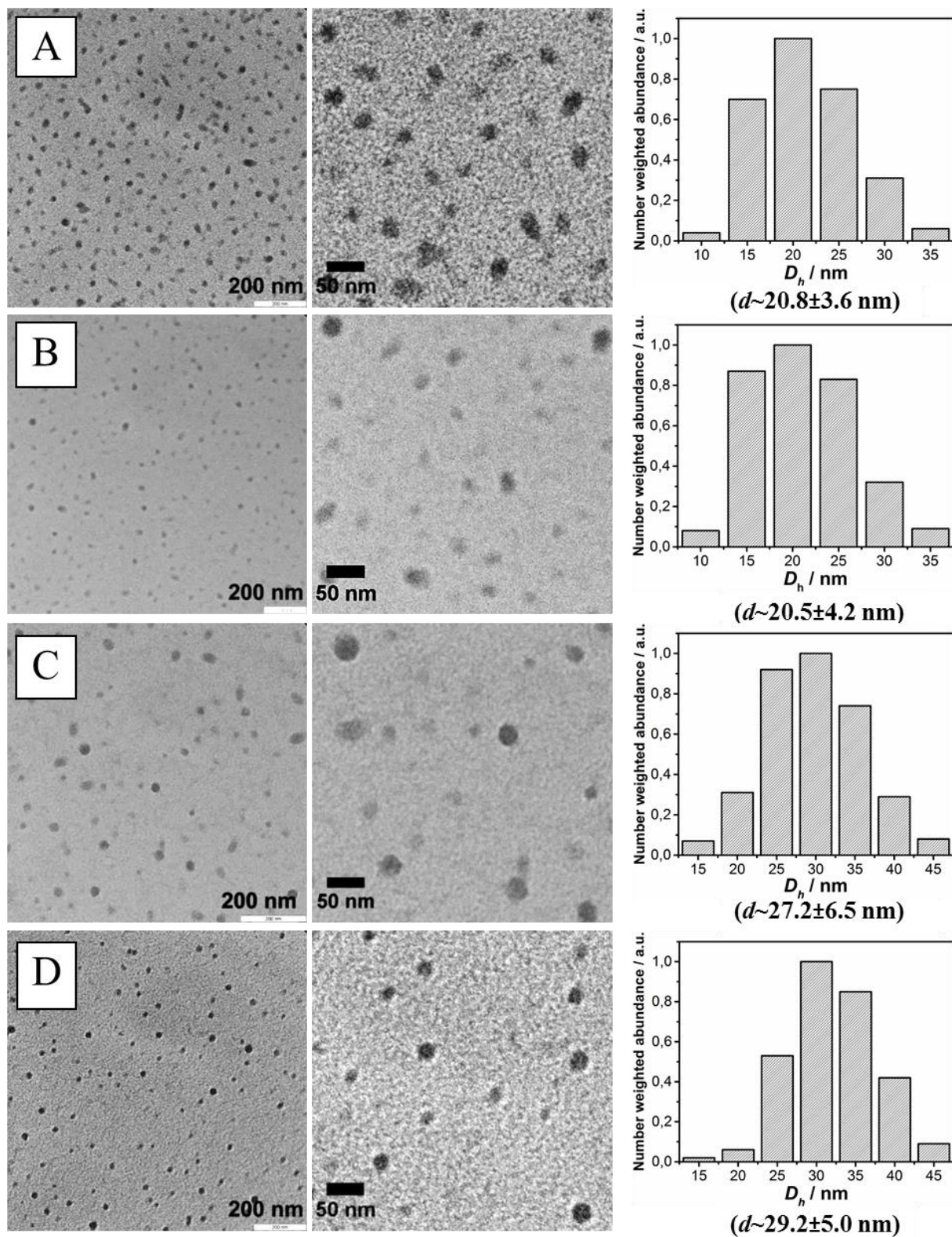


Figure 16. TEM images and number-averaged particle size distributions obtained *via* DLS of poly(TILM-C12I) (A), poly(TILM-C12Br) (B); poly(TILM-C14Br) (C); and poly(TILM-C16Br). All samples are measured in a concentration of 0.4 g/L in water.

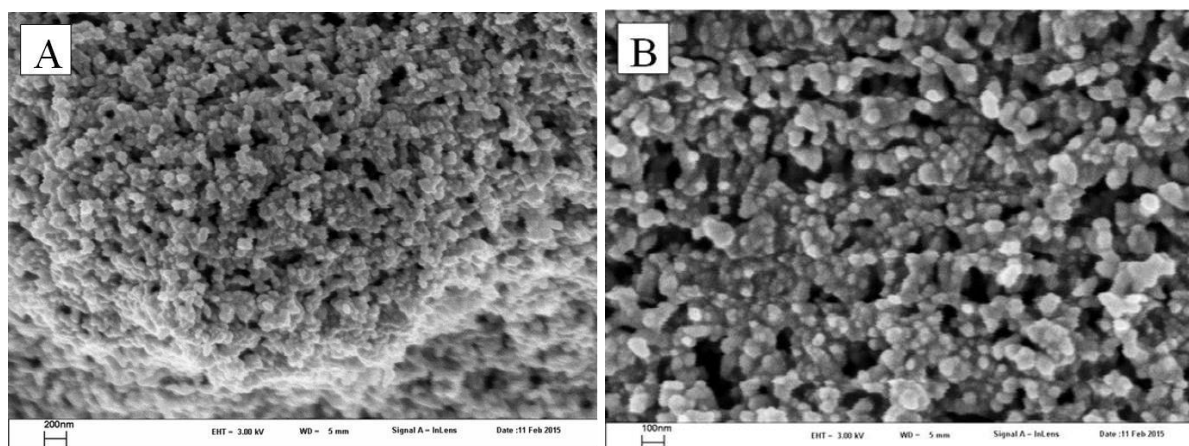


Figure 17. SEM images of poly(TILM-C12Br) nanoparticles prepared *via* drop casting of its aqueous dispersion. (A) overview; (B) close view.

The cryo-EM images of poly(TILM-C12I) and poly(TILM-C_xBr) ($x = 12, 14$ and 16) nanoparticles are collected in **Figure 18** (close view) and **Figure 19** (overview). It is clearly seen that homogeneous striped ellipsoid nanoparticles with wasp-like interior can be visually recognized both in poly(TILM-C12I) (**Figure 18A/19A**) and poly(TILM-C12Br) (**Figure 18B/19B**). Onion-like vesicular nanostructures are uniformly observed in poly(TILM-C16Br) (**Figure 18G/19D**). In poly(TILM-C14Br) (**Figure 18C-F/19C**), wasp-like ellipsoid/spherical and onion-like spherical particles coexist with some intermediate structures, which are identified as transition structure between these two shapes.

In poly(TILM-C12I), besides wasp-like nanoparticles a minor amount of quasi-spheres (~6%) is present, which are the projection of the wasp-like nanoparticles from their polar axis. It should be mentioned that despite variation in particle sizes, all nanoparticles acquire parallel aligned striped inner nanostructure exclusively. The well-distinguishable striped inner structure of poly(TILM-C12I) preferentially grow in the vertical direction (polar axis) of the nanoparticles rather than in the parallel direction when increasing number of bilayers in these nanoparticles. The comparison of particle morphologies reveals that the particle size is therefore simply controlled by the number of bilayers, *i.e.* the size variation in these nanoparticles is caused by different numbers of bilayers packed in individual nanoparticles. The bilayer spacing can be calculated from corresponding images by fast Fourier transform (FFT) and graphical analysis. These two techniques provide the same distance of 3.10 ± 0.5 nm for poly(TILM-C12I). Similar wasp-like vesicles with parallel multilamellar stripes inside are also observed in the cryo-EM images of poly(TILM-C12Br). Negligible difference is found in comparison with **Figure 18A**, except the bilayer spacing slightly increase to

3.20 ± 0.5 nm. Accordingly, variations in the anion of the same type in the PIL nanoparticles seems to have little-to-no effect on their self-assembly behavior.

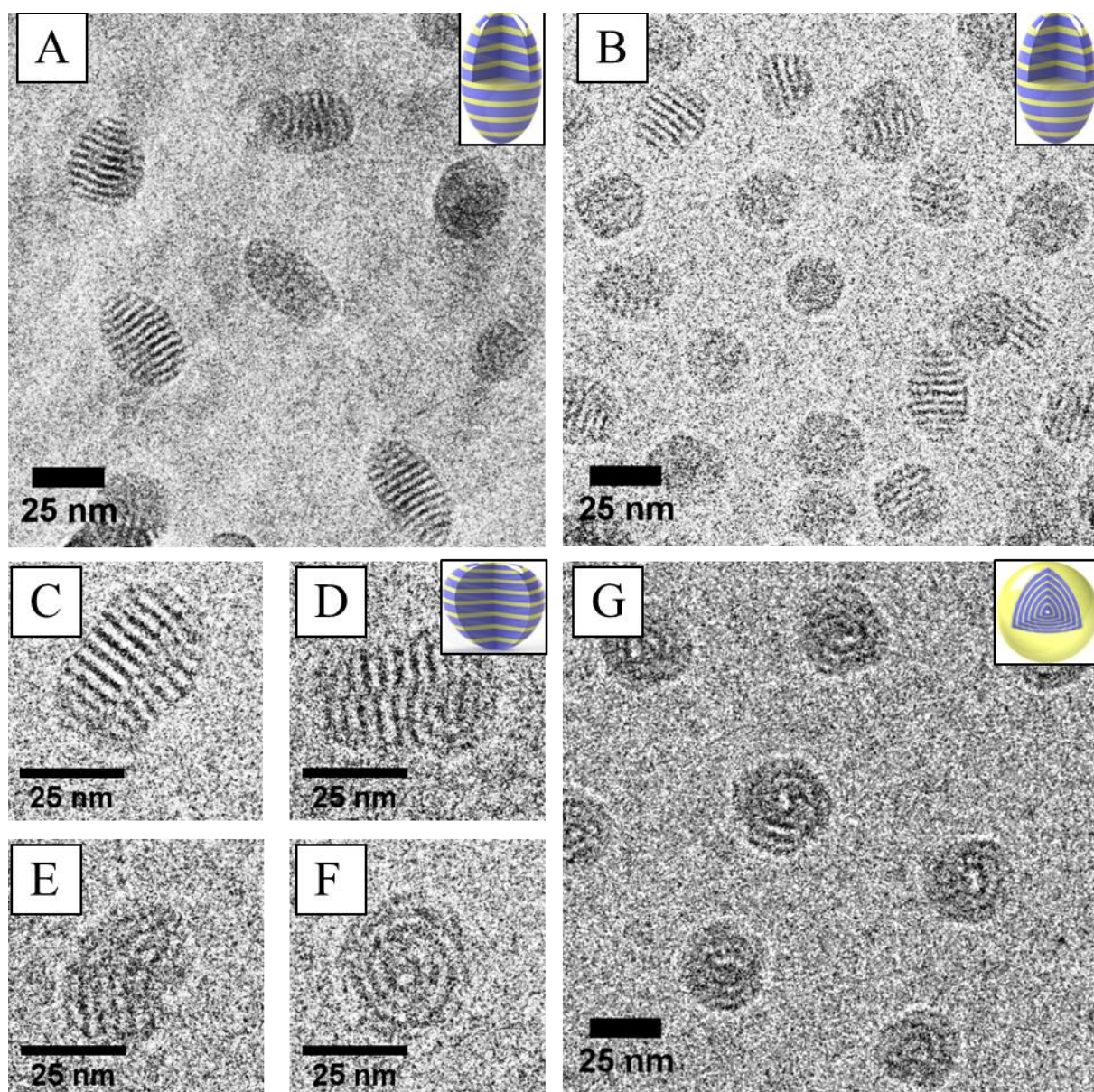


Figure 18. Representative cryo-EM images of PIL nanoparticles in aqueous solution. (A) poly(TILM-C12I); (B) poly(TILM-C12Br); (C-F) poly(TILM-C14Br); (G) poly(TILM-C16Br).

When bromide as anion is kept, by increasing the alkyl chain length to C14 the inner structures of the synthesized nanoparticles change significantly. Multiple hierarchical self-assembled particle shapes are observed. Specifically, in poly(TILM-C14Br) nanoparticles (**Figure 18C—18F**), two phenomena are obvious. On the one hand, ellipsoids with wasp-like parallel aligned multilamellar nanostructure (**Figure 18C**) coexist with onion-like spherically aligned multilamellar (quasi-)spherical nanoparticles (**Figure 18E**). The fraction of the latter

is 40%, slightly bigger than that of ellipsoids (~28%). On the other hand 32% of particles with intermediate shape were found well-distributed throughout the whole sample. In **Figure 18D** and **18F**, two intermediate structures with representative morphology were provided. A “wasp” is under “splitting” process in the former one (**Figure 18D**). All stripes in it were “cut” in the middle and staggered with each other, thus it looks like two “wasps” glue together. The inner stripes of this particle were partially curled and became semi-orbicular. In the latter one (**Figure 18F**), the particle slightly bent over, perpendicularly to its bilayer alignment direction. All the “stripes” inside this particle were found slightly curled toward its bending direction as well, thus it looks more like a distorted “pastry”. Unlike normal wasp-like particles, the bilayers of “pastry” are vertically aligned with its long axis (polar axis) in the ellipsoid. It is concluded from these observations that poly(TILM-C14Br) nanoparticles were in the changing process from ellipsoids with wasp-like morphology to onion-like spheres, or *vice versa*. In the same time, the average bilayer distance measured from FFT is 3.55 ± 0.5 nm, 0.35 nm larger than poly(TILM-C12Br) nanoparticles. Since one $-\text{CH}_2\text{CH}_2-$ unit in a stretched form is 0.22 nm in length and thus a head-to-head non-interdigitated packing will give 0.44 nm, a partial interdigitated chain packing is expected.^[86]

The transformation from ellipsoid to spherical particles is more distinct when further elongating the alkyl substituents. In poly(TILM-C16Br), onion-like circular multilamellar (quasi-)spherical nanoparticles are exclusively obtained (**Figure 18G/19D**). The decreased bilayer number in these nanoparticles expands the bilayer distance to 4.00 ± 0.5 nm (since all these nanoparticles have similar size of 20-30 nm in DLS analysis). As the poly(TILM-C16Br) nanoparticles exhibit uniform onion-like structures, compared with above-mentioned morphology and self-assembly variations, alkyl chain elongation seems to be able to tune the shape and inner nanostructures of 1,2,4-triazolium-based PIL nanoparticles. In other words, shape and morphology of corresponding PIL nanoparticles will be transformed from “wasp”-like inner structure mostly in an elliptical nanoparticle shape to spherically aligned inner “onion”-like structure in a (quasi-)spherical nanoparticles shape when increasing the alkyl chain length from C12 to C16.

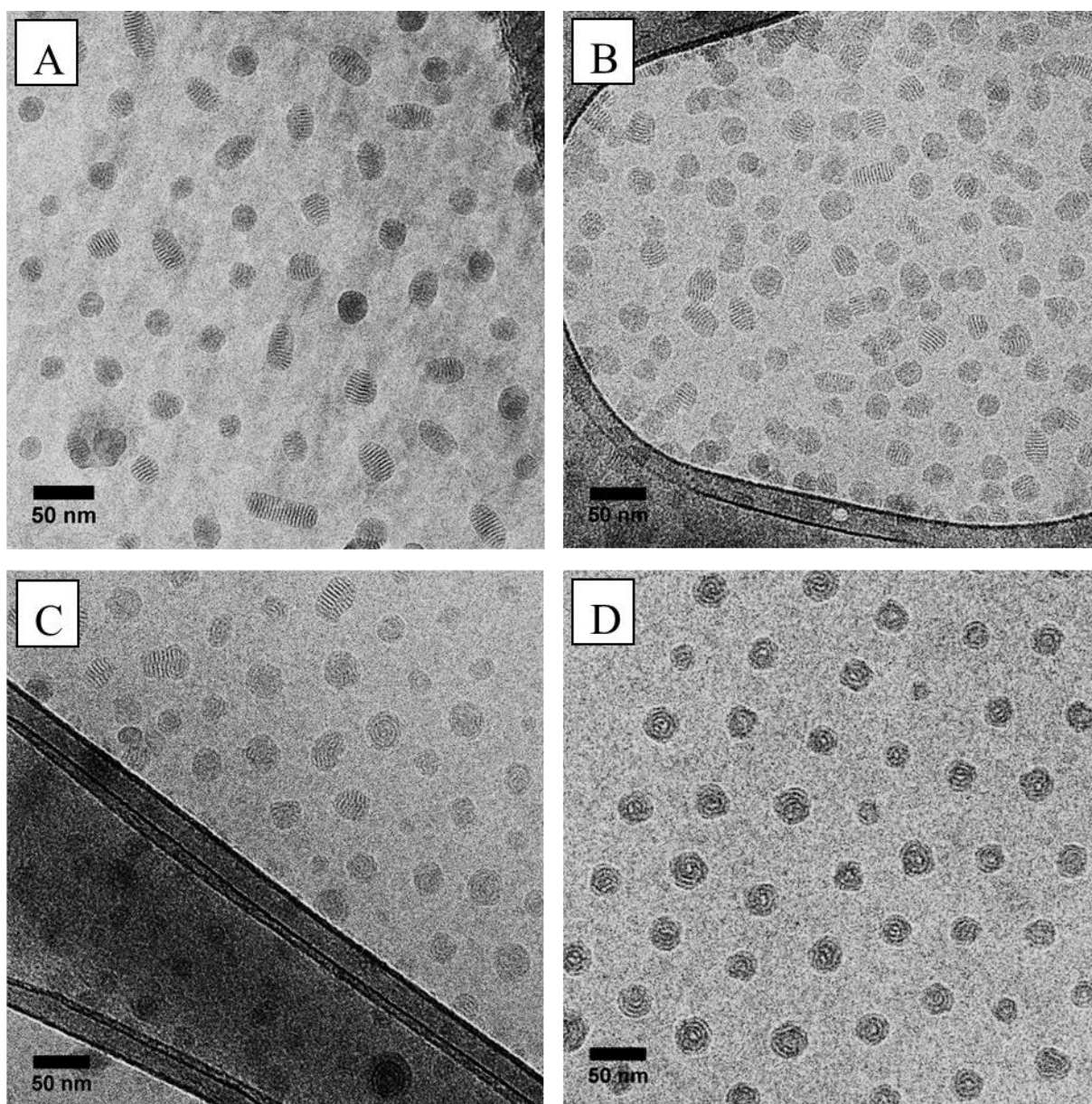


Figure 19. Overview of cryo-EM images of PIL nanoparticles in aqueous solution: (A) poly(TILM-C12I); (B) poly(TILM-C12Br); (C) poly(TILM-C14Br); (D) poly(TILM-C16Br).

In imidazolium-based PIL nanoparticles, liposome-like unilamellar structures—“void”—existed in the long alkyl chain substituted nanoparticles. It is believed that the sample preparation temperature for cryo-EM experiments may induce crystallization that affects the overall shapes. Therefore, DSC measurements (**Figure 20**) of dried PIL samples were conducted. At the sample preparation temperature (here 4 °C), only the alkyl chains in poly(TILM-C16Br) are dominantly in a crystalline state, which is responsible for the edges and facets spotted in poly(TILM-C16Br), as crystallization is one of the driving forces to straighten out curvature.

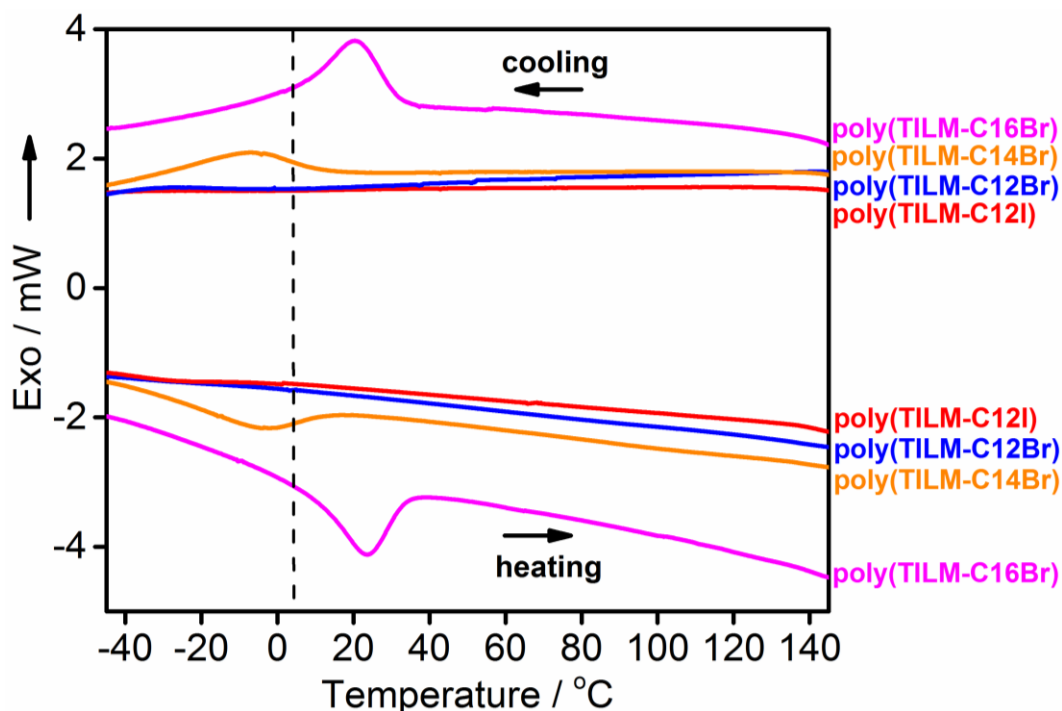


Figure 20. Differential scanning calorimetry curves of the dried solid poly(ionic liquid) polymers. The dashed line indicates the preparation temperature of cryo-EM samples. Thermogravimetric analysis measurements display that all poly(ionic liquid) samples started to decompose at ca. 250 °C under N₂ and left a residue of 1.0 ± 0.5 wt.% at 1000 °C.

To investigate the lamellar packing in PIL nanoparticles in more detail, small-angle X-ray scattering (SAXS) measurements were conducted from aqueous PIL nanoparticle dispersions (concentrated to 50 g/L). As depicted in **Figure 21A**, four primary peaks with different q values for poly(TILM-C12I), poly(TILM-C12Br), poly(TILM-C14Br) and poly(TILM-C16Br) were identified, whose d spacings were calculated to be 2.15±0.5, 2.22±0.5, 2.56±0.5 and 2.99±0.5 nm, respectively. Clearly, d spacings for these four nanoparticle samples increased nearly linearly from C12I/C12Br to C16Br.^[87] However, in comparison with d spacing values received from cryo-EM images (3.10±0.5, 3.20±0.5, 3.55±0.5 and 4.00±0.5 nm), the ones determined from SAXS patterns are ~1.00 nm smaller in all cases (**Table 5**). The difference between the results of the two methods can be ascribed to two different structures measured in these two methods. In **Figure 21B**, distances calculated from cryo-EM images with FFT method were actually the entire length of the bilayers (d_1), *i.e.* backbone-backbone distances; while distances from SAXS patterns presumably refer to the interdigitated alkyl chain domains (d_2). Consequently, the 1 nm difference can be assigned to the thickness of the backbone domains in the bilayers.^[88]

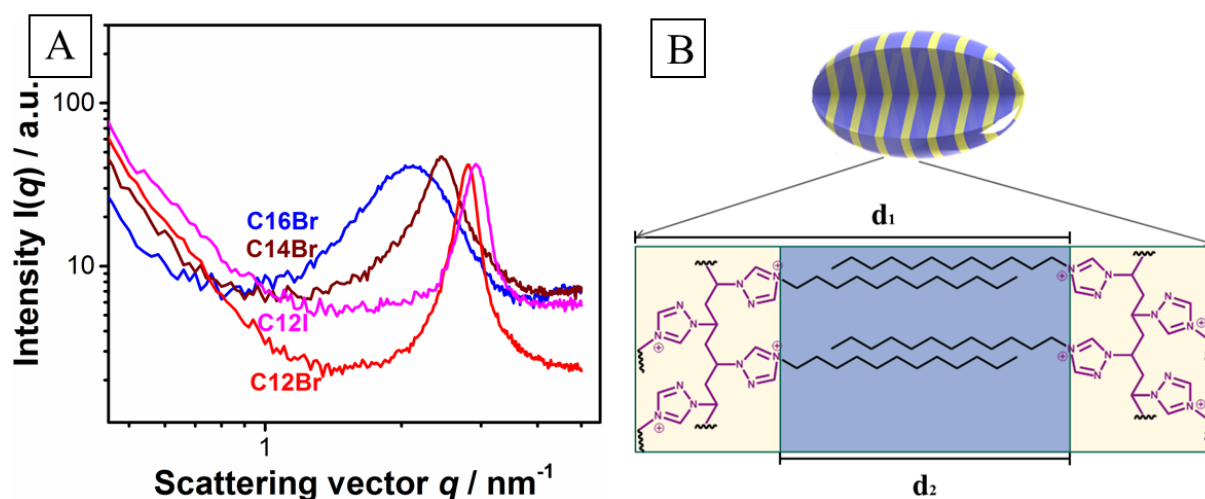


Figure 21. (A) Small-angle X-ray scattering patterns of aqueous dispersions of PIL nanoparticles (50 g/L); (B) Schematic representation of interdigitated packing of alkyl chains in PIL nanoparticles.

As discussed above, one trend for the self-assembly behavior of TPIL nanoparticles can be observed distinctly (**Figure 15**). When using differently alkylated 1,2,4-triazolium monomers for polymerization, namely from poly(TILM-C12I) to poly(TILM-C16Br), the shape of nanoparticles will vary from ellipsoids to (quasi-)spherical particles. Simulations based on amphiphilic diblock copolymers have shown similar hierarchical self-assembly transformations.^[89] Briefly, when polymer nanoparticles are formed in the same size confinement, their inner structures will be determined by their surface preferences—hydrophilicities in aqueous solutions. With decreasing hydrophilicity, the inner particle morphologies will transform from wasp-like to onion-like to reduce unfavorable contact between the hydrophobic domains with water. Since 1,2,4-triazolium-type PIL nanoparticles are more hydrophilic than previously described imidazolium-type PIL nanoparticles^[28] that form exclusively spherical particles with onion-like inner morphology, 1,2,4-triazolium-type PIL nanoparticles tend to form wasp-like ones. Following the predictions, TPIL nanoparticles showed similar “wasps” to “onions” variation, which were in good agreement with simulations for amphiphilic copolymers. The change in inner morphology is accompanied by a change in the overall particle shape as well. Wasp-like inner morphologies lead to ellipsoid particles, while onion-like inner morphologies produce spherical particles to minimize the interface between the hydrophobic alkyl chains and water. The shape differences affect the stability of TPIL nanoparticles in aqueous solutions as well, depicted by *Zeta-potential* measurements of corresponding polymer dispersions (**Table 6**). The stability of particles in

aqueous solutions increased gradually from poly(TILM-C12I) to poly(TILM-C16Br) with the decreasing exposure of their hydrophobic alkyl moieties on outer surface.

Table 5. The d spacing values of poly(TILM-C12I), poly(TILM-C12Br), poly(TILM-C14Br) and poly(TILM-C16Br) nanoparticles received from SAXS measurements and cryo-EM images .

<i>Compound</i>	<i>d spacings (d₂) from SAXS measurements/ nm</i>	<i>d spacings (d₁) from cryo-EM images / nm</i>
poly(TILM-C12I)	2.15±0.4	3.10±0.5
poly(TILM-C12Br)	2.22±0.7	3.20±0.5
poly(TILM-C14Br)	2.56±1.1	3.55±0.5
poly(TILM-C16Br)	2.99±1.9	4.00±0.5

Table 6. Zeta-potential values of poly(TILM-C12I), poly(TILM-C12Br), poly(TILM-C14Br) and poly(TILM-C16Br) nanoparticles in aqueous dispersions.

<i>Compound</i>	<i>Surface Z-potential / mV</i>
poly(TILM-C12I)	29.5±0.1
poly(TILM-C12Br)	36.0±0.8
poly(TILM-C14Br)	42.0±0.2
poly(TILM-C16Br)	52.5±1.2

As studied in our previous work, confined hierarchically self-assembled nanostructures of PIL nanoparticles can be formed in one-step polymerization. For 1,2,4-triazolium-type PIL nanoparticles, the same formation mechanism was expected. The cryo-EM images of TILM-C14Br monomer solution (**Figure 22**) and corresponding DLS measurements show only micelles with a diameter of ~5 nm. In analogy to micro-emulsion polymerization, the formed

polymers are presumably first generated from the pre-assembled TILM micelles. Subsequently they serve as nucleation center for nanoparticle formation. During that process, residue monomers in solution can act as surfactants in the reaction for the stabilization of PIL nanoparticles. To confirm this mechanism, a control experiment was conducted. First, solid powders of poly(TILM-C12Br) sample were obtained from its original aqueous dispersion by freeze-drying. After re-dissolving into DMF and dialysis against deionized water, polymer micelles of ~8 nm in diameter can be observed in TEM images as well as DLS analysis (**Figure 23**). Compared with the original nanoparticle dispersions, re-dispersed polymer micelles were smaller in size in water and no ordered inner structure was identified. The stepwise one-pot self-assembly / polymerization of TILMs fits well into the frequently utilized concept of polymerization induced self-assembly (PISA).^[90] PISA is a unique mechanism and responsible for the structural complex and high ordering observed here in the poly(TILM) nanoparticles.

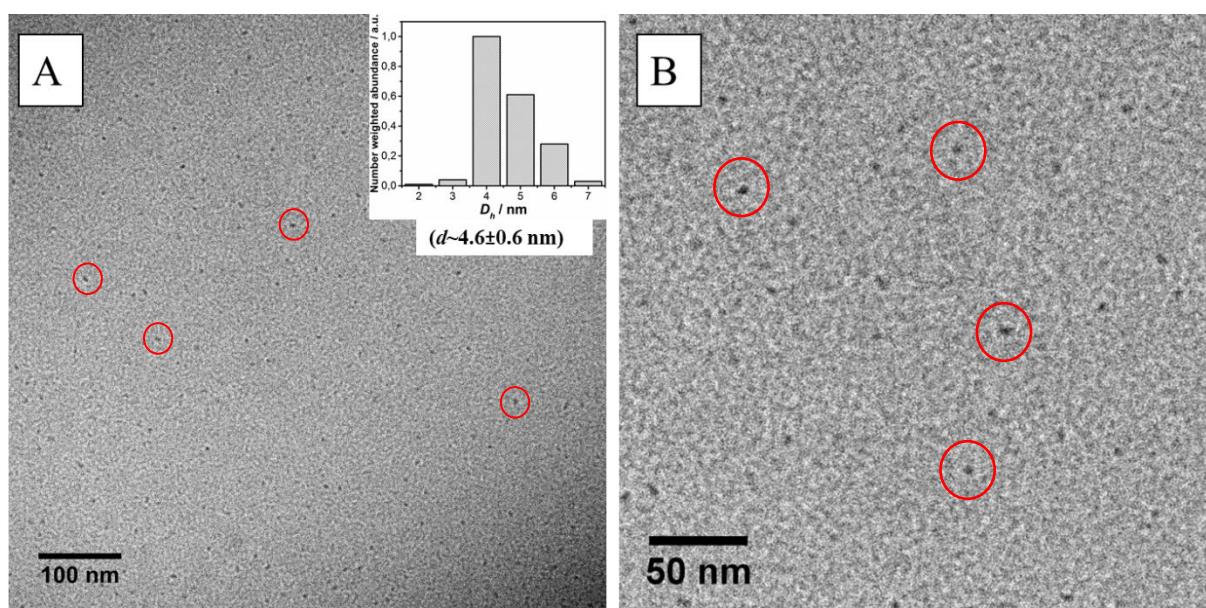


Figure 22. Cryo-EM image of aqueous solution of TILM-C14Br at $c=30$ g/L. (A) Overview. The inset is a size distribution curve derived from DLS measurement of the same sample. (B) Close view of the cryo-EM image, only micelles (dark dots) can be found overall in the suspension. No multilamellar or unilamellar vesicles were identified.

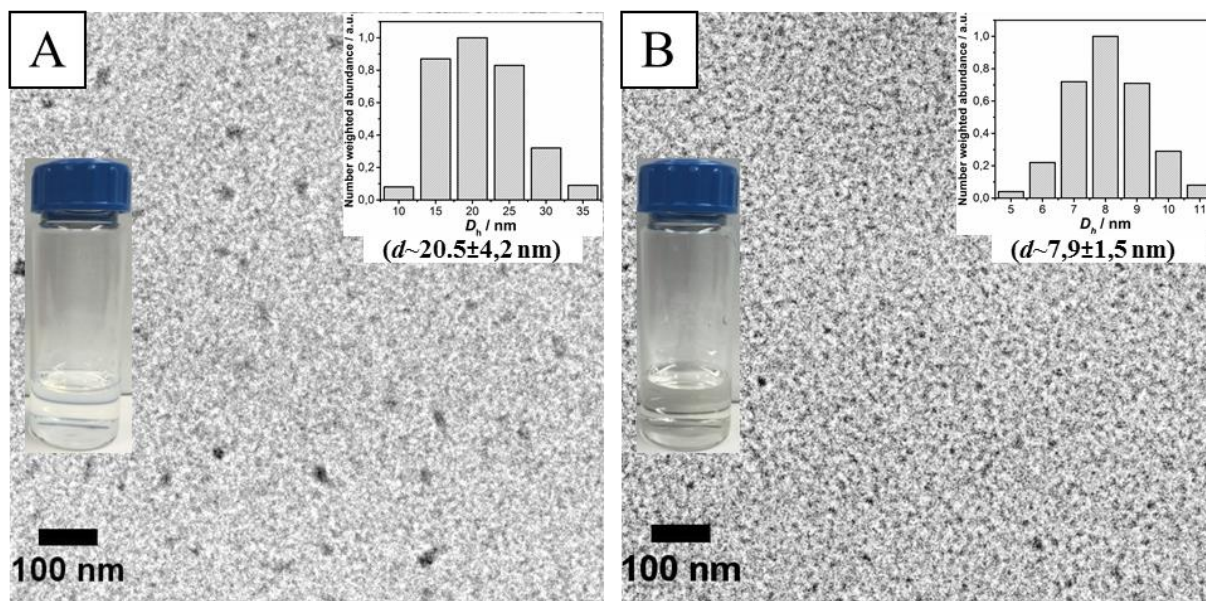


Figure 23. A) a TEM image of the poly(TILM-C12Br) (5 g/L) dispersion when produced *via* dispersion polymerization in water. B) a TEM image of a re-dispersed sample. To prepare this sample, the original PIL nanoparticle dispersion was freeze-dried to produce a white powder. This powder was dissolved in DMF and was then dialyzed in water to produce an aqueous dispersion of 5 g/L.

To obtain further insight in their 3D structures, ellipsoid particles with wasp-like inner morphology poly(TILM-C12Br) and spherical particles with onion-like inner morphology poly(TILM-C16Br) were visualized *via* cryo-ET technique (**Figure 24**). **Figure 24A** and **24D** are central slices from tomographic imaging of poly(TILM-C12Br) and poly(TILM-C16Br). Based on tomography reconstruction, 3D models of “wasp” and “onion” particles were obtained (**Figure 24B, 24E**). The inner structure of the wasp-like particle revealed parallel aligned “plates” along the Z axis of the volume (**Figure 24B; Figure 24C; Figure 25A**), a configuration consistent with the one suggested by the 2D cryo-EM images (**Figure 18B/19B**). Interestingly, surface defects, and also innerstructure optimizations make the single layers connected at a few sites, contributing to the complexity of the structure. It must be underlined that all the beautiful structural details remain of course unseen in an averaging scattering experiment.

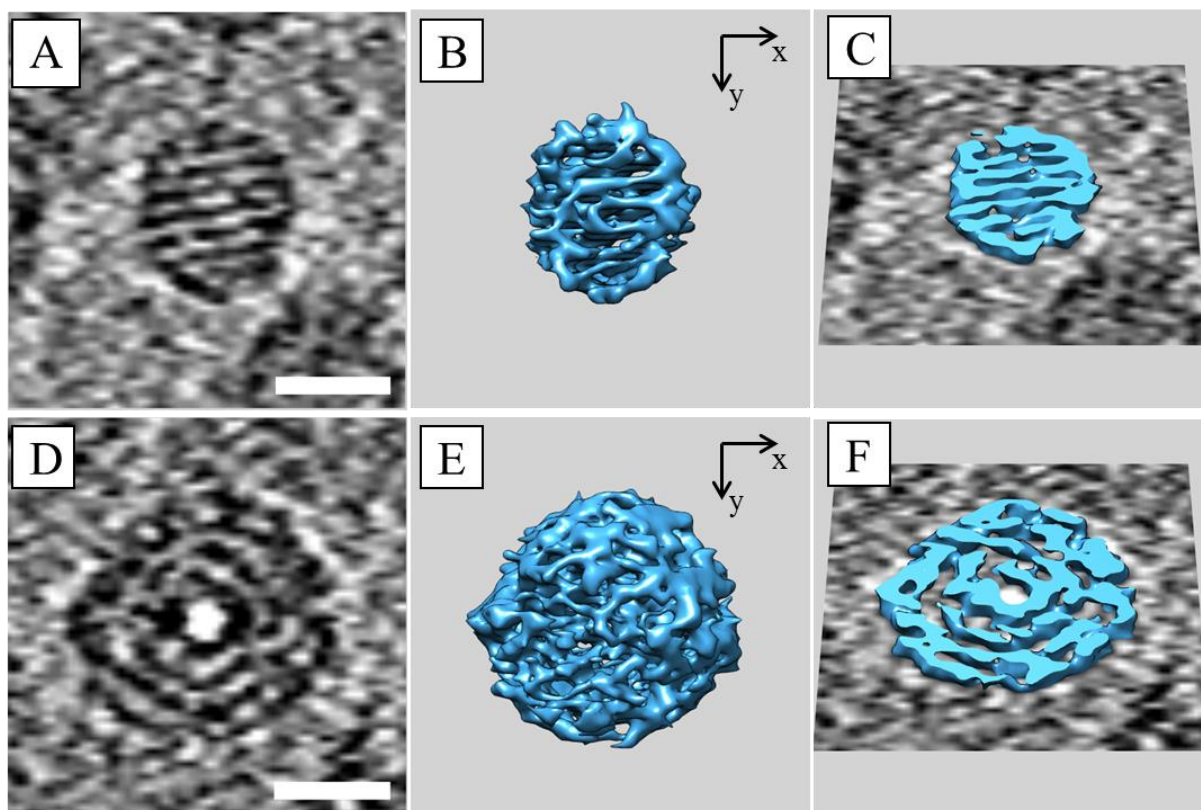


Figure 24. Representative cryo-ET of TPIL nanoparticles. (A, D) Central tomographic slices along the Z axis (normal to the paper surface) of the tomographic volumes of individual poly(TILM-C12Br) and poly(TILM-C16Br) particles, respectively (scale bar: 25 nm). (B, E) 3D volume renderings of the particles in (A) and (D), respectively. (C, F) Same 3D volume renderings as in (B) and (E) but digitally clipped along the Z axis around their central regions and shown together with the tomographic slices from (A) and (D). The 3D images in (C) and (F) have been slightly tilted around the X axis in order to get a better representation of the internal features of the structures.

In comparison with its C12 analogue, the inner structure of the onion-like particle shown in **Figure 24E** revealed a 3D arrangement unexpectedly different from its 2D cryo-EM images (**Figure 18G/19D**). Here a “spaghetti ball” configuration, *i.e.* the individual onion layers of the charged backbones break-up into partly branched cylinders, was observed as a unique onion-like model. In other words: the spherical plain formed by backbone layers are not closed, most presumably due to perforation in the charged backbone lamellae by large-sized alkyl chains.^[91] The cryo-ET derived inner particle morphology nicely shows the family relation to the classical “onion” structure, which in fact is a product of an averaging projection operation of the electron beams. Cryo-EM in the non-tomographic mode simply shows the sum of the electron density through the particle then appearing as an “onion” morphology,

while tomographic TEM elaborates the real inner structure in **Figure 24D**. The appearance of the inner “spaghetti ball” as perforated onion-like structure can be nicely illustrated by central slices (**Figure 24F**, **Figure 25B**). As the sample is side chain-crystalline in the solid state as well as at lower temperatures, we assume that this spaghetti-ball-to-onion-like-sphere transition is fully reversible and contributed to the inner order, but also to a potential functionality of such particles.

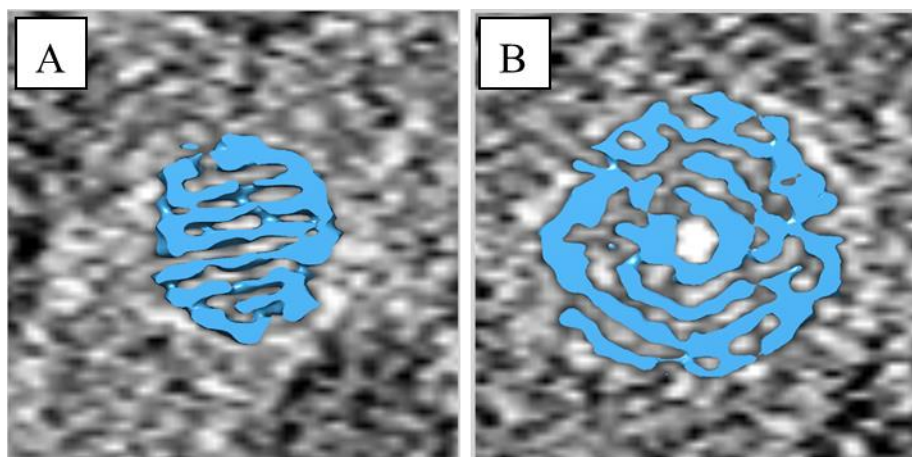


Figure 25. 3D renderings (before tilting) of (A) poly(TILM-C12Br) and (B) poly(TILM-C16Br) PIL nanoparticles that have been clipped along the Z axis at their central regions. Tomographic slices along the Z axis of the tomographic volume at a slight offset with respect to the clipping planes are also shown.

It is worth mentioning that sizes of these PIL nanoparticles are independent of the polymerization temperature or the post-synthesis annealing temperature but increase correlatively at higher monomer concentrations in polymerization due to the formation of anisotropic one-dimensional superstructures. **Table 7** summarized the sizes of poly(TILM-C12Br) nanoparticles prepared at different polymerization temperature and monomer concentrations from 20 g/L (25.5 mM) to 160 g/L (408 mM), as determined by DLS measurements and TEM characterization. For example, when the polymers are synthesized above a critical monomer concentration, *e.g.* 80 g/L (204 mM), poly(TILM-C12Br) increases its size to 75 nm and “nanoworms” as elongated superstructures appear (**Figure 26**). Different from the imidazolium derived particles that can build up nanoworms of several micron long,^[28] the 1,2,4-triazolium-based PIL nanoworms are generally shorter than 300 nm.

Table 7. Nanoparticle sizes obtained from different monomer concentrations in the dispersion polymerization of TILM-C12Br. The initiator concentration (6.50 mM) was kept constant during polymerization in water.

<i>Entry</i>	<i>Monomer [mM]</i>	<i>Temperature [°C]</i>	<i>D_h[nm]^{a)}</i>
1	25.5	70	22
2	51.1	70	21
3	102	70	28
4	204	70	75
5	408	70	120
6	51.1	60	23
7	51.1	80	24
8	51.1	90	26

a) The hydrodynamic diameter D_h was determined from DLS measurement.

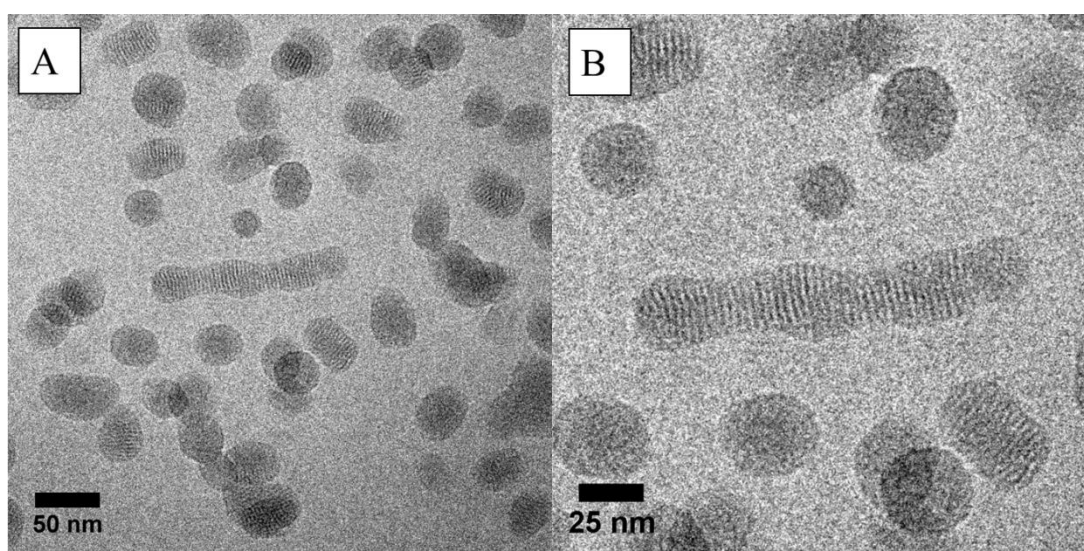


Figure 26. Cryo-EM images of elongated nanoworm superstructures of poly(TILM-C12Br) prepared with monomer concentration at 100 g/L. (A) overview and (B) close view of the nanoworm.

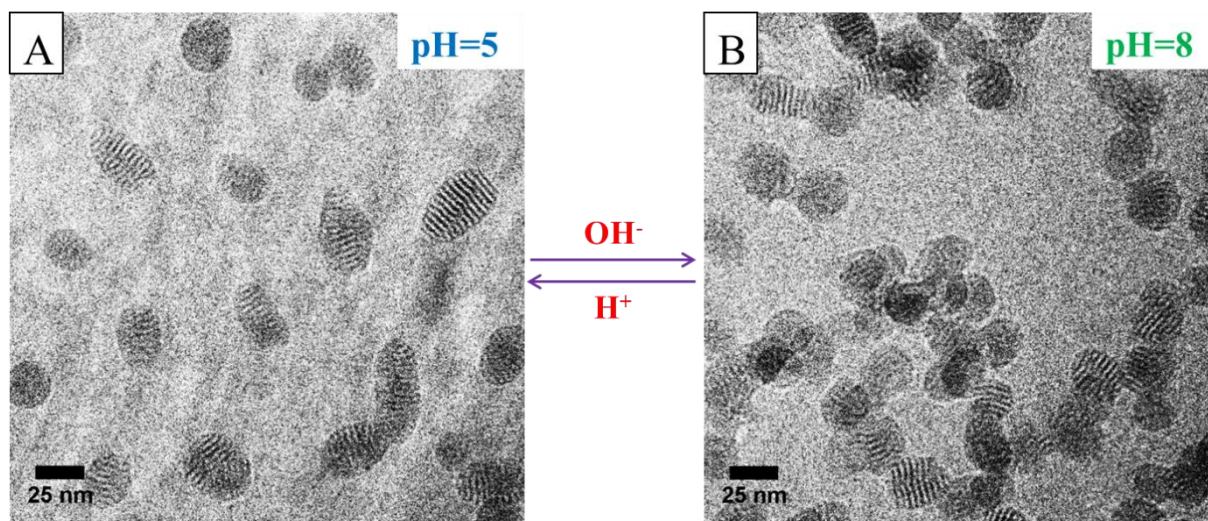


Figure 27. Cryo-EM images of pH responsive TPIL nanoparticles in aqueous dispersion: (A) poly(TILM-C12Br) before adding ammonium hydroxide (pH=5); (B) poly(TILM-C12Br) after adding ammonium hydroxide (pH=8).

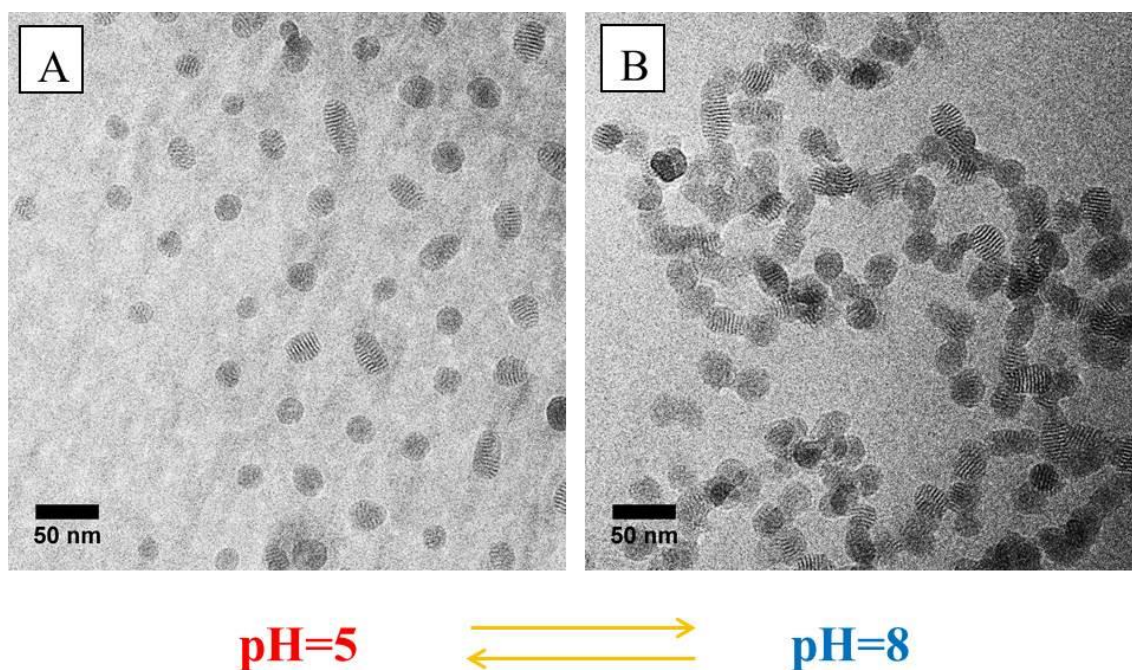


Figure 28. Overview of Cryo-EM images of pH responsive TPIL nanoparticles in aqueous solution: (A) poly(TILM-C12Br) before adding ammonium hydroxide (pH=5); (B) poly(TILM-C12Br) after adding ammonium hydroxide (pH=8).

More interestingly, these PIL nanoparticles are pH responsive. When ammonium hydroxide was added into poly(TILM-C12Br) to reach a final pH of 8, nanoparticles started to aggregate

with each other (**Figure 27** and **Figure 28**) due to lowered *Zeta-potential* and thus colloidal instability. In contrast, addition of hydrochloric acid to bring the pH back to 5 leads to evenly re-dispersed nanoparticles. Therefore the colloidal behavior of these PIL nanoparticles can be adjusted *via* pH, a convenient parameter to control. This effect might be related to the 2 active protons in the 1,2,4-triazolium ring, which are more acid than that in imidazolium ring and are thus pH-responsive.

3.5 Conclusions

In summary, a series of 1,2,4-triazolium-type PIL nanoparticles of well-defined shape with ordered, complex inner nanostructures have been revealed by cryo-EM and cryo-ET. Upon simply altering length of alkyl substitutions, corresponding nanoparticles can adopt either elliptical particle shapes with “wasp”-like inner structure or spherical particles with inner “onion”-like structure, which, to the best of our knowledge, is the first example of shape-tuning nanoparticles for homopolymers below the 50 nm scale with sub 5 nm domain spacings. It is a unique example of shape-changing nanoparticles, which can be formed in a one pot approach and is a good model for further study of tunable hierarchical self-assembly nanomaterials.

4. Crosslinked 1,2,4-triazolium-type poly(ionic liquid) nanoparticles

4.1 Introduction

In previous chapter, a facile synthetic route towards 1,2,4-triazolium-type PIL nanoparticles with an average size of 20~30 nm have been produced by dispersion polymerization of vinyl-1,2,4-triazolium ILMs with long alkyl chains (C12~C16). Cryo-EM revealed that these PIL nanoparticles developed distinctive inner structures. Although these nanoparticles are unusually simple and scalable to access, in organic solvents, such as DMF and methanol, they will dissolve molecularly thus forfeiting their distinctive inner patterns.^[92] It is our interest thus to further extend such a nanoparticle system to crosslinked species,^[93] which are expected to possess improved structural stability in organic media. Additionally, the effect of crosslinking on the self-assembled nanoparticle interior is also to be understood.^[94] In this context, covalently crosslinked PIL nanoparticles were synthesized in this chapter from 1,2,4-triazolium-type ILMs carrying different long-chain alkyls in the presence of a dication crosslinker.^[95] Their self-assembly profile, morphological variations and colloidal behavior in organic solvents were investigated. We further demonstrate their functionality and usefulness as Pickering stabilizers for dispersing carbon nanotubes in both aqueous and organic solvents.

4.2 Experimental Section

Materials, preparation techniques and characterization methods are provided in Appendix.

4.3 Nanoparticle preparation

The synthetic technique of three monomers (**TILM-CnBr**, n=12, 14, or 16) followed the same procedures described in chapter 3. The chemical structures and synthetic routes are illustrated in **Figure 29**. A dication crosslinker, 1,4-butanediyl-4,4'-bis(1-vinyl-1,2,4-triazolium) dibromide (**BVTD**) was prepared *via* quaternization of 1-vinyl-1,2,4-triazole with alkyl bromide in a 2:1 molar ratio relationship. The chemical structure of BVTD is confirmed by ¹H NMR spectrum in **Figure 31**. The vinylic protons *c*, *d*, and *e* can be assigned to peaks at 7.48, 6.01 and 5.53 ppm, respectively, while *a* and *b* protons on the 1,2,4-triazolium ring appear at 10.66 and 9.48 ppm, respectively, as they feature lower electron density due to the delocalization of 1,2,4-triazolium ring. The methylene protons *f* and *g* are observed at 4.38 and 1.96 ppm, respectively. To avoid anion effect to the self-assembly process, the same ion pair was used in the monomers and crosslinker.

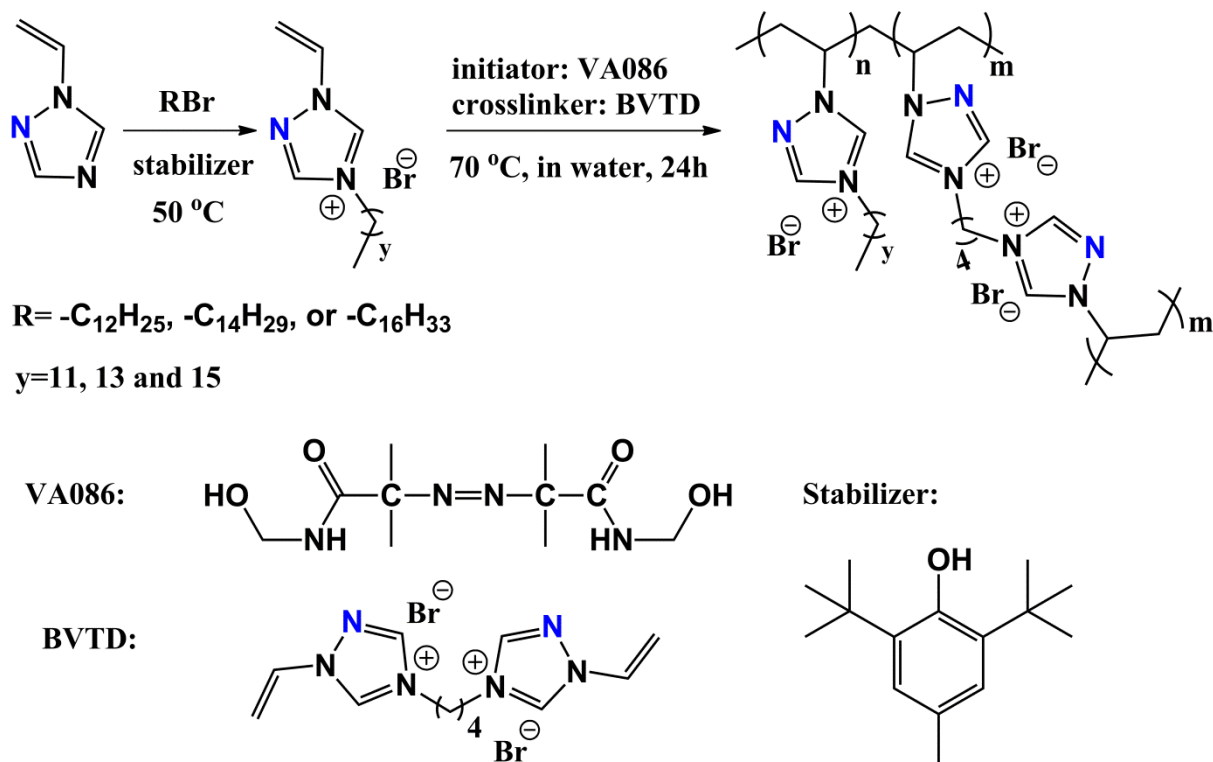


Figure 29. Chemical structures and synthetic route towards covalently crosslinked 1,2,4-triazolium-type poly(ionic liquid) nanoparticles.

To analyze the thermal behavior of the monomer and crosslinker, DSC measurements were conducted. TILM-C12Br, TILM-C14Br, and TILM-C16Br were found to melt at 78, 82 and 86 °C, respectively, indicating the increase in the melting points stepwise upon alkyl chain length extension. These monomers can be strictly referred to as ILs, because they reach a molten state below 100 °C. The crosslinker BVTD did not show obvious liquid state below 150 °C, above which polymerization sets in. In the thermogravimetric analysis measurements (**Figure 30**), TILM-C_nBr monomers start to decompose around 170 °C and the crosslinker BVTD at ca. 200 °C under N₂ flow. At 1000 °C, a residue of 1.0 ± 0.5 wt.% was left for both monomers and BVTD.

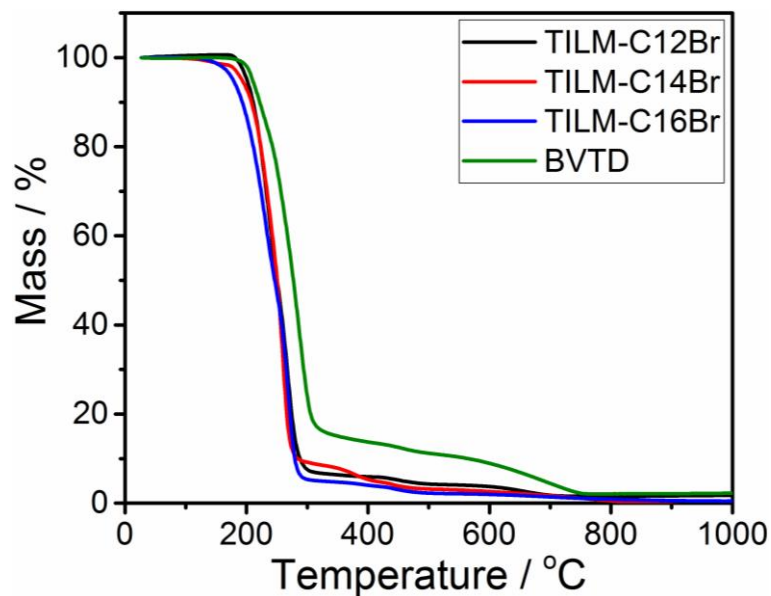


Figure 30. Thermogravimetric analysis curves of **TILM-C12Br**, **TILM-C14Br**, **TILM-C16Br** and **BVTD**.

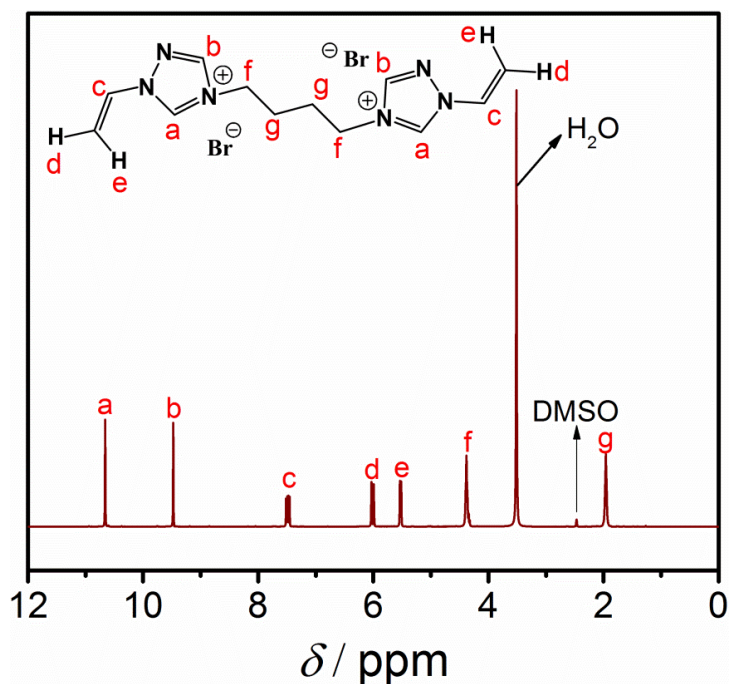


Figure 31. $^1\text{H-NMR}$ spectrum of the 1,2,4-triazolium crosslinker in $\text{DMSO-}d_6$.

Crosslinked PIL nanoparticles were produced by dispersion polymerization in the presence of BVTD. As depicted in **Figure 29**, TILM-C12Br, TILM-C14Br and TILM-C16Br were polymerized at a monomer concentration of 20 g/L (112 mM) and a 10 mol% crosslinker BVTD (with regard to monomer). The initiator concentration is fixed at 3.5 mM. These

polymers are denoted as **poly(TILM-CnBr/BVTD)**, $n=12, 14$ and 16 , respectively. All the polymerization reactions ended up with stable translucent dispersions. It should be mentioned here that the short chain (C2~C4) PILs are fully hydrophilic and molecularly soluble in water, while PIL bearing intermediate alkyl chain length (C6~ C10) precipitated partially and left behind a turbid dispersion. Only in the case of monomers bearing sufficiently long alkyl chains (C12~C16), stable PIL nanoparticle dispersions formed.^[61] Similar to chapter 3, no surfactants were used for the polymerization, as the monomers served as surfactants.

4.4 Characterization and discussion

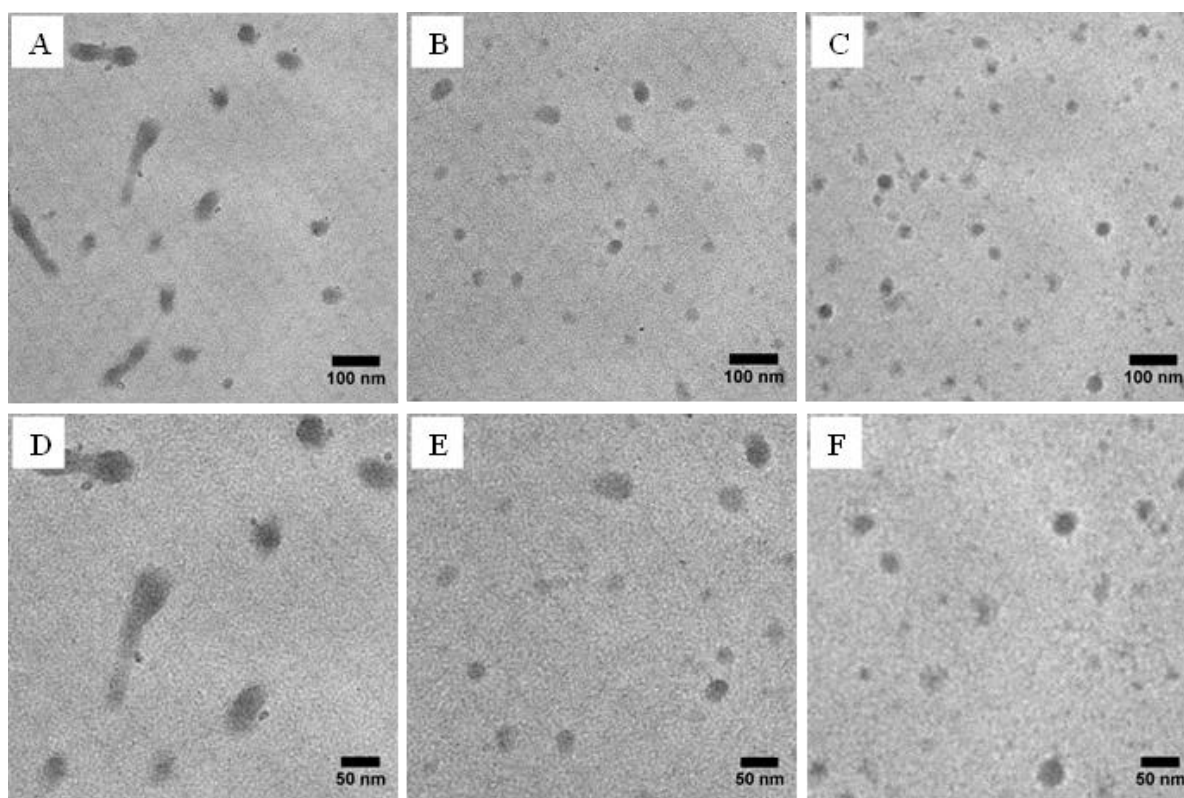


Figure 32. TEM images of crosslinked 1,2,4-triazolium poly(ionic liquid) nanoparticles poly(TILM-C12Br/BVTD) (A&D), poly(TILM-C14Br/BVTD) (B&E) and poly(TILM-C16Br/BVTD) (C&F).

Via DLS, the sizes of crosslinked poly(TILM-CnBr/BVTD) ($n=12, 14$ and 16) nanoparticles were determined to be $42, 29$ and 33 nm, respectively (**Table 9**, Entries 1-3) with a normalized standard size deviation ranging from 0.2 to 0.3 . TEM measurements of these crosslinked PIL nanoparticles were conducted to access their morphology, which were displayed in **Figure 32A—C**. For comparison, the non-crosslinked samples are shown in **Figure 16** in chapter 3. In poly(TILM-C12Br/BVTD) (**Figure 32A&D**), both (quasi-)spherical dark dots and worm-like objects in a short one-dimensional form were found in

abundance of 80% and 20%, respectively. This observation is very much different from its non-crosslinked poly(TILM-C12Br) that did not show any nanoworm. In poly(TILM-C14Br/BVTD) (**Figure 32B&E**) (quasi-)spherical nanoparticles close to its non-crosslinked poly(TILM-C14Br) were the only product. Poly(TILM-C16Br/BVTD) only showed spherical nanoparticles, which are identical to poly(TILM-C16Br). It seems that at an identical crosslinker concentration, the C12 polymer nanoparticles are more prone to changes of their morphology than the C14 and C16 ones. Additionally, it can be explained why the hydrodynamic diameter of poly(TILM-C12Br/BVTD) is much larger than poly(TILM-C14Br/BVTD) and poly(TILM-C16Br/BVTD), as the appearance of the anisotropic elongated nanoworms expands the hydrodynamic size effectively.

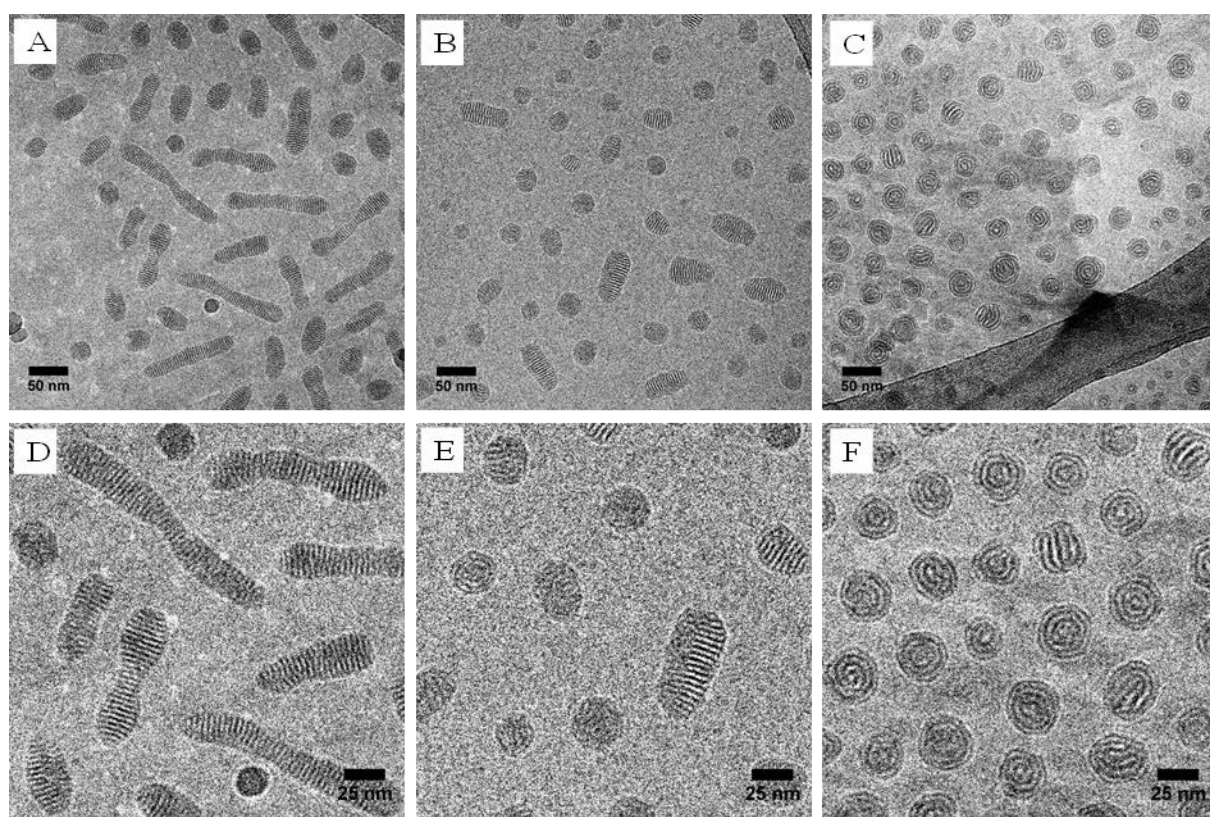


Figure 33. Representative cryo-EM images of crosslinked TPIL nanoparticles in aqueous solution. (A&D) poly(TILM-C12Br/BVTD); (B&E) poly(TILM-C14Br/BVTD); and (C&F) poly(TILM-C16Br/BVTD).

The cryo-EM images in **Figure 33** visualize PIL nanoparticles in aqueous dispersion. For the non-crosslinked TPIL nanoparticles, their cryo-EM analysis was conducted in chapter 3, in which poly(TILM-C12Br) contained striped wasp-like ellipsoids, poly(TILM-C16Br) onion-like nanoparticles and poly(TILM-C14Br) a mixture of both. Poly(TILM-C12Br/BVTD) nanoparticles (**Figure 33A**) consisted of a mixture of ellipsoidal nanoparticles and

nanoworms of irregular length, in good agreement with the TEM observation in **Figure 32A**. The ellipsoidal nanoparticles in **Figure 33D** are in fact wasp-like striped nanoparticles of diameter from 25-40 nm and length from 50-70 nm, similar to that of non-crosslinked ones in chapter 3. The diameter of the nanoworms and the individual wasp-like striped ellipsoids is identical, but the length of nanoworms ranges from 120 nm to 400 nm (**Figure 33A&33D/Figure 34**). Since the shape and contour of individual “compartments” in the nanoworms are similar to an ellipsoid, it is assumed that nanoworms are a linear connection of the ellipsoids along their long axis. The diameter of nanoworms is therefore identical to that of the ellipsoids and their length is controlled by the number of ellipsoids connected in the linear assembly. Theoretically two regular structures can form by connection of individual ellipsoids, either linearly through their long axis (thus a nanoworm) or through the short axis (thus a nanoplate). The reason for the exclusive linear connection of ellipsoids observed here remains unclear and will be a future topic.

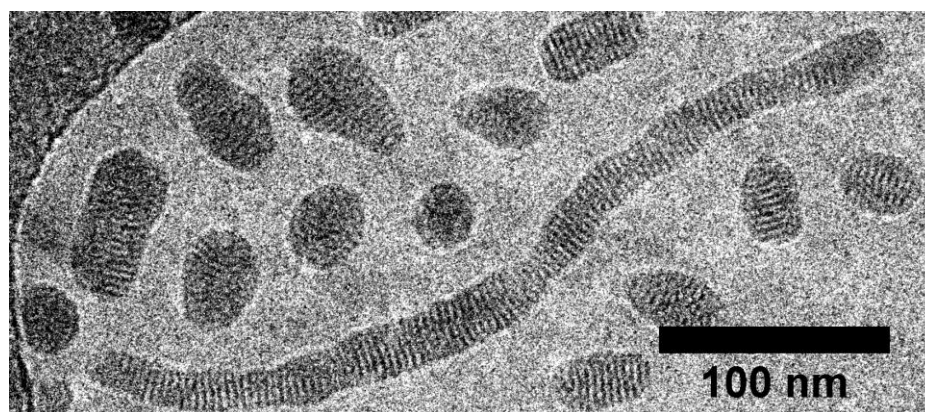


Figure 34. Cryo-EM image of the long (ca. 400 nm) crosslinked **poly(TILM-C12Br/BVTD)** nanoparticle in aqueous solution.

The **poly(TILM-C14Br/BVTD)** (**Figure 33B&33E**) sample consists of both spherical nanoparticles of onion-type, striped ellipsoids with wasp-type and short nanoworms formed from two joint nanoparticles. Hence **poly(TILM-C14Br/BVTD)** is very possibly a transition intermediate from “wasp-like” to “onion-like” in an abundance of 8% and 72%, respectively. The short nanoworms account for the rest 20%. By contrast, the **poly(TILM-C16Br/BVTD)** (**Figure 33C&33F**) nanoparticles with spherical outer shapes are the only product. In these spherical nanoparticles, “onion-type” is dominant (89%) along with a minor part of “wasp-like” ones, which were absent in the non-crosslinked **poly(TILM-C16Br)** sample.

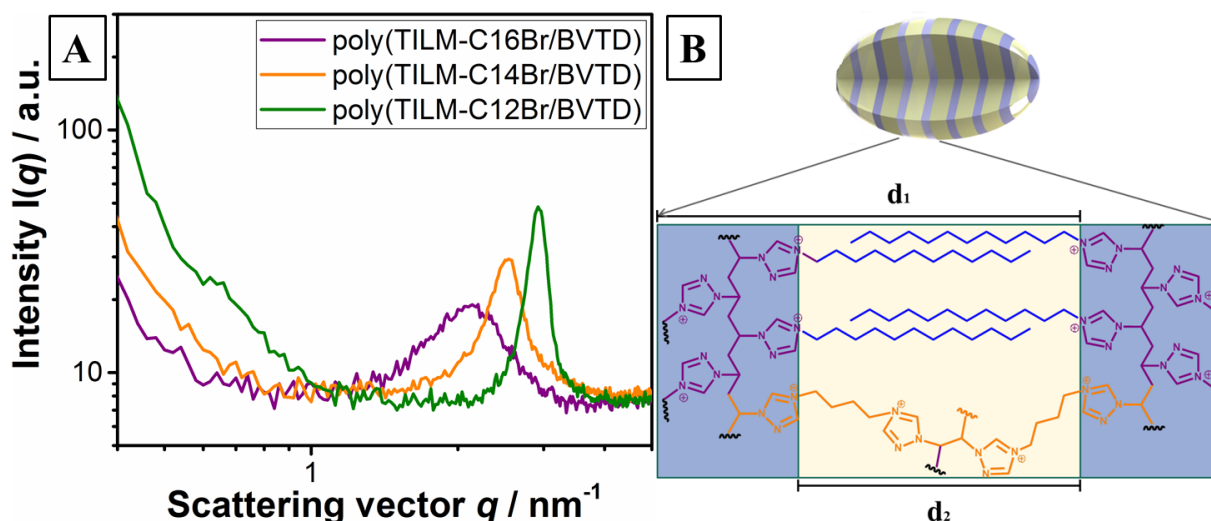


Figure 35. (A) Small-angle X-ray scattering patterns of aqueous dispersions of crosslinked TPIL nanoparticles at 20 g/L. Poly(TILM-C12Br/BVTD) in olive, poly(TILM-C14Br/BVTD) in orange, and poly(TILM-C16Br/BVTD) in purple; (B) Schematic representation of interdigitated packing of alkyl chains in TPIL nanoparticles.

The morphological transition from parallel stripes to concentric lamellae has been discussed in chapter 3. It is related to the energy balance of interface energy between the hydrophobic alkyl chains and the hydrophilic charged backbones as well as the surface energy of the particle. Following the FFT operation of the corresponding cryo-EM images, the average bilayer spacings of poly(TILM-C n Br/BVTD) ($n=12, 14$ and 16) are determined to be 3.20, 3.50 and 4.00 nm, respectively (**Table 8**), which follows the increasing alkyl chain length in polymer nanoparticles.^[87] In the SAXS measurements in **Figure 35A**, the scattering curves of poly(TILM-C n Br/BVTD) ($n=12, 14$ and 16) displayed well-recognized primary peaks, corresponding to spacing of 2.15, 2.49 and 2.97 nm, respectively (**Table 8**). These values are generally 1 nm smaller than the spacings received from the FFT operation. As discussed previously, the spacing obtained from the FFT pattern is assigned to the bilayer distance, *i.e.* the charged backbone region together with the alkyl chain region, while the spacing obtained from the SAXS measurements describes only the thickness of the alkyl chain layer (**Figure 35B**).^[88]

Similar to the non-crosslinked PIL nanoparticles, upon alkyl chain extension in monomers and in the presence of crosslinker, the nanoparticle internal nanopatterns follow a structural transition from parallel stripes to concentric multilamellae. Nevertheless, the outer shapes of crosslinked TPIL nanoparticles can significantly differ from the non-crosslinked ones, for example in poly(TILM-C12Br/BVTD). Furthermore spherical “wasp-like” nanoparticles have

been first found in the crosslinked systems. In previous chapter, it is mentioned that the nanoparticle formation follows a polymerization-induced self-assembly mechanism. The crosslinking in PIL nanoparticles is expected to limit or even lock the mobility of polymer chains. The formation of well-organized inner structure pattern is thus a supportive proof of the PISA mechanism, because these fine patterns can only form during the polymerization when the chains are still mobile before they are crosslinked in the final stage. That is, the self-assembly and polymerization occur side by side in the chain growth process. As expected, crosslinking also enhances stability of the overall nanoparticle shape in organic solvents, such as DMF, that can fully dissolve the non-crosslinked nanoparticles.

Table 8. The d spacing values of poly(TILM-C12Br/BVTD), poly(TILM-C14Br/BVTD) and poly(TILM-C16Br/BVTD) nanoparticles received from SAXS measurements and cryo-EM images.

<i>Compound</i>	<i>d spacings (d₂) from SAXS measurements/ nm</i>	<i>d spacings (d₁) from cryo-EM images / nm</i>
poly(TILM-C12Br/BVTD)	2.15±0.4	3.20±0.5
poly(TILM-C14Br/BVTD)	2.49±0.7	3.50±0.5
poly(TILM-C16Br/BVTD)	2.97±0.9	4.00±0.5

To have a full picture of the effect of crosslinking on the shape and interior self-assembly of 1,2,4-triazolium-based PIL nanoparticles, the reaction parameters (monomer, crosslinker, and added salt concentrations) on nanoparticle size were systematically varied and their effects were studied. In all tests, TILM-C12Br was used as the model monomer, and NaI as externally added salt. The size of the resulting PIL products was determined by DLS characterization and **Table 9** summarized all results.

The influence of anion type, reaction temperature and concentration of initiator on the nanoparticle morphology was excluded from the current work, because in previous reports,^[96] these factors have been investigated and deliver little-to-no effect on the size of the PIL nanoparticles produced by dispersion polymerization.

Table 9. Nanoparticle sizes obtained from different experimental conditions in the dispersion polymerization of TILM-C12Br in the presence of BVTD crosslinking agent. The temperature (70 °C) and initiator concentration (3.5 mM) were kept constant during polymerization in water.

Entry	<i>Monomer</i> [mM]	<i>Crosslinker</i> [mM]	<i>[NaI]</i> [M]	<i>D_h</i> [nm] ^{a)}
1	TILM-C12Br/112	BVTD/11.2	0	42
2	TILM-C14Br/112	BVTD/11.2	0	29
3	TILM-C16Br/112	BVTD/11.2	0	33
4	TILM-C12Br/56	BVTD/11.2	0	34
5	TILM-C12Br/224	BVTD/11.2	0	74
6	TILM-C12Br/448	BVTD/11.2	0	117
7	TILM-C12Br/884	BVTD/11.2	0	201
8	TILM-C12Br/112	BVTD/0.56	0	24
9	TILM-C12Br/112	BVTD/1.12	0	33
10	TILM-C12Br/112	BVTD/2.24	0	35
11	TILM-C12Br/112	BVTD/5.6	0	38
12	TILM-C12Br/112	BVTD/22.4	0	82
13	TILM-C12Br/112	BVTD/33.6	0	133
14	TILM-C12Br/112	BVTD/44.8	0	245

15	TILM-C12Br/112	BVTD/11.2	0.0001	44
16	TILM-C12Br/112	BVTD/11.2	0.001	47
17	TILM-C12Br/112	BVTD/11.2	0.01	50
18	TILM-C12Br/112	BVTD/11.2	0.03	119
19	TILM-C12Br/112	BVTD/11.2	0.04	205
20	TILM-C12Br/112	BVTD/11.2	0.05	865

^{a)} The hydrodynamic diameter D_h was determined from DLS measurement;

The effect of the three experimental parameters, namely concentration of monomer, crosslinker and externally added salt (NaI) on the size of PIL nanoparticles, is discussed in **Figure 36**. Generally speaking, the nanoparticle size changed correlatively when varying these three factors and all samples ended up with larger sizes at higher concentrations of the monomer, crosslinker and salt. A gradual size expansion in a nearly linear order (**Figure 36A**) was observed upon increasing the monomer concentration. Nanoparticle size increases steadily from 34 nm to 74 nm within the concentration range from 56 mM to 224 mM (Entries 4, 5 in **Table 9**). Precipitation started in the dispersion and the solution became largely turbid once the monomer concentration is beyond 224 mM (Entries 6, 7 in **Table 9**). As for crosslinker concentration in **Figure 36B**, the nanoparticle size increase also gradually at increasing crosslinker concentration and no insoluble agglomerates were detected up to 44.8 mM (Entries 8-14 in **Table 9**). In contrast, the concentration of NaI has a very unique impact on the nanoparticle size. In **Figure 36C**, polymer nanoparticle size did not alter upon NaI addition until its concentration of 0.03 M (Entries 15-20, **Table 9**). A rapid size expansion appears beyond this concentration, indicating that polymers started to form insoluble agglomerates in a visible manner and macroscopic phase separation occurs due to the “salting-out” effect.

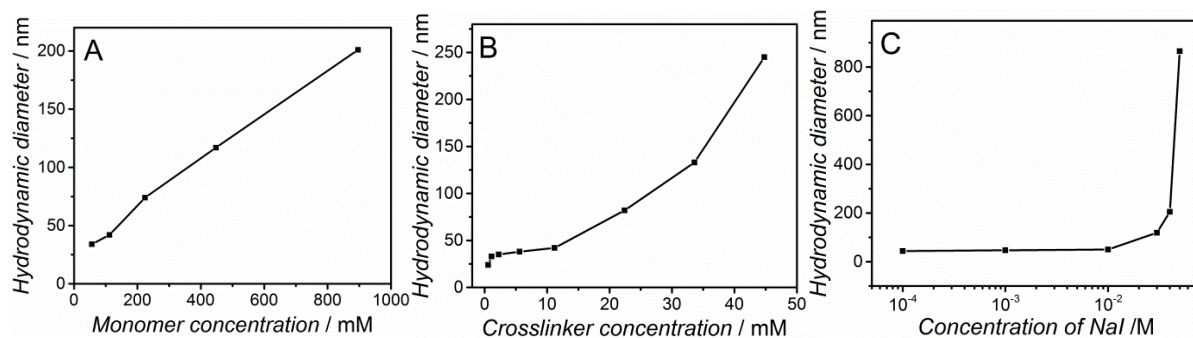


Figure 36. Plots of crosslinked PIL nanoparticle sizes/ D_h versus the concentrations of the monomer TILM-C12Br (A) the crosslinker BVTD (B) and NaI salt (C) in dispersion polymerization.

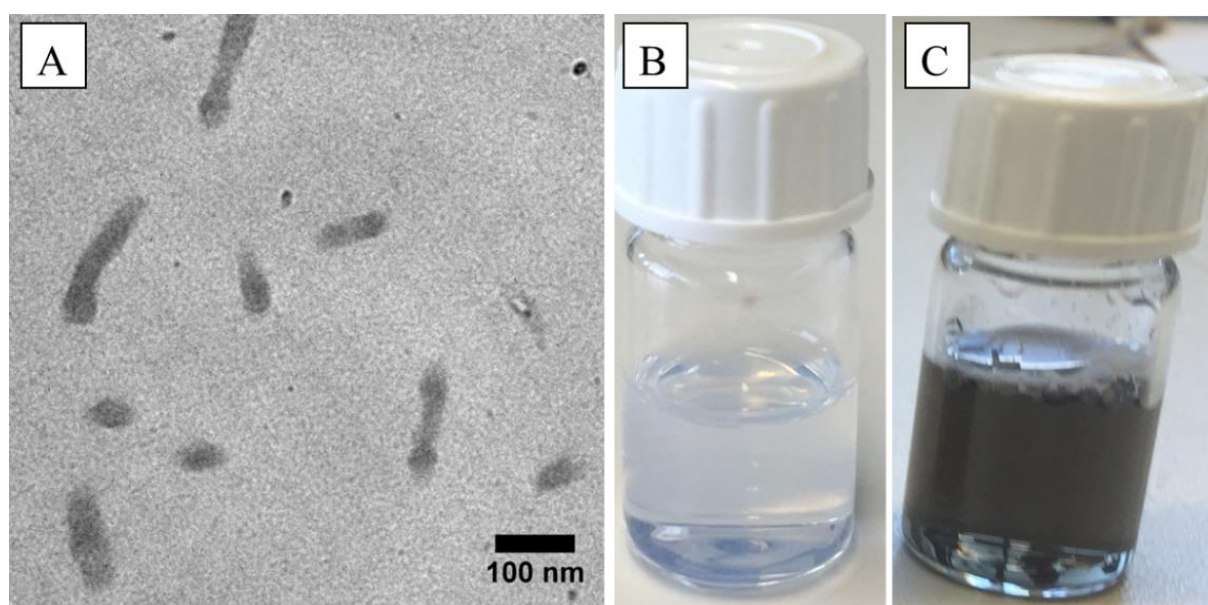


Figure 37. (A) TEM image of poly(TILM-C12Br/BVTD) prepared from their dispersion in DMF. (B and C) Photographs of poly(TILM-C12Br/BVTD) in DMF (left) and the dispersion of CNTs in DMF (right) in the presence of poly(TILM-C12Br/BVTD) after sonication treatment.

PIL nanoparticles represent a powerful materials platform to offer solutions to various materials systems, such as coatings, binders, nanoreactors, dispersants and many more.^[97] Crosslinked PIL nanoparticles, due to their structure stability in organic solvents, expand these advantages into aggressive organic media, *e.g.* DMF and DMSO. As shown in the TEM image in **Figure 37A**, poly(TILM-C12Br/BVTD) nanoparticles can be transferred from their aqueous dispersion into DMF without forfeiting their structural feature. The morphology of polymer colloids in this test is completely intact and identical to particles prepared from aqueous media (**Figure 32D**). In the case of non-crosslinked systems, such as poly(TILM-

C12Br) nanoparticles, once transferred to DMF solution, we failed to trace any nanoparticles, as they are now molecularly dissolved in DMF. One application of these crosslinked PIL nanoparticles is to disperse carbon nanostructures in organic solvents. By addition of multi-wall carbon nanotubes (CNTs) into a dispersion of poly(TILM-C12Br/BVTD), a homogeneous black dispersion of CNTs in both aqueous and organic media was obtained (**Figure 38**). It is well known that the cation- π interaction between the heterocyclic cation ring and the aromatic CNT surface is the driving force to attach polymers onto CNTs and eventually bring CNTs into solution. **Figure 37B&C** shows a native TPIL nanoparticle dispersion in DMF and a stable CNTs dispersion in it *via* sonication treatment, respectively. The crosslinked PIL nanoparticles serve as pickering dispersant to stick onto the CNTs and bring them into stable dispersion. This dispersion possesses long-term stability of more than one week (**Table 10**), which is confirmed by DLS measurements of the dispersion sample at different storage period.

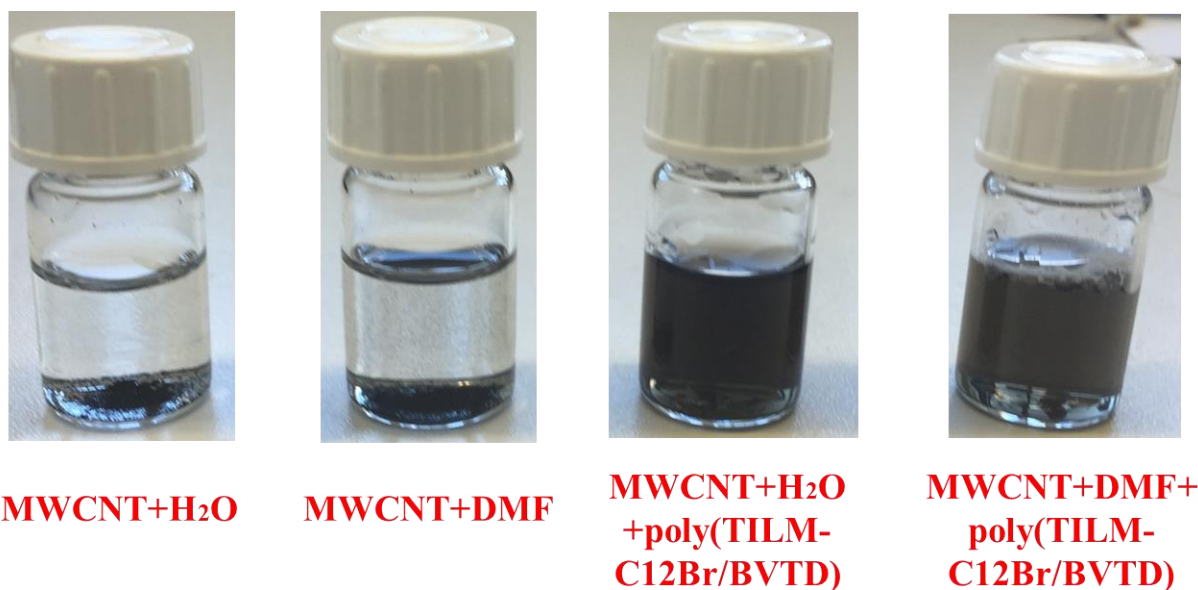


Figure 38. Photographs of treated multi-wall carbon nanotubes in water and DMF with and without poly(TILM-C12Br/BVTD) nanoparticles.

Table 10. Nanoparticle sizes obtained from different still standing days in the poly(TILM-C12Br-112/BVTD-11.2) dispersion with stabilized multi-wall carbon nanotubes.

<i>Entry</i>	<i>Time</i> [Day ⁻¹]	<i>D_h</i> [nm]
1	1	68.0
2	3	68.4
3	5	69.2
4	7	72.0

4.5 Conclusions

In summary, covalently crosslinked 1,2,4-triazolium-type PIL nanoparticles of different shape and size and distinctive interior patterns were obtained *via* one-pot dispersion polymerization in water. The interiors and morphological variation of these nanoparticles observed by cryo-EM characterization are similar to non-crosslinked ones discussed in chapter 3. Nevertheless it is the first time to observe spherical “wasp-like” nanoparticles. The size of the PIL nanoparticles is controllable by polymerization conditions, *i.e.* concentration of monomer, crosslinker and also externally added salt. As a proof-of-concept, crosslinked nanoparticles were tested in DMF to be stable in a particle form and were successfully used as dispersants for multi-wall carbon nanotubes in DMF.

5. Poly(1,2,4-triazolium) poly(ionic liquid) bearing triiodide anions: synthesis, basic properties and electrochemical behaviors

5.1 Introduction

The constant need for polymers of task-specific functions results in a non-stop search for unexplored polymer structures and functions. In the previous chapters, 1,2,4-triazolium-based PILs, which were much unknown before this thesis, have been examined in terms of their basic physical properties and self-assembly behavior to form fine inner nanostructure in their colloidal nanoparticles. Compared to imidazolium or 1,2,3-triazolium type PILs, 1,2,4-triazolium-based species indeed have high hydrophilicity, and strong acidity due to 2 active protons in the cation ring, and enhanced metal ion loading capacity. Since in IL/PIL chemistry ion metathesis/modification is a facile way to produce new PILs, 1,2,4-triazolium PILs with other counter anions are of interest to be explored, which might bring new knowledge in PILs.

In literature, PILs, due to their high ion density, have been used by Ohno *et al.* as polymer electrolytes^[9] for applications in supercapacitors, fuel cells, dye-sensitized solar cells, *etc.*^[17, 98] Generally speaking, PILs are thermodynamically more stable than conventional liquid-state or quasi-solid state electrolytes, and can be stable upon exposure to air when carrying hydrophobic anions, thus possessing a long shelf life. Chemically, the polymerizable cations or anions are associated to the polymer backbone thus have limited, sometimes negligible mobility, but the counter-ions of related PILs are fairly movable and can transport ions in the whole system, which make PILs naturally single-ion conductors.^[99] In this chapter we introduce poly(1,2,4-triazolium) PIL as a new solid-state polymer electrolyte bearing enhanced ion mobility and acidic protons.^[78] Triiodide is purposely incorporated into 1,2,4-triazolium PIL as the counter-anion, which minimizes interactions between the heterocyclic cation ring and the anion due to its large size thus enhanced steric hindrance. While triiodide has been explored previously as additives to polymers for its charge carrying properties,^[100, 101] they have not been examined in the context of PILs. After the introduction of I_3^- , the electrochemical and thermal behaviors of the PILs were altered, and a highly ion conductive polyiodide “network” can be expected according to Grotthuss mechanism. This makes triiodide-based PILs promising materials for high-performance polyelectrolyte.

5.2 Experimental Section

Materials, synthetic route, characteristic methods and additional experimental data are available in Appendix.

5.3 Results and discussion

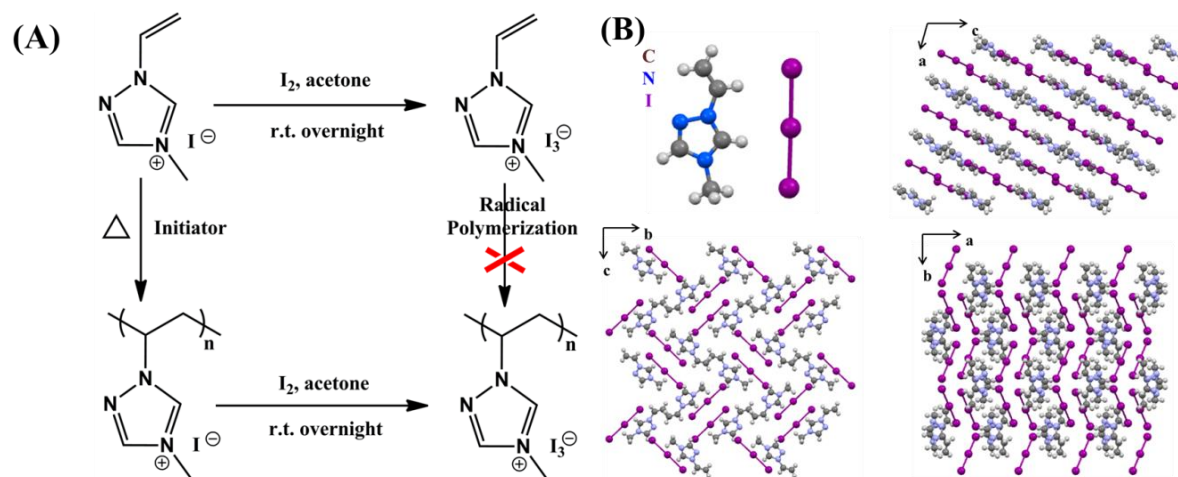


Figure 39. (A) Synthetic route towards 4-methyl-1-vinyl-1,2,4-triazolium triiodide monomer and poly(4-methyl-1-vinyl-1,2,4-triazolium triiodide). (B) Single crystal structure and crystallographic packing model of 4-methyl-1-vinyl-1,2,4-triazolium triiodide (CCDC 1436279 contains the supplementary crystallographic data for this article. These data can be found from the Cambridge Crystallographic Data Centre *via* www.ccdc.cam.ac.uk/data_request/cif.)

Our initial effort in synthesizing poly(4-methyl-1-vinyl-1,2,4-triazolium triiodide) followed the traditional free radical polymerization approach starting from its monomer. First, 4-methyl-1-vinyl-1,2,4-triazolium triiodide (TILM-CI₃) was synthesized directly from its iodide analogue. The synthesis route towards 4-methyl-1-vinyl-1,2,4-triazolium iodide as well as poly(4-methyl-1-vinyl-1,2,4-triazolium iodide) was reported in chapter 2 and two obtained compounds were used here directly as precursors. Treatment of the iodide-based IL monomer with a 1:1 molar equivalent amount of I₂ produces I₃⁻ which can be viewed as the neutralization of a Lewis base (I⁻) and Lewis acid (I₂).^[102] Triiodide-based IL was obtained as a solid powder *via* precipitation of the reaction mixture in cyclohexane to remove unreacted iodine. In order to elucidate the solid state structure of TILM-CI₃, single crystal X-ray diffraction of the single crystals grew from triiodide monomer-acetone solution was performed.

Table 11. Crystallographic data and structural refinement for 4-methyl-1-vinyl-1,2,4-triazolium triiodide.

Bond precision:	C-C = 0.0400 Å	Wavelength=0.71073
Cell:	$a=7.2685(14)$ $b=11.616(4)$ $c=15.038(4)$	
	$\alpha=90$ $\beta=106.472(19)$ $\gamma=90$	
Temperature:	293 K	
	Calculated	Reported
Volume	1217.6(6)	1217.6(6)
Space group	P 21/c	P 1 21/c 1
Hall group	-P 2ybc	-P 2ybc
Moiety formula	C5 H8 N3, I3	C5 H8 N3, I3
Sum formula	C5 H8 I3 N3	C5 H8 I3 N3
M_r	490.84	490.84
$D_x, g\text{ cm}^{-3}$	2.678	2.678
Z	4	4
$M_u\text{ (mm}^{-1}\text{)}$	7.658	7.658
F000	872.0	872.0
F000'	866.65	
h, k, l_{max}	8, 13, 18	8, 13, 18
N_{ref}	2229	2211
$T_{\text{min}}, T_{\text{max}}$	0.173, 0.252	0.253, 1.000
T_{min}'	0.023	
Correction method=	# Reported T Limits: $T_{\text{min}}=0.253$ $T_{\text{max}}=1.000$	
AbsCorr =	MULTI-SCAN	
Data completeness=	0.992	Theta(max)= 25.330
R(reflections)=	0.0781(1489)	wR ₂ (reflections)= 0.2332(2211)
S =	1.050	$N_{\text{par}}= 102$

As shown in **Table 11**, TILM-CI₃ monomer crystallizes in the monoclinic space group $P2_1/c$, and cell parameters are $a=7.2685(14)$ Å, $b=11.616(4)$ Å, $c=15.038(4)$ Å and $\beta=106.472(19)^\circ$. Single crystal data analysis reveals the successful formation of I₃⁻ anion in TILM-CI₃. The distances for I-I bonds in I₃⁻ anion are 2.91 and 2.88 Å, and the I-I-I bending angle is 178.94(6)°, which are consistent with triiodide reported in the previous literatures.^[103] **Figure 39B** shows the packing model of TILM-CI₃ along a , b and c axes individually. It is clear that the I₃⁻ anions are sandwiched between adjacent 1,2,4-triazolium rings, which further extend to supramolecular 3D “network” by the intramolecular electrostatic interaction. Owing to Grotthuss mechanism, in which the charge transfer is achieved *via* construction and simultaneous destruction of covalent bonds among neighboring species, *i.e.* “hopping” of atoms instead of mass movement,^[104] enhanced transportation of I⁻ in such 3D supramolecular “network” is foreseeable for solid-state ILs. Additionally, the unique alignment of I₃⁻ anions

finally result in a shorter distance of 4.4 Å between adjacent triiodide chains. Considering the radius of I⁻ (2.2 Å), bond length of I₂ (2.7 Å) and above mentioned “hopping” mechanism, the effective ion conduction can be inferentially expected in triiodide systems.

Table 12. Elemental analysis result of poly(4-methyl-1-vinyl-1,2,4-triazolium) triiodide.

poly(TILM-C1I ₃)	%C	%H	%N	%I
Calculated	12.23	1.64	8.56	77.56
Measured	12.73	1.80	8.52	76.23

Since the radical quenching capability of triiodide is well-known^[105] and prevents direct radical polymerization of I₃⁻ containing monomers (**Figure 39A**), which was proven by our experimental efforts, post-modification of the iodide PIL was the left choice. Triiodide-based PILs were produced following the same procedure used for triiodide-based IL monomers, *i.e.* anion modification. It is worth mentioning that iodide-based polymer poly(TILM-C1I) is insoluble in acetone. The addition of 1:1 molar equivalent I₂ led to the formation of a transparent dark yellow acetone solution plus a tiny fraction of residue solid (< 5 wt%) that was filtered off. After precipitation of the mixture solution in cyclohexane to remove any I₂ species and further purified *via* dialysis in acetone using a dialysis tube with molecular weight cutoff of 3,500 Da to remove impurities, dark brown powders were obtained when solvent was evaporated. The change in the solubility of the iodide PIL after the treatment of I₂ indicated that triiodide-based PILs were successfully synthesized, which was further identified by elemental analysis (**Table 12**).

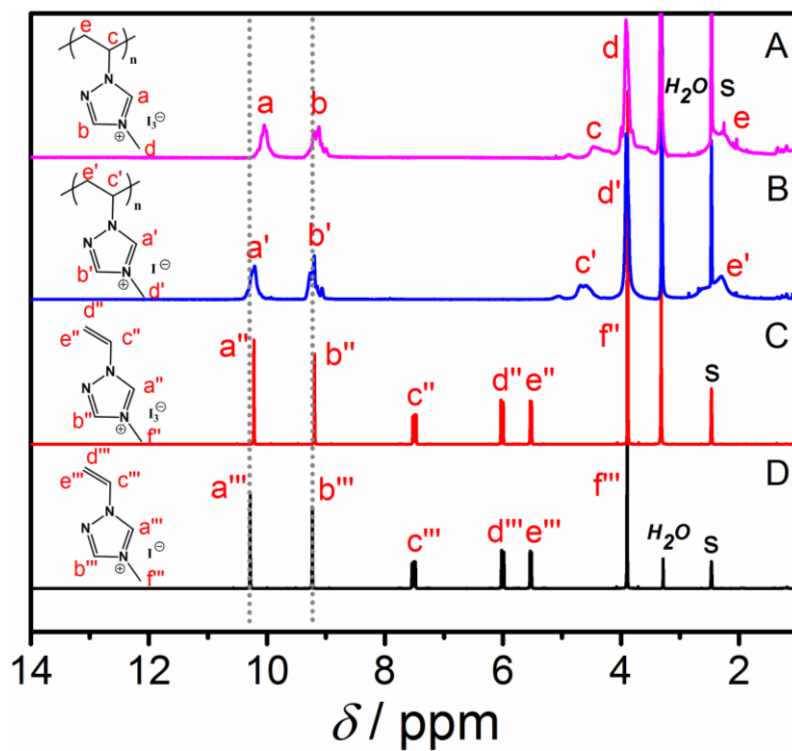


Figure 40. ^1H -NMR spectra of (A) poly(4-methyl-1-vinyl-1,2,4-triazolium triiodide); (B) poly(4-methyl-1-vinyl-1,2,4-triazolium iodide); (C) 4-methyl-1-vinyl-1,2,4-triazolium triiodide; and (D) 4-methyl-1-vinyl-1,2,4-triazolium iodide.

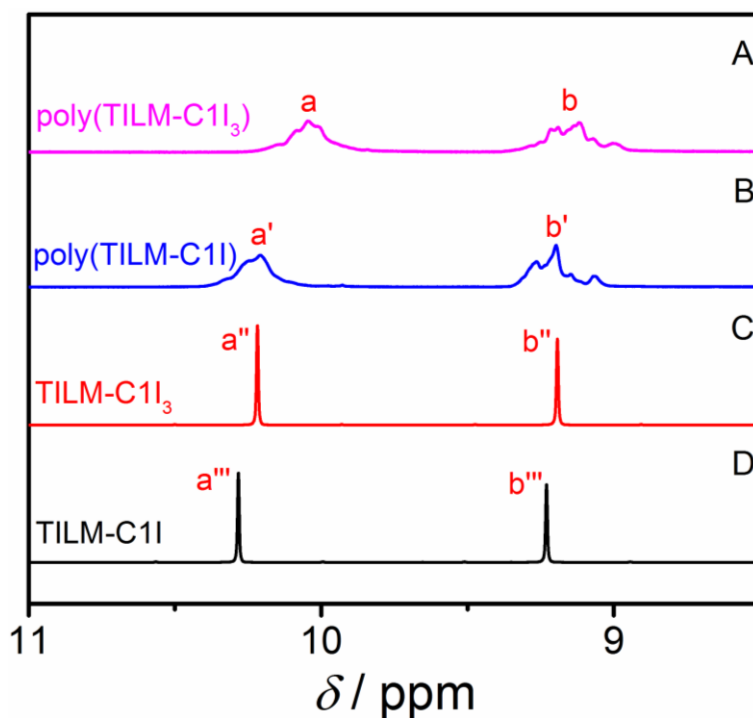


Figure 41. Enlarged ^1H -NMR spectra of (A) poly(TILM-C1I₃); (B) poly(TILM-C1I); (C) TILM-C1I₃; (D) TILM-C1I.

Slight differences were observed in the ^1H NMR spectra for the triiodide-based monomer and polymer relative to their iodide congeners. **Figure 40** shows the resonances corresponding to two acidic protons in 1,2,4-triazolium rings are slightly shielded when the anion is triiodide. This trend is consistent with other anion-exchanged PILs, where the replacement of anions may result in varied shielding of the protons.^[18] In the low field of PILs in **Figure 41**, peak *a* and *b* related to protons in 1,2,4-triazolium rings in poly(TILM-C1I₃) were shielded in comparison to poly(TILM-C1I), one from 10.23 (*a'*) to 10.03 ppm (*a*) and the other from 9.21 ppm (*b'*) to 9.11 ppm (*b*). Similar behaviors were observed as well for monomers TILM-C1I and TILM-C1I₃ from 10.28 (*a''*) to 10.21 ppm (*a''*) and from 9.23 (*b''*) to 9.19 ppm (*b''*). As reported, triiodide anions are existed in an isolation state in solutions because they are electronically more stable instead of I₂-I pair in solvents,^[106] we believe that the delocalized negative charge in triiodide *vs* iodide leads to weakened interaction of anions with hydrogens in the 1,2,4-triazolium heterocycle ring, which eventually results in shielding of those acidic protons.

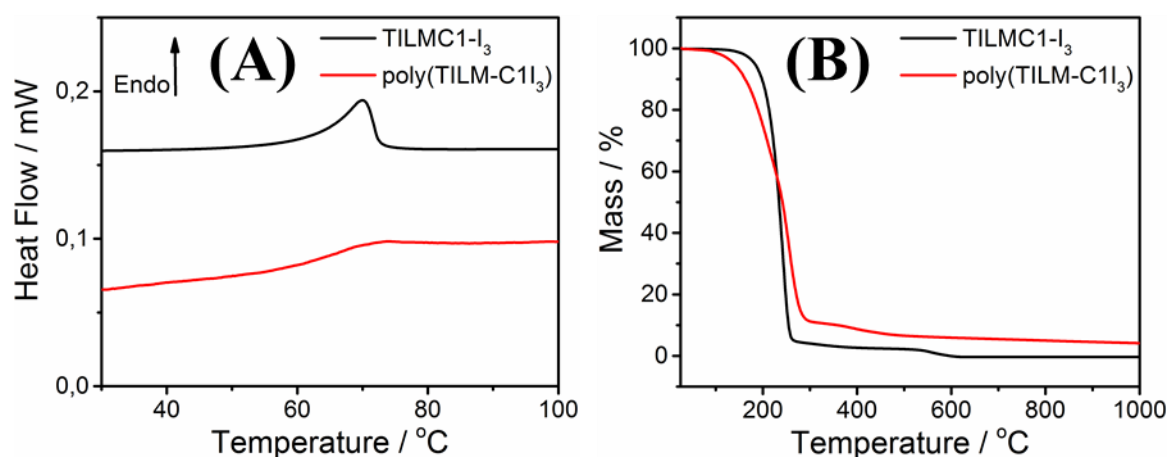


Figure 42. (A) DSC curves of poly(TILMC1-I₃) and TILM-C1I₃; (B) TGA curves of poly(TILMC1-I₃) and TILM-C1I₃.

The thermal behaviors of ILMs and their polymers strongly depend on the types of cations, anions, and interactions between them. Differential scanning calorimetry (**Figure 42A**) and thermogravimetric analysis (under N₂, **Figure 42B**) were applied to measure the melting points, glass transition temperature (T_g), and thermal stabilities of the monomers/polymers. TILM-C1I₃ melts at approximately ~70 °C, and is considered an IL by conventional definition. Owing to the inhibition effect of iodine as well as triiodide towards radical propagation, exothermal peaks for thermal radical polymerization are not found till 100 °C. Poly(TILM-C1I₃) possesses a T_g at ~68 °C, which is very close to the melting point of its

monomer. Compared to poly(TILM-C1I) which didn't show glass transition temperature before its thermal decomposition, poly(TILM-C1I₃) acquired T_g in consistent with the trend corroborated by the monomers. According to the thermal stability, triiodide PIL and IL here start to decompose (defined as 5 wt% mass loss) at 139 and 183 °C, respectively. Compared to their iodide analogues, the stability of triiodide monomer is consistent with the iodide monomer (180 °C for TILM-C1I), while triiodide PIL drops significantly lower than 237 °C for poly(TILM-C1I).

Anion differences in PILs/ILs will not only induce variations in their thermal properties, but also their hydrophilicity/hydrophobicity. **Table 13** exhibits the solubility of triiodide-based 1,2,4-triazolium type monomer and polymer performed at a concentration of 1.0 wt% at room temperature. In good accordance with their iodide analogues, both TILM-C1I₃ and poly(TILM-C1I₃) are insoluble in chloroform and toluene, and soluble in DMF/DMSO, which indicates the solubility in these hydrocarbon solvents is irrelevant or less relevant to anion types. Opposite to their iodide precursors, poly(TILM-C1I₃) and TILM-C1I₃ were both insoluble in water but soluble in tetrahydrofuran and acetone/acetonitrile. In addition, poly(TILM-C1I₃) and TILM-C1I₃ differentiate each other slightly in their solubility in methanol and ethyl acetate, in which only the triiodide monomer is soluble. The contrary solubility appeared here between triiodide monomer and polymer can stem from the linear connection of the monomer units through the vinyl group in the cation, which makes the triiodide more exposed to the solvent environment. In general, the presence of the triiodide anion results in more hydrophobic salts relative to the iodide ones due to the weakened ionic bond.

Table 13. Solubility of triiodide-type monomer and polymer in different solvents.

Compound	H ₂ O	MeOH	Acetone/AC	THF	CHCl ₃ /toluene	EtOAc	DMF/DMSO
TILM-C1I	+	+	+	-	-	-	+
TILM-C1I ₃	-	+	+	+	-	+	+
poly(TILM-C1I)	+	-	-	-	-	-	+
poly(TILM-C1I ₃)	-	-	+	+	-	-	+

(+) – soluble at 1.0 wt%; (-) – insoluble at 1.0 wt%

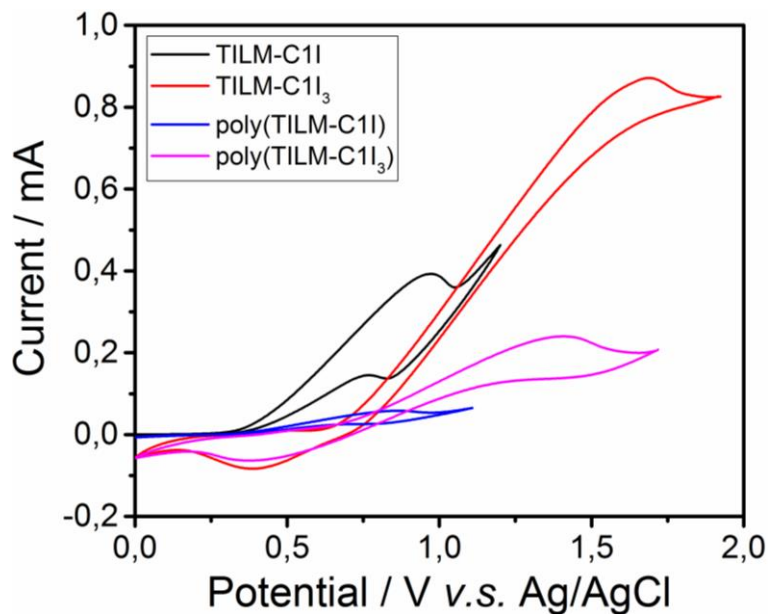


Figure 43. Cyclic voltammetry curves of TILM-C1I, TILM-C1I₃, poly(TILM-C1I) and poly(TILM-C1I₃) (50 mmol in 10 mL DMF).

In order to understand the electrochemical behavior of triiodide type IL and PIL, cyclic voltammetry and electrochemical impedance spectroscopy (EIS) analyses in DMF (with Ag/AgCl standard electrode and Pt/C electrode) was performed. Additionally, iodide-based TILM-C1I and poly(TILM-C1I) were measured as references. In **Figure 43**, triiodide PIL/IL exhibit a higher current density than iodide counterparts, which is possibly contributed by the more ion-conductive triiodide species because of their better charge transportation ability realized *via* “hopping” of I⁻.

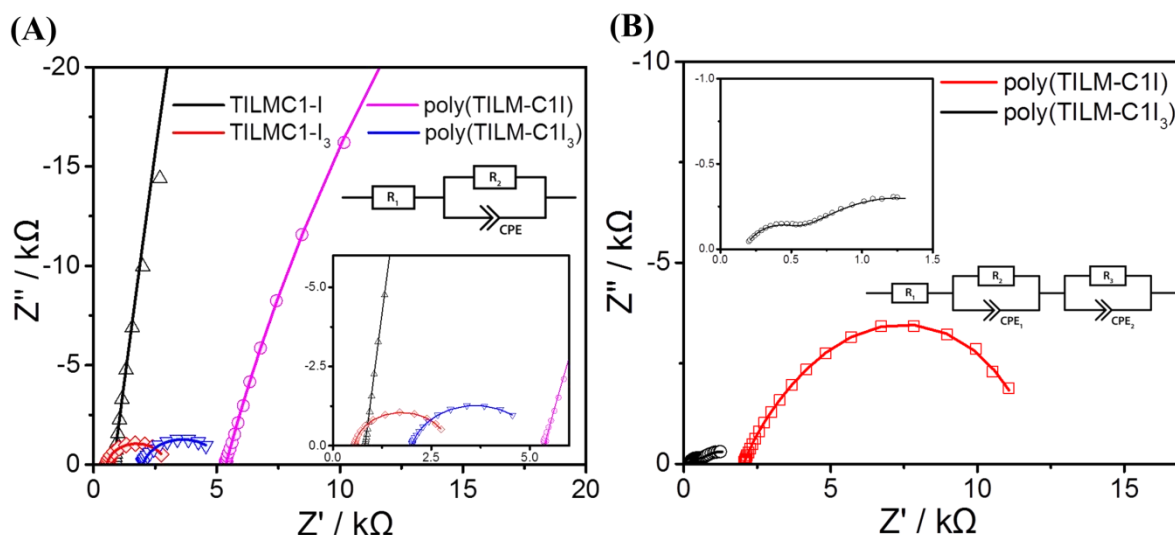


Figure 44. Nyquist plots from electrochemical impedance spectroscopy analysis of (A) 50 mmol TILM-C1I, TILM-C1I₃, poly(TILM-C1I) and poly(TILM-C1I₃) in 10 mL DMF and equivalent electrical circuit model used for fitting (inset); (B) 0.1 mol anhydrous poly(TILM-

C1I) and poly(TILM-C1I₃) sample with two blocking electrodes (graphite sheets, 6 cm*1 cm; electrolyte area, 0.6-0.8 cm*1 cm). The scattered symbols and solid lines represent experimental and fitting results, respectively.

In **Figure 44A**, EIS data from iodide and triiodide-type IL and PIL is plotted as a Nyquist plot. The equivalent circuit (**Figure 44A**, inset) is a typical Randles circuit consisting of an ohmic resistor, R_1 , in series with a $R_2||CPE_1$ circuit element representing the resistance of the electrolyte and the charge transfer at the double layer from the electrode/electrolyte interface, respectively.^[107] The fitting results can be found in the **Table 14**. It becomes apparent that the high frequency series resistance, R_1 , is smaller for triiodide type samples in comparison to iodide IL or PIL. This is consistent with the idea that the use of triiodide anion will increase ion conductivity.^[101] Since polycations possess relatively lower mobility in solution compared to their monomers, *i.e.* the formed polymer chains are more restricted from free random motions according to chain tangling and shearing, that R_1 for PILs is larger than the one for ILs. The double layer resistance, R_2 , can be drastically reduced by using I_3^- and/or by polymerization. These results underline the differences in charge transportation in these four compounds, in which triiodide-based ones outperform the iodide ones.

Table 14. Fitting results obtained from analysis of EIS data (**Figure 44A**).

Samples	R_1 (Ω)	R_2 (Ω)	CPE_1T (-)	CPE_2P (-)
TILM-C1I	814	$3.26 \cdot e^6$	$1.72 \cdot e^{-6}$	0.935
TILM-C1I ₃	545	$2.40 \cdot e^3$	$2.04 \cdot e^{-6}$	0.918
poly(TILM-C1I)	$5.37 \cdot e^3$	$225 \cdot e^3$	$2.04 \cdot e^{-6}$	0.866
poly(TILM-C1I ₃)	$2.00 \cdot e^3$	$3.22 \cdot e^3$	$3.51 \cdot e^{-6}$	0.851

Since, from a practical point of view, solid state electrolytes are more reliable in long-term safety and fabrication process,^[108] we further perform EIS measurements on bulk poly(TILM-C1I₃) and compared it with poly(TILM-C1I) as a reference. Due to its low T_g (thus sticky) and relatively high electrochemical stability, it might be used as solid electrolyte and binder at the same time. **Figure 44B** shows the measured and fitted EIS data of poly(TILM-C1I) and poly(TILM-C1I₃) in solid state. As shown in the inset, the equivalent circuit consists of an ohmic resistor in series with two $R||CPE$ circuits to mimic the influence of the electrode/electrolyte double-layer ($R_2||CPE_1$) as well as the charge transport resistance in the solid electrolyte ($R_3||CPE_2$) on the overall impedance.^[109]

Table 15. Fitting results obtained from analysis of EIS data (**Figure 44B**).

Samples	R_1 (Ω)	R_2 (Ω)	CPE_1T (-)	CPE_1P (-)	R_3 (Ω)	CPE_2T (-)	CPE_2P (-)
poly(TILM-C1I)	$2.04 \cdot e^3$	$2.64 \cdot e^3$	$2.28 \cdot e^{-5}$	0.656	$7.40 \cdot e^3$	$1.33 \cdot e^{-5}$	0.849
poly(TILM-C1I ₃)	167	346	$6.98 \cdot e^{-6}$	0.688	$1.49 \cdot e^3$	$2.90 \cdot e^{-4}$	0.482

The results from fitting can be found in **Table 15**. It is apparent that the use of the triiodide anion results in significantly reduced R_1 , R_2 , and R_3 emphasizing the importance of I_3^- in the bulk as well as at the electrode/electrolyte interface. We found that the value for CPE_2P is decreased from 0.85 to 0.48 when using I_3^- instead of I^- . It means that a transition from a capacitive-like circuit element to a diffusion-like element was observed.^[110] We believe that our primary result is indicative of diffusion of ionic species through the Grotthuss mechanism when I_3^- is present. Based on above results, it is fair to say that poly(1-vinyl-1,2,4-triazolium triiodide) is a promising material in the field of sustainable energy generation and conversion where it can be utilized as solid polymer electrolyte.

5.4 Conclusions

In conclusion, a 1,2,4-triazolium triiodide-type PIL was synthesized from its iodide precursor for the first time. Compared to its iodide analogues, both triiodide type IL and PIL exhibit visibly different behaviors in solubility, thermal properties, and especially in electrochemical properties. According to the single crystal structure of TILM-C1I₃, we believe that the triiodide “network” can largely enhance conductivity and electrochemical efficiency of triiodide type PIL, and it has been confirmed by cyclic voltammetry test as well as EIS measurement both in solution and in bulk as solid electrolyte. Consequently, poly(TILM-C1I₃) as a new PIL is a promising candidate as solid polymer electrolyte for future energy devices to be investigated.

6. Dispersed Palladium clusters stabilized by poly(1,2,4-triazolium) poly(ionic liquid) vesicle

6.1 Introduction

Palladium clusters (PdCs) with dimensions between single metal atoms and nanoparticles of > 2 nm, have attracted growing attention due to their unique electronic structures and the associated unusual physical and chemical properties.^[111] The size of PdCs approaches the Fermi wavelength of electrons, resulting in molecule-like characters including discrete energy levels, size-dependent fluorescence, photostability and sometimes biocompatibility.^[112] However, the tiny size of PdCs brings difficulty to their synthesis in comparison to the relatively easier preparation of nanoparticles beyond 2 nm, because they are naturally prone to aggregation driven by high surface energy.^[113] Although various synthetic techniques and routes have been developed to prepare PdCs over the past few years,^[111, 114] these procedures often require stringent experimental conditions or necessitate tedious multistep reactions and purifications. Therefore, the development of simple and efficient route for preparing PdCs of precise size is highly desirable.

In this chapter, we introduced an approach toward synthesis of PdCs with controlled size of averagely 1 nm by applying 1,2,4-triazolium-PIL vesicle as a robust stabilizer. By joint effects of designable binding sites and well-defined hydrophilicity/hydrophobicity balance of PILs, poly(4-hexyl-1-vinyl-1,2,4-triazolium iodide) (denoted as poly(TILM-C6I)) serves as stabilizer for PdCs in organic medium. The stabilizing power in poly(TILM-C6I) is expected to be related to an *in-situ* polycarbene formation process.

6.2 Experimental section

Materials, synthetic route, characteristic methods and additional experimental data are available in Appendix.

6.3 Results and discussion

The synthetic route of PIL with pending hexyl chain from the 1,2,4-triazolium ring is illustrated in **Figure 45**. 1-vinyl-1,2,4-triazole was first reacted with 1-iodohexane to form the 1,2,4-triazolium monomer, which in the next step was radically polymerized to form the targeted poly(TILM-C6I) PIL. The existence of the hydrophilic 1,2,4-triazolium iodide ion

pair enables the PIL to be dissolved in polar solvent such as methanol, while the pending *n*-hexyl chains on the 1,2,4-triazolium ring expand their solubility scope to moderate polar solvent such as dichloromethane. Therefore, a mixture of methanol and dichloromethane is chosen as the solvent for the current PIL system.

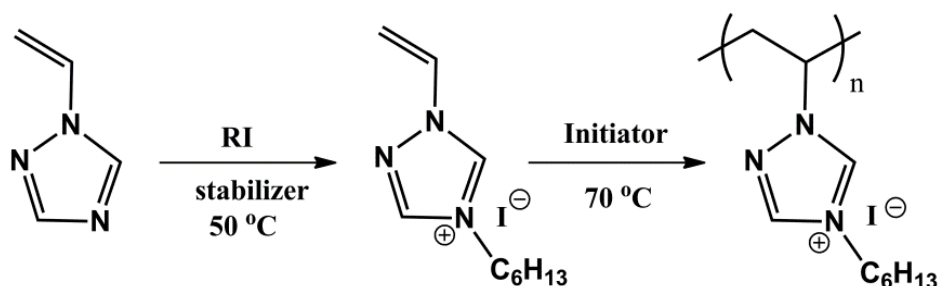


Figure 45. Synthetic route towards poly(TILM-C6I). R: *n*-hexyl group.

In the following step, Pd cluster synthesis was conducted by using poly(TILM-C6I) as stabilizer. The Pd/poly(TILM-C6I) nanohybrid was prepared by a solution process (**Figure 46**). Briefly, a solution (9 mL) of dichloromethane and methanol mixture (volume ratio = 2:1) was added to a flask containing dried PIL (5 mg) to give a light yellow solution. Since poly(TILM-C6I) contains both hydrophobic and hydrophilic subdomains in its repeating molecular structure, as discussed above, cryo-EM measurements were conducted to this solution in order to approach the real dispersing state of poly(TILM-C6I) PIL. Indeed, intriguing vesicular structures with the size ranging from 50 to 250 nm and the shell thickness of 15 ~ 35 nm were observed in sample (**Figure 47**). These vesicles maintain a fairly long (for months) stability as colloids in solution.

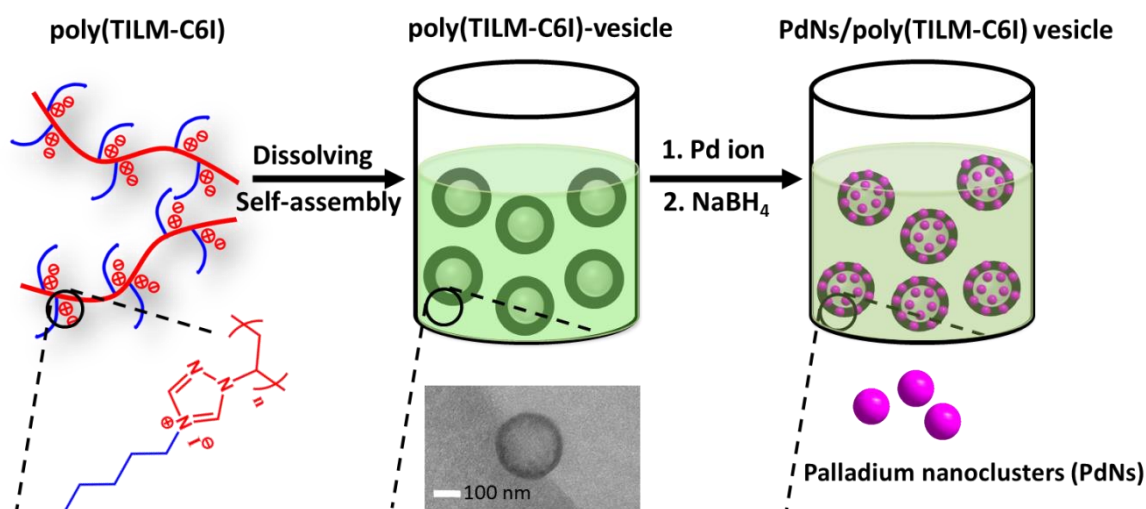


Figure 46. Schematic illustration of the general procedure toward the synthesis of Pd clusters stabilized by poly(TILM-C6I) vesicles.

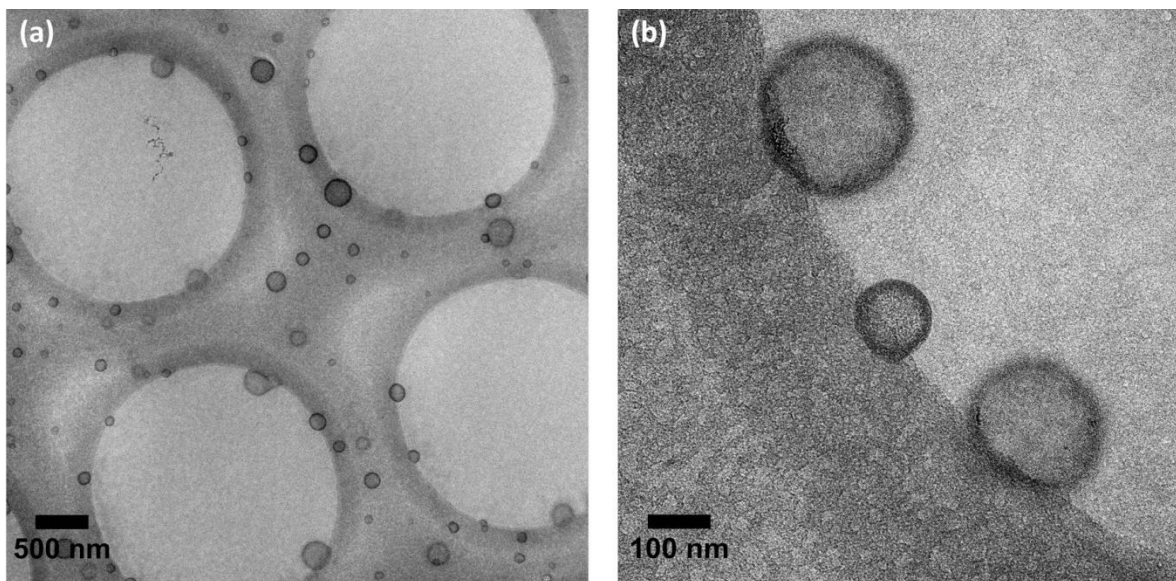


Figure 47. Cryo-EM images of poly(TILM-C6I) vesicles in dichloromethane and methanol mixture (volume ratio = 2:1)

The color of the poly(TILM-C6I) in methanol/dichloromethane mixture solution is light yellow, which became dark brown (**Figure 48**) immediately upon adding palladium nitrate (Pd content = 0.5 mg). After aging the sample for 20 min, the mixture was subsequently reduced with a methanol solution of sodium borohydride (5 mg, room temperature). The solution immediately changed its color from dark brown to light brown (**Figure 48**) without any precipitates, indicating the rapid Pd(II) reduction as well as simultaneous stabilization of the resultant Pd clusters by poly(TILM-C6I) vesicles.



Figure 48. Photographs of the Pd(II)/poly(TILM-C6I) solution (left) and the corresponding Pd/poly(TILM-C6I) solution (right) in dichloromethane and methanol mixture solvent (volume ratio = 2:1).

The diameter and size distribution of Pd

clusters were characterized by scanning transmission electron microscopy (STEM). The sample was prepared using a solution of Pd/poly(TILM-C6I), which was drop-cast onto a

carbon-coated copper grid and allowed to dry before the measurements. The morphology of Pd clusters was revealed by high-angle annular dark field scanning transmission electron microscopy (HAADF-STEM) images (**Figure 49a**), in which the PdCs appear as light dots. The average diameter of Pd clusters is measured to be 1.0 ± 0.2 nm. Its size histogram is visualized in **Figure 49b**, displaying a monomodal size distribution. X-ray photoelectron spectroscopy (XPS) analysis identifies the formation of Pd clusters with binding energies at 335.3 and 340.6 eV (**Figure 50**), corresponding to Pd $3d_{5/2}$ and Pd $3d_{3/2}$ of metallic Pd, respectively.

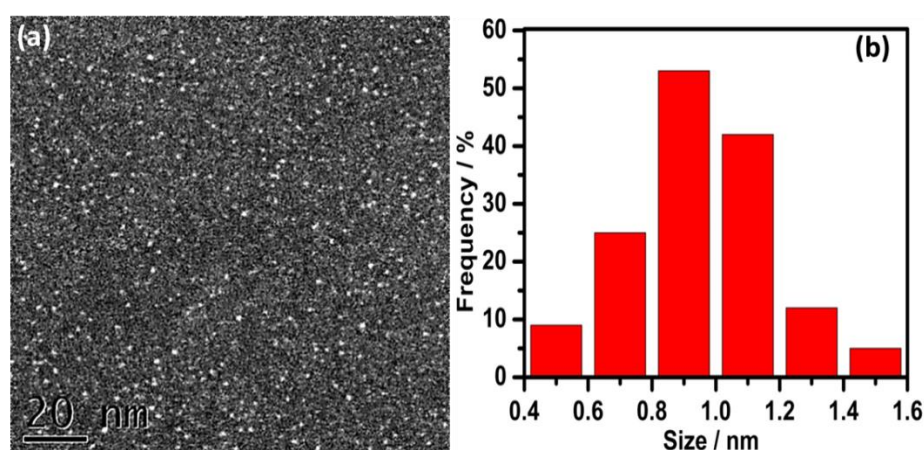


Figure 49. (a) HAADF-STEM images of Pd/poly(TILM-C6I); (b) the corresponding size histogram of Pd clusters.

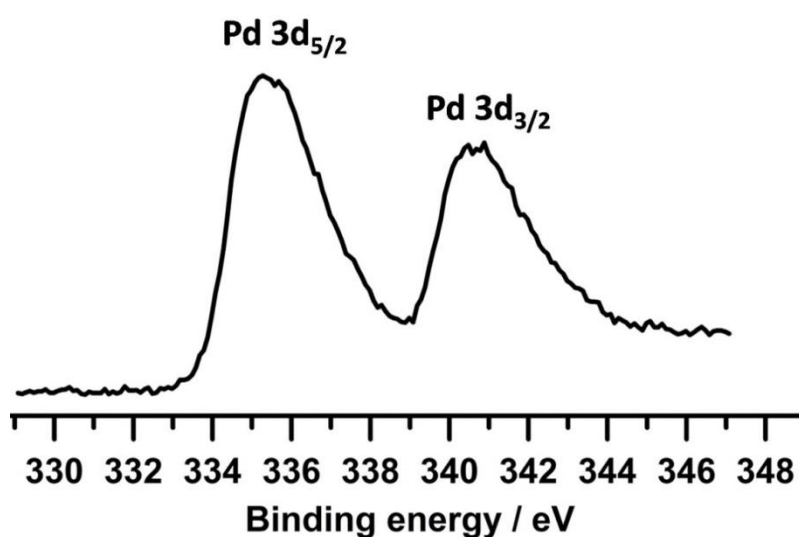


Figure 50. XPS spectrum of Pd/poly(TILM-C6I) showing Pd $3d_{5/2}$ (335.3 eV) and Pd $3d_{3/2}$ (340.6 eV) peaks of metallic Pd after Ar etching.

Despite their ultrasmall size, the obtained Pd clusters show excellent non-aggregation behavior. They are stable in solution without agglomeration and noticeable color change over months. More importantly, they can be dried under N₂ flow and purified by water washing but then re-dissolved in a solution of dichloromethane and methanol mixture (volume ratio = 2:1). This behavior is very much polymer-like. As we know that the re-dispersion of Pd nanoparticles after drying of their initial dispersion has been often a problem due to weak binding interaction between the supports/stabilizers and Pd nanoparticles, easily leading to particle aggregation that cannot be re-dispersed in solution even under strong sonication treatment.^[115]

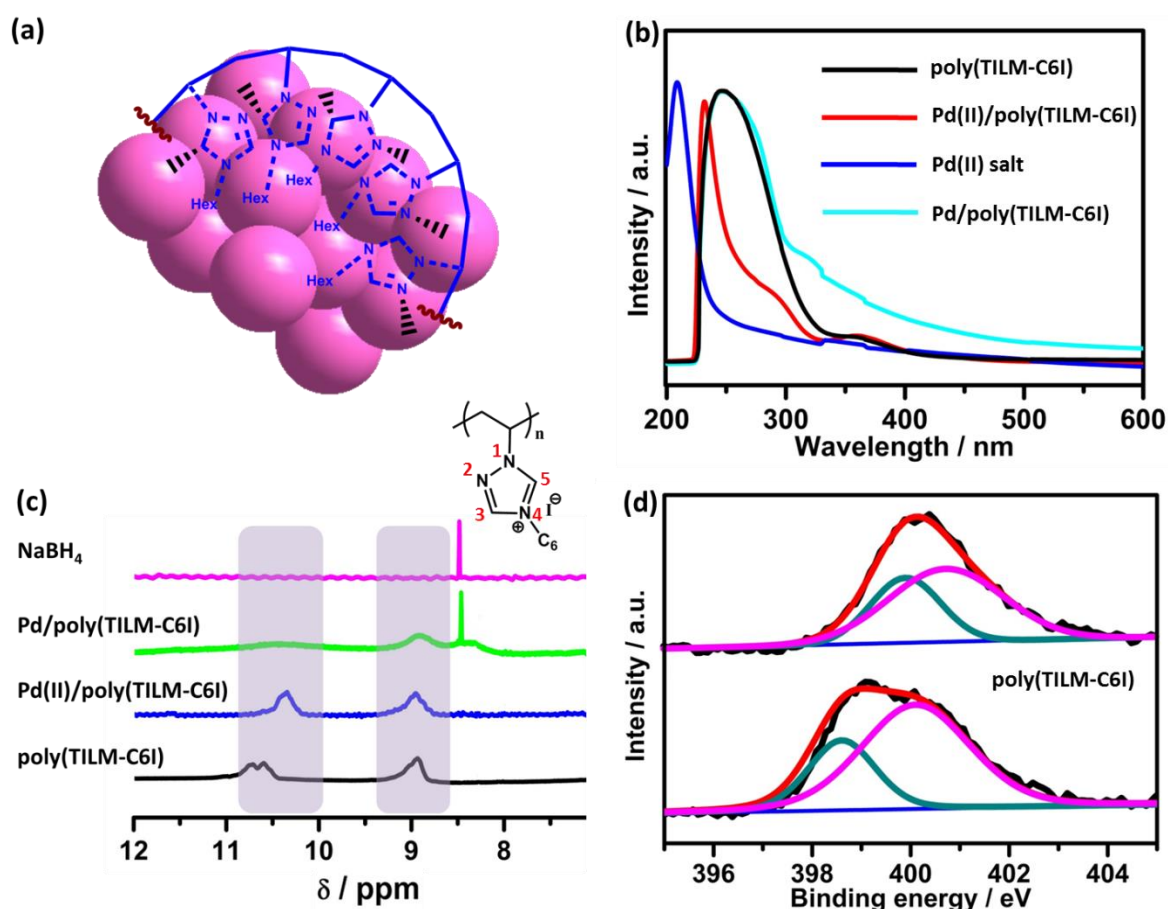


Figure 51. (a) Schematic illustration of poly(TILM-C6I)-derived polycarbene binding Pd cluster. (b) The UV-Vis spectra monitoring the process of formation of Pd/poly(TILM-C6I) in dichloromethane-methanol mixture (volume ratio = 2:1). (c) The ¹H NMR spectra recorded during the process of formation of Pd/poly(TILM-C6I) in CD₂Cl₂ and CH₃OH (volume ratio = 2:1). (d) XPS spectra for N 1s signals of poly(TILM-C6I) and Pd/poly(TILM-C6I). In both spectra, the N1s spectra could be fitted by the sum of two separated peaks with 1:2 area ratios that correspond to naked nitrogen (N2) and the two nitrogen atoms (N1 and N4) of the 1,2,4-triazolium groups, respectively.

We move next to investigate the intrinsic role of poly(TILM-C6I) toward stabilization and immobilization of Pd clusters. The UV-Vis (ultraviolet-visible) spectra were firstly recorded to monitor the interaction between poly(TILM-C6I) and Pd(II). Notably, an obvious shift of absorption band in Pd(II)/poly(TILM-C6I) mixture in comparison to individual Pd(II) or poly(TILM-C6I) in solution is distinguishable. For example, in the Pd(II)/poly(TILM-C6I) system, compared with the absorption of Pd(II) ion at 209 nm and poly(TILM-C6I) at 247 nm, respectively, new peaks at 231 and 295 nm are observed in Pd(II)/poly(TILM-C6I) (**Figure 51b**), indicative of complexation between both. It is well-known that the support with strong coordination sites is essential to bind metal ions and thus control over the nucleation and particle growth of Pd clusters.^[116] To specify the binding site of poly(TILM-C6I), ¹H NMR measurement was employed to monitor the cluster formation process. As shown in **Figure 51c**, there is an obvious low-field shift of 0.3 ppm (from 10.6 to 10.3 ppm) of hydrogen signal at C5 position in 1,2,4-triazolium ring upon addition of Pd(II) ions. It is noteworthy mentioning that the C5 hydrogen signal decreases after reduction by NaBH₄, (**Figure 51c**). Since the C5 hydrogen atoms in native poly(TILM-C6I) (metal free) could be removed by a weak base to form carbene species (**Figure 51c**), the observed phenomenon in Pd/poly(TILM-C6I) system suggests the generation of carbene carbons in the 1,2,4-triazolium rings, which due to its preferential interaction with Pd species serve as *in-situ* binding species to Pd clusters. Through integration of ¹H NMR spectra, ca. 33 % of the 1,2,4-triazolium units in poly(TILM-C6I) were calculated to participate in carbene formation, corresponding to one metal atom per 1 monomer unit.

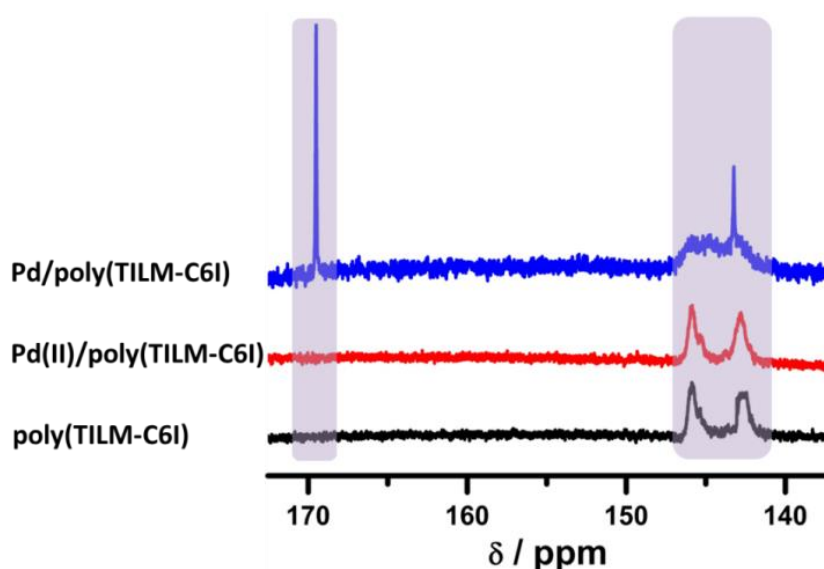


Figure 52. ¹³C NMR spectra of poly(TILM-C6I), Pd(II)/poly(TILM-C6I) and Pd/poly(TILM-C6I) in CD₂Cl₂ and CH₃OH mixture (volume ratio = 2:1).

Further evidence of carbene generation and its assisted stabilization of Pd cluster was demonstrated by ^{13}C NMR spectra (**Figure 52**), in which a new peak appears at 169.6 ppm after reduction of Pd(II)/poly(TILM-C6I) by NaBH_4 , a typical chemical shift for metal-carbene coordination.^[117] It should be mentioned that there is a naked nitrogen atom (N2) in the 1,2,4-triazolium ring, which binds the Pd species strongly as well. The XPS measurements of the resultant Pd/poly(TILM-C6I) hybrid show an obvious shift of N2 signal from 398.6 eV in native poly(TILM-C6I) (green line in **Figure 51d**) to a high binding energy position (399.8 eV). In comparison, the shift of signal from the other two quarternized nitrogens (N2 and N4) is rather weak (< 0.5 eV), indicating complexation between the metallic Pd and 1,2,4-triazolium cation through the N2 position (**Figure 51d**). Thus in poly(TILM-C6I) both the nitrogen atoms and the *in-situ* generated polycarbene join this stabilization process.

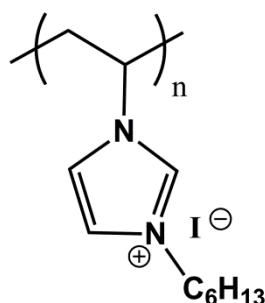


Figure 53. Chemical structure of poly(ImILM-C6I).

The important role of poly-1,2,4-triazolium-derived polycarbene toward efficient control over the size of Pd clusters was further demonstrated in a control experiment by using its imidazolium analogue poly(4-hexyl-1-vinylimidazolium iodide) (denoted as poly(ImILM-C6I), chemical structure in **Figure 53**). In poly(ImILM-C6I), the cation rings contains two nitrogen atoms at 1 and 3 position with a $-\text{CH}_2-$ unit in between that serves in the presence of a strong base as carbene precursor. Following the same procedure, the resultant Pd nanoparticles are broadly distributed in size from 1.5 to 11 nm as visualized by TEM image (**Figure 54**). Thus, the N2 atom in the 1,2,4-triazolium ring is a crucial structural motif in the Pd cluster synthesis, not only because it binds the most strongly with Pd cluster but also because it facilitates the formation of carbene species of poly(1,2,4-triazolium) PIL.

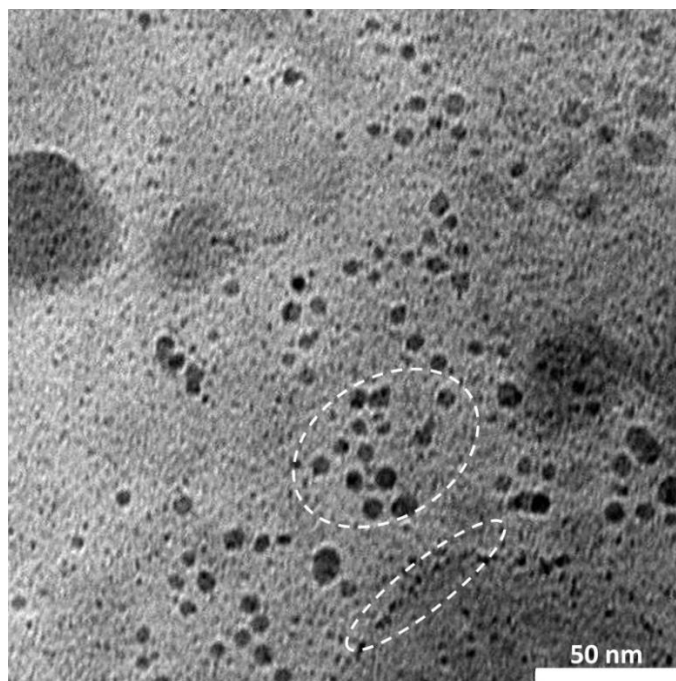


Figure 54. The bright field of TEM image of Pd/poly(ImILM-C6I). The white ellipses indicate that both cluster and large nanoparticle exist in it.

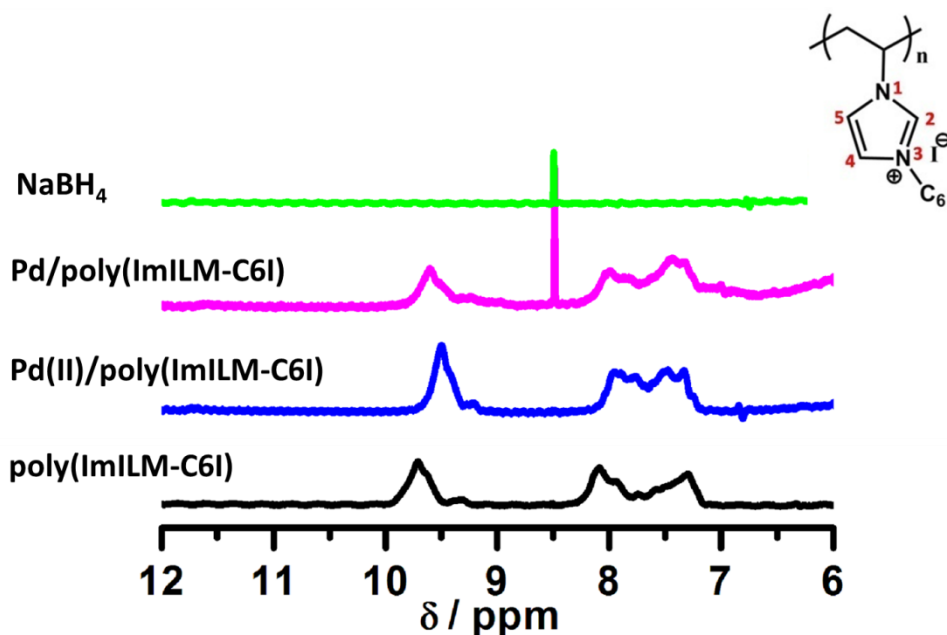


Figure 55. The ^1H NMR recorded during the formation process of Pd/poly(ImILM-C6I) in CD_2Cl_2 and CH_3OH (volume ratio = 2:1).

The ^1H NMR spectra (**Figure 55**) confirmed that in the presence of NaBH_4 as weak base, the C2-H in the imidazolium ring is more inert to produce carbene than that in 1,2,4-triazolium. Its chemical shift has little-to-no change after reduction by NaBH_4 , so does the C2 carbon according to its ^{13}C NMR spectrum (**Figure 56**), indicating the C2 position in imidazolium

ring is less active in forming carbene-metal complex. In comparison with poly(TILM-C6I), the decrease in signal intensity at 135 ppm corresponding to the C2 of imidazolium ring is not obvious in Pd/poly(ImILM-C6I), and meanwhile only a weak single signal at 169.6 ppm appeared after reduction, *i.e.* the involvement of polycarbene stabilization is weak in Pd/poly(ImILM-C6I). This is also consistent with the observation in TEM image of non-uniform distribution of particles in Pd/poly(ImILM-C6I) (**Figure 54**).

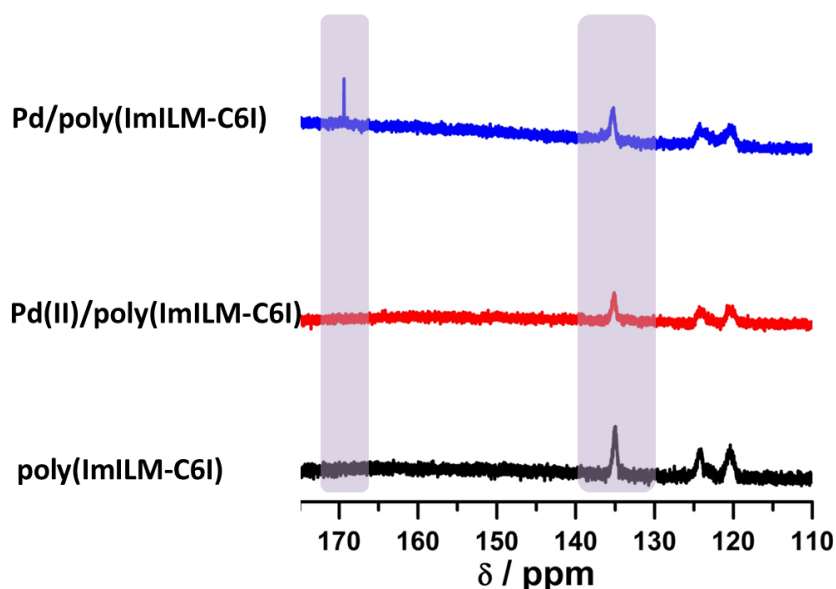


Figure 56. ^{13}C NMR spectra of poly(ImILM-C6I), Pd(II)/poly(ImILM-C6I) and Pd/poly(ImILM-C6I) in CD_2Cl_2 and CH_3OH mixture (volume ratio = 2:1).

It is clear that intensive involvement of polycarbene is a prerequisite toward successful stabilization and strict size control of ultrasmall Pd clusters. This role cannot be replaced by monocarbene compounds. If the 1,2,4-triazolium monomer, a low molecular weight carbene precursor (**Figure 58**), was used instead of poly(TILM-C6I) as stabilizer (**Figure 57**), freshly prepared Pd particles after a few minutes were observed to aggregate severely in solution at room temperature. These aforementioned experiments unequivocally justify the function of poly(TILM-C6I) derived polycarbene as strong and extra binding power, which work synergistically and effectively with co-existent heterocyclic cation ring to enhance the metal-support interaction for size control and long-term stability.

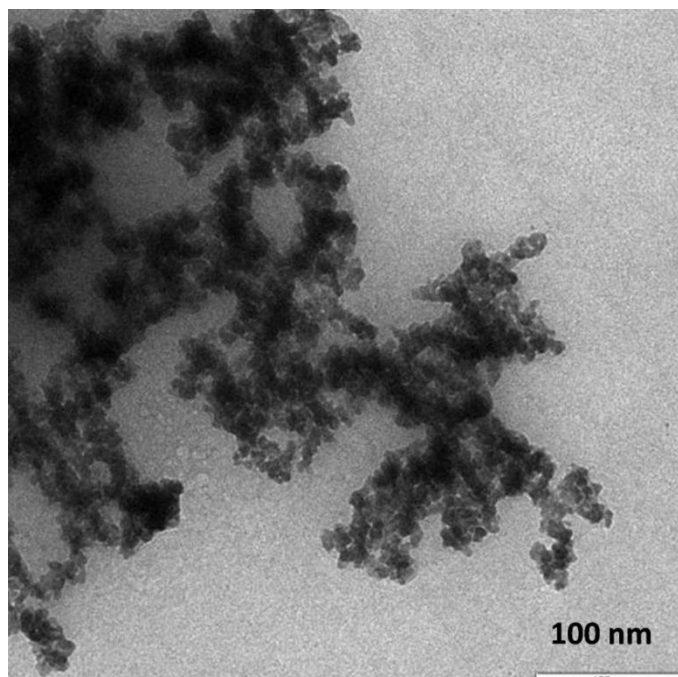


Figure 57. The TEM image of Pd/1,2,4-triazolium monomer prepared by NBH_4 reduction.

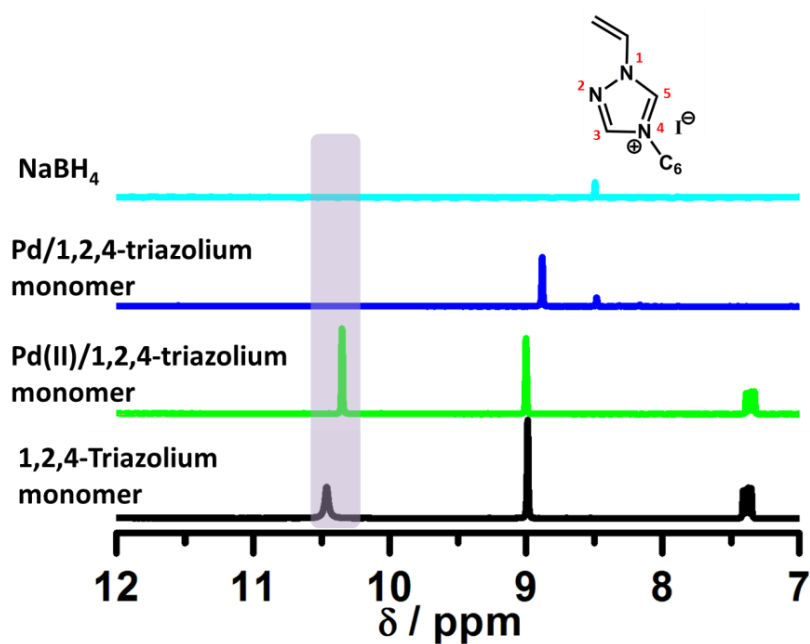


Figure 58. The ^1H NMR spectra recorded during the formation process of Pd/1,2,4-triazolium monomer in CD_2Cl_2 and CH_3OH (volume ratio = 2:1). The signal at 10.4 ppm at C5 position in pure 1,2,4-triazolium monomer disappears in Pd/1,2,4-triazolium monomer after reduction by NaBH_4 (shown in violet rectangle), indicative of the formation of carbene carbon in 1,2,4-triazolium monomer.

6.4 Conclusions

In conclusion, 1,2,4-triazolium PIL poly(TILM-C6I) has been applied as strong stabilizer to prepare Pd clusters with precisely controlled size of 1 nm. Cryo-EM measurements showed a vesicular morphology of this PIL in a mixture of methanol and dichloromethane solution. The key to the success of this approach is the synergistic effect of multiple binding sites of the polymeric support, including the original binding sites in the heterocyclic cation ring and the extra polycarbene binding power, which was generated by deprotonation of the C5 proton by the reductant NaBH_4 . We experimentally confirmed that the polycarbene contribution here is vital to control the cluster size. Due to the excellent dispersing state and superior stability, the Pd clusters are expected to be active catalysts.

7. Summary

This thesis aims at introducing a new series of poly(ionic liquid)s—poly(1,2,4-triazolium)s—into the common scope of PILs. After the investigation as well as discussion on novel features and phenomena that were discovered in poly(1,2,4-triazolium) PILs in this thesis, it became obvious, as we expected, that a tiny variation in the chemical structure—*e.g.* replace a carbon atom in the imidazolium ring with a nitrogen atom—can induce huge effect in their materials function. The whole thesis includes fundamental synthesis, self-assembly behavior, characterization, and the materials application of poly(1,2,4-triazolium) PILs in stabilization of Pd metal clusters. We expect all these evidences and findings can help researchers understand this new class of PILs, and possibly initiate further research activity on this topic. The followings are detailed contents of each chapter.

In chapter 2, we report synthesis of a series of poly(4-alkyl-1-vinyl-1,2,4-triazolium) PILs either *via* straightforward free radical polymerization of their corresponding ILMs, or *via* anion metathesis of the polymer precursors bearing halide as counter anion. The ILMs were first prepared *via* *N*-alkylation reaction of commercially available 1-vinyl-1,2,4-triazole with alkyl iodides, followed by anion metathesis with targeted fluorinated anions. The thermal properties and solubility of these PILs have been systematically investigated. It was found that the poly(4-ethyl-1-vinyl-1,2,4-triazolium TFSI) PIL exhibited an improved loading capacity of transition metal ions in comparison with its imidazolium counterpart.

In chapter 3, we studied the internal morphology-controllable self-assembly in 1,2,4-triazolium-based PIL nanoparticles with long alkyl chains. Precise control of the interior and outer shapes of polymer nanoparticles has found broad interest in nanoscience, *e.g.* in fundamental studies of their physical properties, colloidal behavior and corresponding applications. Realizing such control below the 50 nm scale (*i.e.* a size scale approaching some individual macromolecules) requires accurate manipulation of polymerization techniques and a judicious choice of the chemical structure in monomers and/or polymers. Here, a series of well-defined sub-50 nm homopolymer nanoparticles with controllable shape and highly ordered, complex internal structures with sub-5 nm domain spacings were prepared and studied. *Via* cryogenic electron microscopy and tomography, a unique morphological evolution of particle shape and interior at this extremely small size end, unusual for polymer colloids, was identified and investigated in detail.

In chapter 4, we extended the study to covalently crosslinked poly(1,2,4-triazolium) PIL nanoparticles. Compared to their non-crosslinked counterparts, the crosslinked ones showed improved structural integrity in aggressive organic media. Assisted by cryogenic electron microscopy, these nanoparticles were analyzed in detail and found to present vastly diverse shapes and highly ordered inner mesostructures. Additionally, the size variation of these colloidal nanoparticles was investigated systematically by polymerizations at different concentrations. Finally, the crosslinked PIL nanoparticles were able to readily disperse multi-walled carbon nanotubes in water and organic media without losing their structural integrity.

In chapter 5, we synthesized poly(4-methyl-1-vinyl-1,2,4-triazolium triiodide) PIL and investigated its ion conduction property. They were prepared from their iodide precursors *via* facile anion reaction of iodide with iodine. The variation from iodide (I^-) to triiodide (I_3^-) was found to introduce obvious variations in the physical properties. The triiodide IL monomer and the PIL polymer present lower melting point/glass transition temperature and altered solubility. Electrochemical behaviors of the triiodide monomer and polymer were studied in solution and in bulk. Compared with their iodide analogues, the triiodide ones exhibited lower electrical impedance and higher current in cyclic voltammetry. Moreover, poly(4-methyl-1-vinyl-1,2,4-triazolium triiodide) was proven to be promising solid polymer electrolyte candidate.

In chapter 6, the poly(1,2,4-triazolium) PILs were used to stabilize Pd clusters. Specifically, colloidally stable poly(4-hexyl-1-vinyl-1,2,4-triazolium iodide) vesicles were used as the stabilizer and support. This unique structural scaffold enables successful control of Pd clusters with average size of ~ 1 nm. It was found that poly(4-hexyl-1-vinyl-1,2,4-triazolium iodide) serves as precursors to polycarbenes, which are generated in the *in-situ* reduction process with multiple binding sites and featured excellent binding capability to stabilize the Pd clusters. All these enable us a high degree of control over the size, dispersibility, and stability of resultant Pd clusters.

As a class of versatile materials, PILs are thriving, growing, and ripe for new discoveries and opportunities. Here the introduction of 1,2,4-triazolium type PILs in this thesis further broadens the horizon of PIL materials as well as their application scopes. In our opinion these efforts will inspire the PIL researchers and foster their enthusiasm to explore more unknown field in PILs.

Appendix

A Materials and Methods

Materials

1-Vinyl-1,2,4-triazole ($C_4H_5N_3$, 98%), iodomethane (CH_3I , 99%), iodoethane (CH_3CH_2I , 99%), 1-iodobutane (C_4H_9I , 99%), 1-iodohexane ($C_6H_{13}I$, 99%), 1-iododecane ($C_{10}H_{21}I$, 99%), 1-iodododecane ($C_{12}H_{25}I$, 98%), 1-bromododecane ($C_{12}H_{25}Br$, 97%), 1-bromotetradecane ($C_{14}H_{29}Br$, 97%), 1-bromohexadecane ($C_{16}H_{33}Br$, 97%), 1,4-dibromobutane (BrC_4H_8Br , 99%), 1-vinylimidazole ($C_5H_6N_2$, 99%), butylated hydroxytoluene (BHT, 98%), N,N'-azobisisobutyronitrile (AIBN, 98%, recrystallized from methanol), potassium hexafluorophosphate (KPF_6 , 98%), and all organic solvents were purchased from Sigma-Aldrich. Iodine (I_2 , 99.8%) was obtained from Acros Organics. Graphite sheets were purchased from LairdTech. 2,2'-Azobis[2-methyl-N-(2-hydroxyethyl) propionamide] (VA086, 98%) was purchased from Wacker-Chemie. Chloroethane (CH_3CH_2Cl , ca. 15% in tetrahydrofuran; ca. 2 mol/L), and lithium bis(trifluoromethylsulfonyl)imide (LiTFSI, >98%) were obtained from TCI chemicals. All solvents used were of analytical grade.

Methods

Thermogravimetric analyses (TGA) were performed on a Netzsch TG209-F1 apparatus using a heating rate of 10 K min^{-1} under constant N_2 flow.

Differential scanning calorimetry (DSC) measurements were carried out under N_2 flow on a Perkin-Elmer DSC-1 instrument at a heating/cooling rate of 10 K min^{-1} . The melting points were determined from the heating curves and recorded in the second heating cycle.

Fourier transform infrared spectroscopy (FT-IR) spectra were on a BioRad 6000 FT-IR spectrometer; samples were measured in solid states using a Single Reflection Diamond ATR.

1H NMR and ^{13}C NMR spectra were performed on a Bruker DPX-400 spectrometer in deuterated solvents using residual solvent as reference.

Gel permeation chromatography (GPC) was performed using NOVEMA Max linear XL column with a mixture of 80% of aqueous acetate buffer and 20% of methanol. Conditions: flow rate 1.00 mL min^{-1} , PSS standards using RI detector-Optilab-DSP-Interferometric Refractometer (Wyatt-Technology).

Metal elemental analyses and elemental analyses (EA) of triiodide compounds were performed by Mikroanalytisches Laboratorium Kolbe (www.mikro-lab.de).

Cyclic voltammetry (CV) (50 mV s^{-1}) was performed with a Gamry reference 3000 potentiostat in a voltage window of 0.0-2.0 V for all samples.

Impedance spectra were recorded using a Gamry reference 3000 potentiostat by applying a sine wave with amplitude of 10 mV over the frequency range from 0.1 or 0.5 Hz to 20 kHz. The data was fitted using ZPlot software from Scribner Associates Inc.

Single crystal X-ray diffraction was conducted on a Gemini A Ultra X-ray Diffraction System (from Rigaku Oxford Diffraction), equipped with Atlas CCD detector.

Transmission electron microscopy (TEM) was performed on a Zeiss EM 912 Omega microscope using an operating voltage of 120 kV. The TEM samples were obtained as follows: one drop of diluted nanoparticles dispersion (in water) was placed onto a 400 mesh carbon-coated copper grid and the grid was dried in air.

Scanning electron microscopy (SEM) was performed on a GEMINI LEO 1550 microscope operating at 3 kV. Samples were sputtered with gold before measurement.

Dynamic light scattering (DLS) was performed with an ALV-7004 multiple tau digital correlator equipped with CGS-3 compact goniometer system, 22 mW He-Ne laser (wavelength $\lambda = 632.8 \text{ nm}$) and a pair of avalanche photodiodes operated in a pseudo-cross-correlation mode. Number-averaged polymer particle size distributions were obtained *via* CONTIN analysis.

Small-angle X-ray scattering (SAXS) was measured using a NONIUS rotating anode instrument (4 kW, Cu K_{α}) with pinhole collimation and a MARCCD detector (pixel size = 79) calibrated using silver behenate. The samples of poly(ionic liquid) nanoparticle dispersion (concentrated to 50 g/L) were transferred in a glass capillary. The observed scattering patterns were standardized by pure water scattering. The 1D radial average of the scattering intensity was transformed from 2D diffraction patterns using the Fit2D software.

Cryo-electron microscopy (cryo-EM) was performed with a JEOL JEM-2100 transmission electron microscope (JEOL GmbH, Eching, Germany). Cryo-EM specimens were prepared by applying a 4 μL drop of sample dispersion to lacey carbon-coated copper TEM grids (200

mesh, Electron Microscopy Sciences, Hatfield, PA) and plunge-frozen into liquid ethane at its freezing point with an FEI vitrobot Mark IV set at 4 °C and 95% humidity. In the case of samples for cryo-electron tomography (Cryo-ET), a 3 μ L drop of 10 nm colloidal gold solution (Aurion) was applied to the grids and allowed to dry before plunge freezing. Vitrified grids were either transferred directly to the microscope cryo transfer holder (Gatan 914, Gatan, Munich, Germany) or stored in liquid nitrogen. All grids were glow-discharged before use. Imaging was carried out at temperatures around 90 K. The TEM was operated at an acceleration voltage of 200 kV and a defocus of the objective lens of about 1.5–2 μ m was used to increase the contrast. Cryo-EM micrographs were recorded at a number of magnifications with a bottom-mounted 4*4k CMOS camera (TemCam-F416, TVIPS, Gauting, Germany). The total electron dose in each micrograph was kept below 20 $e^-/\text{\AA}^2$. Tomographic tilt series were collected using the Serial-EM software [<http://www.ncbi.nlm.nih.gov/pubmed/16182563>] to $\pm 60^\circ$ with a 2° angular increment and a total dose of 100 $e^-/\text{\AA}^2$ at a magnification of 50,000 x, corresponding to a pixel size of 2.32 \AA at the specimen level.

Cryo-electron tomography (**Cryo-ET**) **image processing**. Tomographic tilt series were aligned and reconstructed with the IMOD software package [Reference: <http://www.ncbi.nlm.nih.gov/pubmed/8742726>]. Tomographic volume segmentation was performed with Amira (FEI Company, Eindhoven, The Netherlands) while three-dimensional volume rendering and movie generation was performed with UCSF Chimera [Reference: <http://www.ncbi.nlm.nih.gov/pubmed/15264254>].

Powder X-ray diffraction (PXRD) was carried out with an X-ray diffractometer of Rigaku, Ultima IV.

X-ray photoelectron spectroscopy (XPS) studies were performed with a Thermo-Fisher ESCALAB250 X-ray photoelectron spectrometer (powered at 150 W) using Al K α radiation ($\lambda = 8.357 \text{\AA}$). To compensate for surface charging effects, all XPS spectra were referenced to the C 1s neutral carbon peak at 284.6 eV.

Absorption UV-Vis measurements in solution were recorded on a Lambda 900 spectrophotometer.

B Experimental Part

All 1,2,4-triazolium type monomers in this thesis are denoted as **TILM-C_nX**, (n=1, 2, 6, 12, 14, or 16; X=I, Br, PF₆, TFSI, I₃), polymers as **poly(TILM-C_nX)**.

General synthetic procedures of ILMs&PILs

Monomer synthesis: A mixture of 1-vinyl-1,2,4-triazole (5 mL, 5.5 g, 57.83 mmol) and an excess stoichiometric amount (1.2 equivalent) of n-iodoalkane/n-bromoalkane were added into a 100 mL round flask, accompanied with 2,6-di-tert-butyl-4-methylphenol (50 mg, 0.227 mol) as the stabilizer. After heated at 50 °C overnight, crude products were precipitated in diethyl ether and washed with the same solvent for three times. White powders were obtained.

Polymerization process: A mixture of monomers with AIBN (1.5 mol%) as initiator was dissolved in anhydrous DMF inside a 100 mL round-bottom Schlenk flask, (concentration: ~1 g monomer in 10 mL solvent) then purged with three freeze-pump-thaw cycles. The reaction was stirred at 70 °C for 24 h under Ar protection. Yellow/brown powders were obtained after dialysis against water and vacuum drying process.

Solubility tests (for chapter 2&5)

10 mg of the monomer/polymer was put into 1 mL of solvent (water, methanol, acetone, acetonitrile, THF, ethyl acetate, toluene, chloroform or DMF). After shaking fiercely for 10 min, the solubility of corresponding monomer/polymer at ambient temperature was checked.

Chapter 2

Synthesis of 4-methyl-1-vinyl-1,2,4-triazolium iodide (2/TILM-C1I)

A pale yellow solid (13.21 g, 96.4%) was obtained. ¹H NMR (400 MHz, DMSO-*d*₆, δ, ppm): 10.36 (s, 1H), 9.28 (s, 1H), 7.55 (dd, 1H, *J*₁=16 Hz, *J*₂=8 Hz), 6.03 (d, 1H, *J*=16 Hz), 5.57 (d, 1H, *J*=8 Hz), 3.94 (s, 3H); ¹³C NMR (400 MHz, DMSO-*d*₆, δ, ppm): 146.02, 142.67, 129.63, 110.85, 35.34.

Synthesis of 4-ethyl-1-vinyl-1,2,4-triazolium iodide (3/TILM-C2I)

A pale yellow solid (13.76 g, 94.8%) was obtained. ¹H NMR (400 MHz, DMSO-*d*₆, δ, ppm): 10.57 (s, 1H), 9.44 (s, 1H), 7.46 (dd, 1H, *J*₁=16 Hz, *J*₂=8 Hz), 6.01 (d, 1H, *J*=16 Hz), 5.57 (d, 1H, *J*=8 Hz), 4.32 (q, 2H, *J*=8 Hz), 1.49 (t, 3H, *J*=8 Hz); ¹³C NMR (400 MHz, DMSO-*d*₆, δ, ppm): 145.04, 141.94, 129.66, 110.97, 44.15, 14.70.

Synthesis of poly(4-methyl-1-vinyl-1,2,4-triazolium iodide) (7/poly(TILM-C1I))

A yellow powder was received after removal of solvents, the yield was 3.6 g (72%). ¹H NMR (400 MHz, DMSO-*d*₆, δ, ppm): 10.25 (br, 1H), 9.24 (m, 1H), 4.62 (br, 1H), 3.91 (br, 3H), 2.34 (br, 2H).

Synthesis of poly(4-ethyl-1-vinyl-1,2,4-triazolium iodide) (8/poly(TILM-C2I))

A yellow powder was obtained with a yield of 3.25 g (65%). ¹H NMR (400 MHz, DMSO-*d*₆, δ, ppm): 10.51 (br, 1H), 9.33 (m, 1H), 4.95 (m, 1H), 4.31 (br, 2H), 2.55 (br, 2H), 1.56 (br, 3H).

Synthesis of TILM-C1PF₆, TILM-C1TFSI and TILM-C2TFSI via anion exchange

Anion exchange was performed by dropwise addition of solution 2) into solution 1) : 1) 1 g of **TILM-C1I** or **TILM-C2I** dissolved in 50 mL of deionized water, and 2) 1.05 eq. of potassium hexafluorophosphate or lithium bis(trifluoromethanesulfonyl)imide in 20 mL deionized water. Concerning **TILM-C1PF₆**, it was extracted by ethyl acetate after vigorous stirring, followed by solvent evaporation to yield pale yellow product. **TILM-C1TFSI** or **TILM-C2TFSI**, precipitated as white powders, and was filtered off and washed with deionized water for 3 times, before it was dried at 40°C under high vacuum.

Synthesis of poly(TILM-C1PF₆), poly(TILM-C1TFSI) and poly(TILM-C2TFSI) via anion exchange

Anion exchange was performed by dropwise addition of solution 2) into solution 1) : 1) 1 g of **poly(TILM-C1I)** or **poly(TILM-C2I)** dissolved in 50 mL of deionized water, and 2) 1.05 eq. of potassium hexafluorophosphate or lithium bis(trifluoromethanesulfonyl)imide in 20 mL deionized water. The resulting white precipitate was filtered off and washed with deionized water for 3 times, before it was dried at 100 °C under high vacuum.

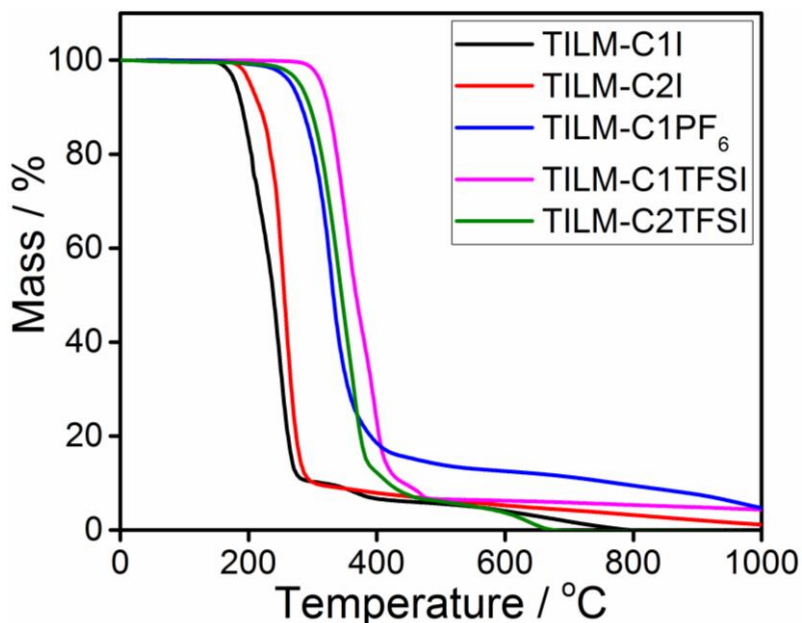


Figure B1. TGA curves of 4-alkyl-1-vinyl-1,2,4-triazolium monomers. Heating rate: 10 K/min under nitrogen atmosphere.

Chapter 3

Dispersion polymerization process. Dispersion polymerization procedures were performed as follows. A 100 mL Schlenk flask was filled with a mixture of 1 g of triazolium-type ionic liquid monomer, 60 mg of water-soluble initiator VA086, and 50 mL of deionized water (monomer concentration 51.1 mM). Then the mixtures were treated with three freeze-pump-thaw cycles to replace air with argon atmosphere. The mixtures were then stirred at 70 °C for 24 h. After cooling down to room temperature, stable translucent dispersions were obtained. The stable dispersions were then purified *via* dialysis against deionized water (>10 folds volume) for two days. The elongated “nanoworms” PIL aggregates were acquired in the same polymerization conditions, except using 5 g ionic liquid monomer instead of 1 g.

4-n-dodecyl-1-vinyl-1,2,4-triazolium iodide (TILM-C12I) (12.23 g, 54%). ^1H NMR (400 MHz, CDCl_3 , δ , ppm): 11.37 (s, 1H), 9.30 (s, 1H), 7.45 (dd, 1H, $J_1=16$ Hz, $J_2=8$ Hz), 6.16 (d, 1H, $J=16$ Hz), 5.42 (d, 1H, $J=8$ Hz), 4.49 (t, 2H, $J=8$ Hz), 1.93 (m, 2H), 1.20 (m, 18H), 0.72 (t, 3H, $J=8$ Hz); ^{13}C NMR (400 MHz, CDCl_3 , δ , ppm): 144.34, 140.65, 128.33, 111.66, 49.25, 31.76, 29.94, 29.49, 29.47, 29.40, 29.30, 29.20, 28.87, 26.07, 22.54, 14.02.

4-n-dodecyl-1-vinyl-1,2,4-triazolium bromide (TILM-C12Br) (10.20 g, 51%). ^1H NMR (400 MHz, CDCl_3 , δ , ppm): 11.82 (s, 1H), 9.61 (s, 1H), 7.56 (dd, 1H, $J_1=16$ Hz, $J_2=8$ Hz), 6.21 (d, 1H, $J=16$ Hz), 5.43 (d, 1H, $J=8$ Hz), 4.55 (t, 2H, $J=8$ Hz), 1.97 (m, 2H), 1.24 (m,

18H), 0.78 (t, 3H, $J=8$ Hz); ^{13}C NMR (400 MHz, CDCl_3 , δ , ppm): 144.56, 141.24, 128.43, 111.31, 77.34, 49.08, 31.79, 30.13, 29.51, 29.42, 29.32, 29.23, 28.90, 26.14, 22.58, 14.04.

4-n-tetradecyl-1-vinyl-1,2,4-triazolium bromide (TILM-C14Br) (14.1 g, 65%). ^1H NMR (400 MHz, CDCl_3 , δ , ppm): 11.88 (s, 1H), 9.53 (s, 1H), 7.59 (dd, 1H, $J_1=16$ Hz, $J_2=8$ Hz), 6.24 (d, 1H, $J=16$ Hz), 5.46 (d, 1H, $J=8$ Hz), 4.57 (t, 2H, $J=8$ Hz), 2.00 (m, 2H), 1.29 (m, 22H), 0.82 (t, 3H, $J=8$ Hz); ^{13}C NMR (400 MHz, CDCl_3 , δ , ppm): 144.74, 141.20, 128.46, 111.24, 49.06, 31.79, 30.12, 29.56, 29.54, 29.53, 29.51, 29.42, 29.31, 29.23, 28.90, 26.13, 22.56, 14.02.

4-n-hexadecyl-1-vinyl-1,2,4-triazolium bromide (TILM-C16Br) (16.5 g, 71%). ^1H NMR (400 MHz, CDCl_3 , δ , ppm): 11.63 (s, 1H), 9.60 (s, 1H), 7.47 (dd, 1H, $J_1=16$ Hz, $J_2=8$ Hz), 6.08 (d, 1H, $J=16$ Hz), 5.31 (d, 1H, $J=8$ Hz), 4.46 (t, 2H, $J=8$ Hz), 1.88 (m, 2H), 1.14 (m, 26H), 0.68 (t, 3H, $J=8$ Hz); ^{13}C NMR (400 MHz, CDCl_3 , δ , ppm): 144.79, 141.12, 128.47, 110.98, 48.96, 33.84, 32.66, 31.74, 30.01, 29.53, 29.50, 29.39, 29.27, 29.19, 28.86, 28.59, 28.00, 26.07, 22.50, 13.95.

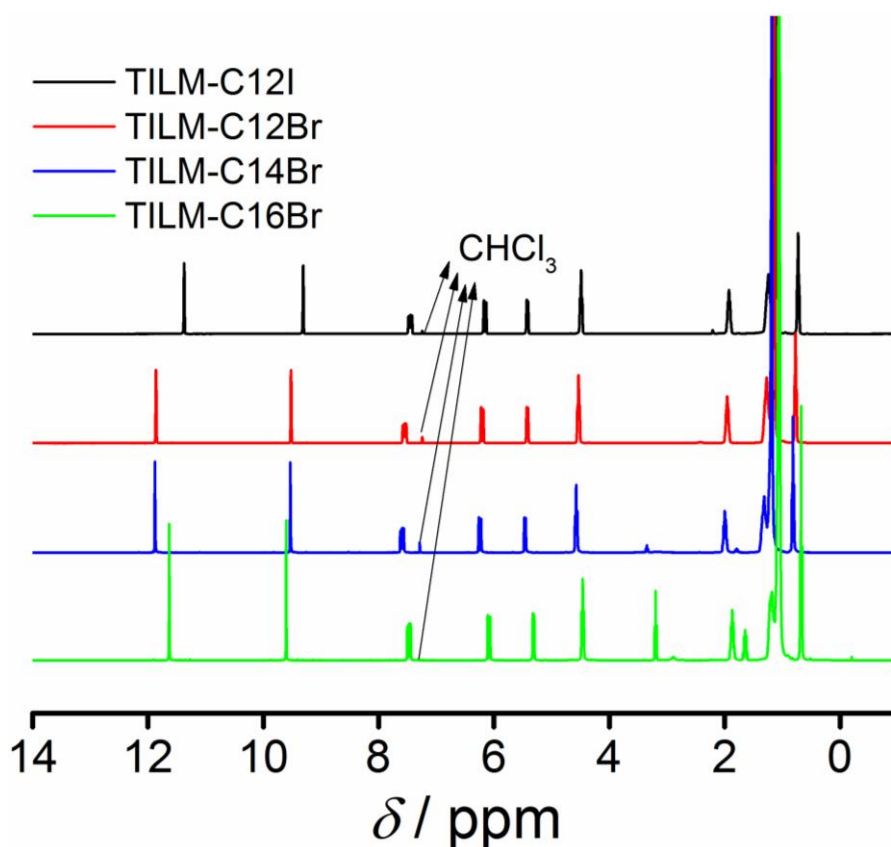


Figure B2. ^1H -NMR spectra of the triazolium ionic liquid monomers in CDCl_3 .

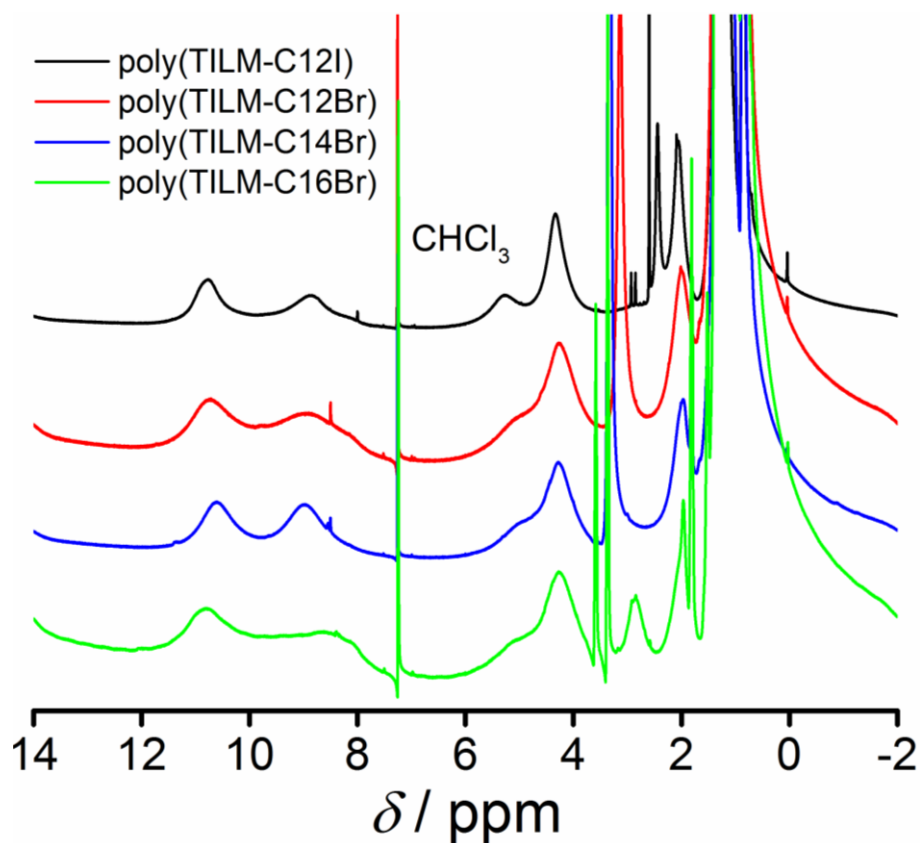


Figure B3. ^1H -NMR spectra of poly(ionic liquid)s in CDCl_3 .

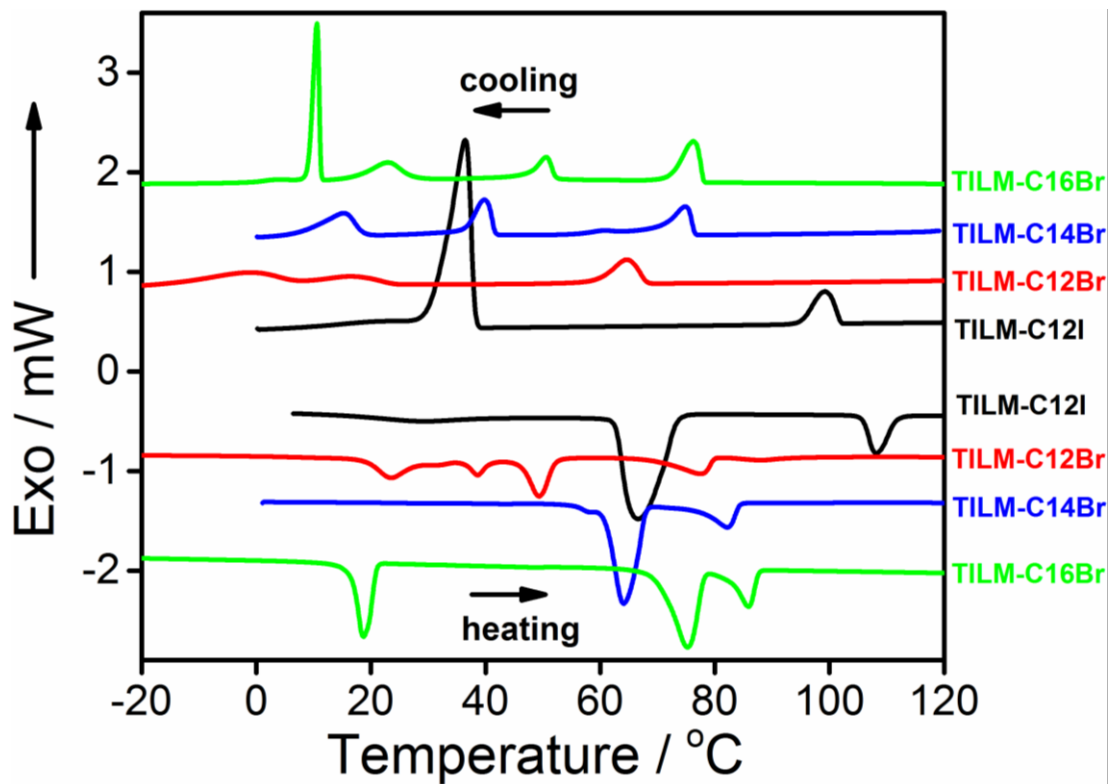


Figure B4. Differential scanning calorimetry curves of the solid 1,2,4-triazolium-type ionic liquid monomers.

Chapter 4

Crosslinker 1,4-butanediyl-4,4'-bis(1-vinyl-1,2,4-triazolium) dibromide (BVTD). In a 100 mL flask, 1-vinyl-1,2,4-triazole (5.0 mL, 5.5 g, 57.8 mmol), 1,4-dibromobutane (3.4 mL, 6.15 g, 28.5 mmol) and BHT as stabilizer (50 mg, 0.23 mmol) were mixed in 10 ml of ethanol. After stirring the mixture in an oil bath at 60 °C for 24 h, the crude product was precipitated in diethyl ether. Then the product was washed with diethyl ether for three times and filtered off. A white solid was obtained. Yield: 10.5 g (89%). ¹H NMR (400 MHz, DMSO-*d*₆, δ, ppm): 10.66 (s, 2H), 9.48 (s, 2H), 7.48 (dd, 2H, *J*₁=16 Hz, *J*₂=8 Hz), 6.01 (d, 2H, *J*=16 Hz), 5.53 (d, 2H, *J*=8 Hz), 4.38 (m, 4H), 1.96 (m, 4H); ¹³C NMR (400 MHz, DMSO-*d*₆, δ, ppm): 145.25, 142.07, 129.61, 110.86, 47.48, 25.58.

Dispersion polymerization process. Dispersion polymerization reactions were performed as follows: a 250 mL Schlenk flask was filled with a mixture of 0.6 g of 1,2,4-triazolium-type ionic liquid monomer, crosslinker **BVTD** (from 0.5 mol% to 40 mol% with regard to the monomer), 30 mg of water-soluble initiator VA086, and 30 mL of deionized water (monomer concentration 20 g/L). After treatment with three freeze-pump-thaw cycles, to replace air with argon inside the flask, the mixtures were stirred at 70 °C for 24 h. After cooling down to room temperature, stable translucent dispersions were obtained. The stable dispersions were then purified *via* dialysis against deionized water for two days.

Chapter 5

Synthesis of 4-methyl-1-vinyl-1,2,4-triazolium triiodide (TILM-C1I₃)

A 50 mL round-bottom flask was filled with a mixture of 4-methyl-1-vinyl-1,2,4-triazolium iodide (2 g, 4.21 mmol) and iodine (1.07 g, 4.21 mmol) with 30 mL acetone. After stirring for 24 h, a tiny fraction of solid residue was filtered off and the transparent solution was dropped into cyclohexane and the resulting precipitate was collected and subsequently washed with cyclohexane for three times. The product was obtained in form of a dark brown solid (4.10 g, 99.0%). ¹H NMR (400 MHz, DMSO-*d*₆, δ, ppm): 10.21 (s, 1H), 9.19 (s, 1H), 7.49 (dd, 1H, *J*₁=16 Hz, *J*₂=8 Hz), 6.01 (d, 1H, *J*=16 Hz), 5.52 (d, 1H, *J*=8 Hz), 3.88 (s, 3H); ¹³C NMR (400 MHz, DMSO-*d*₆, δ, ppm): 146.02, 142.67, 129.63, 110.85, 35.34.

Synthesis of poly(4-methyl-1-vinyl-1,2,4-triazolium triiodide) (poly(TILM-C1I₃))

Following the same procedures described in the synthetic route of triiodide monomer, a dark brown solid (3.5 g, 98.5%) was obtained. ^1H NMR (400 MHz, $\text{DMSO-}d_6$, δ , ppm): 10.03 (br, 1H), 9.12 (m, 1H), 4.45 (br, 1H), 3.91 (br, 3H), 2.34 (br, 2H).

Crystal growth

The single crystal of 4-methyl-1-vinyl-1,2,4-triazolium triiodide (TILM-C1I₃) was obtained by vapor diffusion method: the monomer was dissolved in acetone and stored inside a 5 mL open vial, then the vial was fixed at the bottom of a 250 mL closed bottle containing surrounding diethyl ether. After diethyl ether diffuses through the gas phase into acetone, crystals of the triiodide monomer slowly grew up. The single crystals were stored in the mother solution until testing. The growth of single crystals of TILM-C1I was similar.

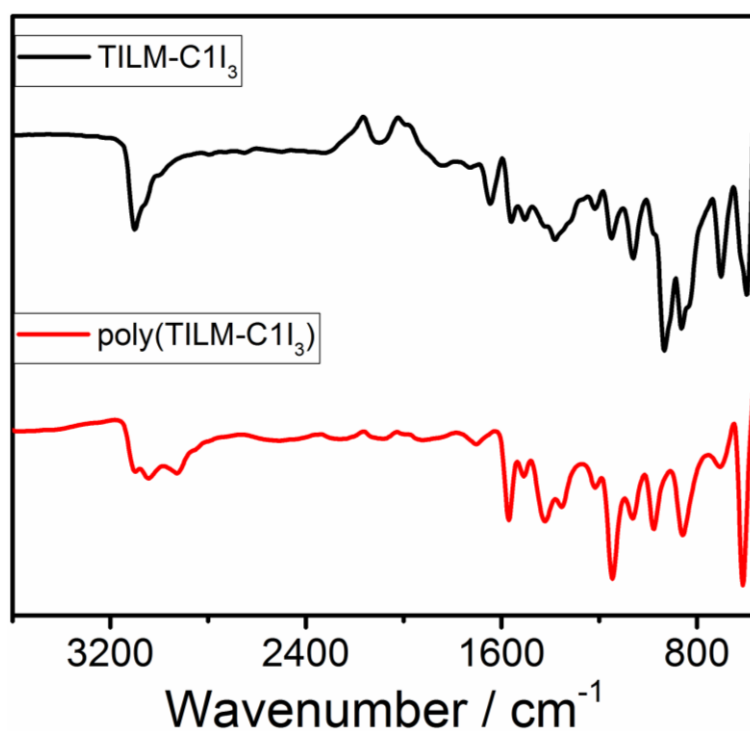


Figure B5. FTIR spectra of TILM-C1I₃ and poly(TILM-C1I₃).

Chapter 6

4-Hexyl-1-vinyl-1,2,4-triazolium iodide (TILM-C6I) (Yield: 96%, 17.04 g): ^1H NMR (400 MHz, $\text{DMSO-}d_6$, δ , ppm): 10.55 (s, 1H), 9.45 (s, 1H), 7.51 (dd, 1H, $J_1=16$ Hz, $J_2=8$ Hz), 6.04 (d, 1H, $J=16$ Hz), 5.58 (d, 1H, $J=8$ Hz), 4.31 (t, 2H, $J=8$ Hz), 1.88 (m, 2H), 1.26 (m, 6H), 0.83 (t, 3H, $J=8$ Hz); ^{13}C NMR (400 MHz, $\text{DMSO-}d_6$, δ , ppm): 145.25, 142.15, 129.76, 110.72, 48.41, 31.00, 28.94, 25.58, 22.29, 14.31.

Poly(4-hexyl-1-vinyl-1,2,4-triazolium) iodide (poly(TILM-C6I)) (Yield: 76%, 2.78 g): ^1H NMR (400 MHz, $\text{DMSO-}d_6$, δ , ppm): 10.51 (br, 1H), 9.33 (m, 1H), 4.75 (m, 1H), 4.23 (br, 2H), 2.58 (br, 2H), 1.90 (br, 2H), 1.30 (br, 6H), 0.85 (br, 3H).

Synthesis of metal cluster stabilized by PILs

Synthesis of Pd/poly(TILM-C6I). In a typical synthesis, 9 mL of dichloromethane and methanol mixture (volume ratio = 2:1) containing 5 mg of poly(TILM-C6I) were added to 0.5 mL of methanol containing $\text{Pd}(\text{NO}_3)_2 \cdot 2\text{H}_2\text{O}$ (0.5 mg of Pd in content). The resulted mixture was further homogenized and subsequently aged for 20 min. Then, a solution of 5 mg of NaBH_4 in 0.5 mL of methanol was immediately added into the above described solution with vigorous shaking, resulting in a well transparent solution of Pd/poly(TILM-C6I).

Synthesis of Pd/poly(ImILM-C6I). Pd/poly(ImILM-C6I) was obtained following the same procedures described for the synthesis of Pd/poly(TILM-C6I), by using 9 mL of dichloromethane and methanol mixture (volume ratio = 2:1) containing poly(ImILM-C6I) (5 mg) in place of poly(TILM-C6I).

Synthesis of Pd/1,2,4-triazolium monomer. The synthetic procedure used to prepare Pd/poly(TILM-C6I) was followed using 9 mL of dichloromethane and methanol mixture (volume ratio = 2:1) containing 1,2,4-triazolium monomer (5 mg) in place of poly(TILM-C6I).

The preparation methods of **4-hexyl-1-vinyl-imidazolium iodide** and **poly(4-hexyl-1-vinyl-imidazolium) iodide** (simplified as “**poly(ImILM-C6I)**”) were described in the literature.^[81]

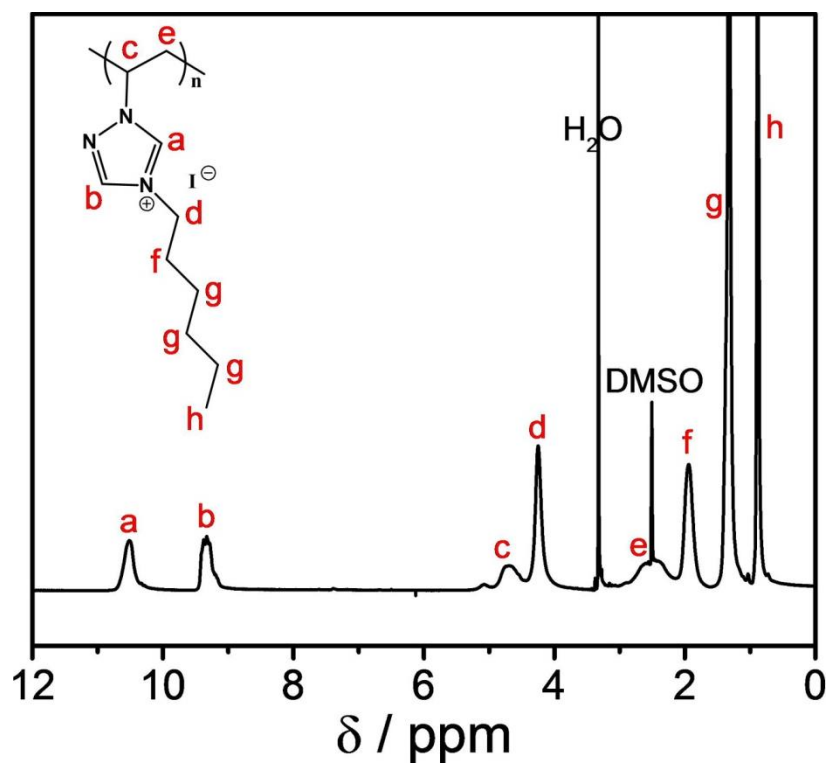


Figure B6. Chemical structure and ¹H-NMR spectrum of (poly(4-hexyl-1-vinyl-1,2,4-triazolium iodide)) (poly(TILM-C6I)).

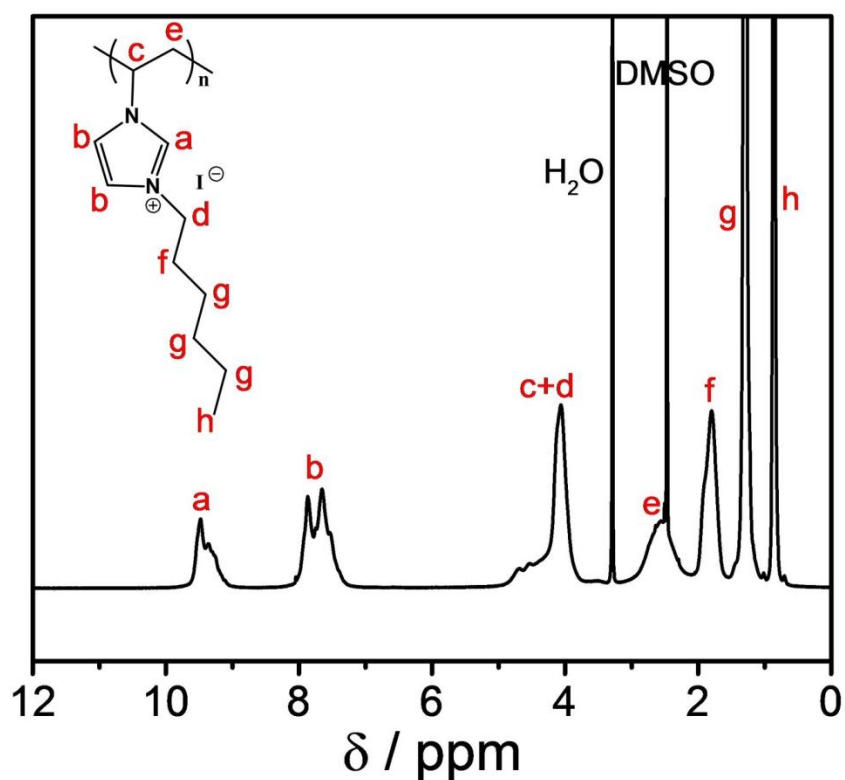


Figure B7. Chemical structure and ¹H-NMR spectrum of (poly(4-hexyl-1-vinyl-imidazolium iodide)) (poly(ImLM-C6I)).

C Co-Authorship Statement

The work described in chapter two was coauthored by Zhang, W. and Yuan, J. *Macromolecular Rapid Communications* 37 (14), pp. 1124-1129 (2016). Weiyi Zhang conducted all the experiments and co-wrote the paper with Jiayin Yuan.

The work described in chapter three was coauthored by Zhang, W.; Kochovski, Z.; Lu, Y.; Schmidt, B. V. K. J.; Antonietti, M. and Yuan, J. *ACS Nano* 10 (8), pp. 7731-7737 (2016). Weiyi Zhang synthesized all polymers and performed all measurements except Cryo-EM & ET. Zdravko Kochovski conducted Cryo-EM & ET. Bernhard V.K.J. Schmidt and Jiayin Yuan designed all experiments. Weiyi Zhang, Zdravko Kochovski, Yan Lu, Bernhard V.K.J. Schmidt, Jiayin Yuan and Markus Antonietti co-wrote the paper.

The work described in chapter four was coauthored by Zhang, W.; Kochovski, Z.; Schmidt, B. V. K. J.; Antonietti, M. and Yuan, J. *Polymer* 107, pp. 509-516 (2016). Weiyi Zhang synthesized all polymers and performed all measurements except Cryo-EM & ET. Zdravko Kochovski conducted Cryo-EM & ET. Weiyi Zhang and Jiayin Yuan designed all experiments. Weiyi Zhang, Zdravko Kochovski, Bernhard V.K.J. Schmidt, Jiayin Yuan and Markus Antonietti co-wrote the paper.

The work described in chapter five was coauthored by Zhang, W.; Willa, C.; Sun, J.-K.; Gutterman, R. and Yuan, J. Awaiting for submission. Weiyi Zhang synthesized all polymers and performed all measurements. Christoph Willa analysed EIS data. Weiyi Zhang and Jiayin Yuan designed all experiments. Weiyi Zhang, Christoph Willa, Jian-Ke Sun, Ryan Guterma and Jiayin Yuan co-wrote the paper.

The work described in chapter six was coauthored by Sun, J.-K.; Kochovski, Z.; Zhang, W.-Y.; Kirmse, H.; Lu, Y.; Antonietti, M. and Yuan, J. Awaiting for submission. Weiyi Zhang synthesized all polymers and measured all the NMR (^1H NMR & ^{13}C NMR) and all the normal TEM. Zdravko Kochovski and Holm Kirmse conducted Cryo-EM and STEM-HAADF. Jian-Ke Sun and Jiayin Yuan designed all experiments and Jian-Ke conducted most of the experiments except mentioned ones. Jian-Ke Sun, Weiyi Zhang, Yan Lu, Markus Antonietti and Jiayin Yuan co-wrote the paper.

D List of publications

1. **Zhang, W.**; Yuan, J.: Poly(1-Vinyl-1,2,4-triazolium) Poly(Ionic Liquid)s: Synthesis and the Unique Behavior in Loading Metal Ions. *Macromolecular Rapid Communications* 37 (14), pp. 1124-1129 (2016)
2. **Zhang, W.**; Kochovski, Z.; Lu, Y.; Schmidt, B. V. K. J.; Antonietti, M.; Yuan, J.: Internal Morphology-Controllable Self-Assembly in Poly(Ionic Liquid) Nanoparticles. *ACS Nano* 10 (8), pp. 7731-7737 (2016)
3. **Zhang, W.**; Kochovski, Z.; Schmidt, B. V. K. J.; Antonietti, M.; Yuan, J.: Crosslinked 1,2,4-triazolium-type poly(ionic liquid) nanoparticles. *Polymer* 107, pp. 509-516 (2016)
4. Grygiel, K.; **Zhang, W.**; Detrembleur, C.; Yuan, J.: Unexpected LCST-type phase behaviour of a poly(vinyl thiazolium) polymer in acetone. *RSC Advances* 6 (62), pp. 57117-57121 (2016)
5. Gao, M.-R.; Yu, S.-H.; Yuan, J.; **Zhang, W.**; Antonietti, M.: Poly(ionic liquid)-Mediated Morphogenesis of Bismuth Sulfide with a Tunable Band Gap and Enhanced Electrocatalytic Properties. *Angewandte Chemie* 128 (41), pp. 13004-13008 (2016)
6. H. Wang, S. Min, C. Ma, Z. Liu, **W. Zhang**, Q. Wang, D. Li, Y. Li, S. Turner, Y. Han, H. Zhu, E. Abou-hamad, M. N. Hedhili, J. Pan, W. Yu, K.-W. Huang, L.-J. Li, J. Yuan, M. Antonietti, T. Wu, *Nature Communications* 8, pp. 13592-13962 (2017).
7. Jian-Ke Sun, Hui-Juan Lin, **Wei-Yi Zhang**, Min-Rui Gao, Markus Antonietti & Jiayin Yuan*: A tale of two membranes: from poly(ionic liquid) to metal-organic framework membranes via pseudomorphic replication. Submitted.
8. **Wei-Yi Zhang**, Christoph Willa, Jian-Ke Sun, Ryan Guterman, Jiayin Yuan*: Poly(1-vinyl-1,2,4-triazolium triiodide): synthesis, basic properties and electrochemical behaviors. Awaiting for submission.
9. Jian-Ke Sun, Zdravko Kochovski, **Wei-Yi Zhang**, Holm Kirmse, Yan Lu, Markus Antonietti, and Jiayin Yuan*: Highly dispersed metal clusters stabilized by hollow-like poly(ionic liquid)s. Awaiting for submission.
10. Jian-Ke Sun#, **Wei-Yi Zhang**#, Hui-Juan Lin, Markus Antonietti, and Jiayin Yuan*: New trick of old chemistry: Ultrasensitive PH-responsive Poly(1,2,4-triazolium) Membranes based on Asymmetric Carbene Distribution. Awaiting for submission. (#:co-first author)

E List of abbreviations

PIL	Poly(ionic liquid)
IL	Ionic liquid
ILM	Ionic liquid monomer
TFSI	Bis(trifluoromethylsulfonyl)imide
PF ₆	Hexafluorophosphate
Ppm	Parts per million
BF ₄	Tetrafluoroborate
CF ₃ SO ₃	Trifluoromethanesulfonate
CRP	Controlled radical polymerizations
ATRP	Atom transfer radical polymerization
RAFT	Reversible addition–fragmentation chain-transfer polymerization
CMRP	Cobalt-mediated radical polymerization
T_g	Glass transition temperature
Poly(NHC)s	Poly(<i>N</i> -heterocyclic carbene)s
Poly(NHC-CO ₂)	Poly(<i>N</i> -heterocyclic carbene-CO ₂) adducts
DSC	Differential scanning calorimetry
GPC	Gel permeation chromatography
TILMs	1,2,4-Triazolium-based ionic liquids
TPIL	1,2,4-Triazolium-based poly(ionic liquid)
Cryo-EM	Cryogenic electron microscopy
Cryo-ET	Cryogenic electron tomography
VA086	2,2'-Azobis[2-methyl- <i>N</i> -(2-hydroxyethyl)propionamide]
DLS	Dynamic light scattering

D_h	Hydrodynamic diameter
TEM	Transmission electron microscopy
SEM	Scanning electron microscopy
AIBN	Azobisisobutyronitrile
FFT	Fast Fourier transform
SAXS	Small-angle X-ray scattering
DMF	N,N-dimethylformamide
DMSO	Dimethyl sulfoxide
PISA	Polymerization induced self-assembly
ATR	Attenuated total reflection
FTIR	Fourier transform infrared spectroscopy
BVTD	1,4-Butanediyl-4,4'-bis(1-vinyl-1,2,4-triazolium) dibromide
TILM-CnX	4-alkyl-1-vinyl-1,2,4-triazolium X (X=halide, or TFSI, PF ₆ , I ₃)
Poly(TILM-CnX) I ₃)	Poly(4-alkyl-1-vinyl-1,2,4-triazolium) X (X=halide, or TFSI, PF ₆ , I ₃)
EA	Elemental analysis
CNTs	Multi-wall carbon nanotubes
¹ H NMR	Proton nuclear magnetic resonance
¹³ C NMR	Carbon nuclear magnetic resonance
TGA	Thermogravimetric analysis
UV/Vis	Ultraviolet-visible spectroscopy
XPS	X-ray photoelectron spectroscopy
XRD	X-ray diffraction

Pd	Palladium
STEM	Scanning transmission electron microscopy
HAADF-STEM microscopy	High-angle annular dark field scanning transmission electron
EIS	Electrochemical impedance spectroscopy
CV	Cyclic voltammetry
PdCs	Palladium clusters

F Declaration

Hiermit erkläre ich, dass ich die vorliegende Arbeit selbstständig angefertigt und keine anderen als die angegebenen Hilfsmittel und Quellen verwendet habe.

Weiyi Zhang

Potsdam, den 20.01.2017

Thesis reviewer:

Prof. Dr. Markus Antonietti

Prof. Dr. Andreas Taubert

Prof. Dr. Eric Drockenmüller

G Acknowledgements

This dissertation has been developed during the last two and half years at the Max Planck Institute of Colloids and Interfaces in Golm. Without the intensive work in the lab as well as the help from people in the institute, this achievement will not be possible. Here I want to express my gratitude to all the people who helped/inspired/encouraged me during these tough years.

First, I really appreciate my supervisor Prof. Dr. Markus Antonietti for giving me the opportunity to work in such creative department. His fine sense of science and broad knowledge in chemistry guided and inspired everyone in this institute and makes us benefit a lot.

I heartedly thank my co-supervisor Prof. Dr. Jiayin Yuan, for his kind and careful supervising over last two and half years. Without him, I will not be able to discover the unknown area of PILs alone and understand the beauty of chemistry. Furthermore, we will start another new journey in the United States, I am looking forward to that.

Words are not enough to express my great appreciation for all the members in and out of our PILs group: they are Martina Amborgi, Haojie Song, Jie Yang, Alessandro Dani, Jiang Gong, Huijuan Lin. Han Miao, Guipeng Yu, Karoline Tauber, Konrad Grygiel, Simon Prescher, Yongjun Men, Ana M. Fernandez, Congxiao Cao, Christoph Willa, Jingyang Yu. Chris, thanks for the EIS! Zdravko! Thanks for the Cryo-EM/ET!

I would specially thank four members in our group: Ryan Guterman, Jian-Ke Sun, Min-Rui Gao and Antje Voelkel. Ryan gets a good humor sense and he helped me a lot in English writing as well as academic thinking and discussion. Jian-Ke is an excellent collaborator and tutor in the research topics, his sense of hot frontier of science and the efforts in work is impressive and encouraging for me. Min-Rui is also a good collaborator and he is an idol in academy who deserve respect. Now Min-Rui is a full professor in USTC, China. Cong! Antje! Thanks for the pumpkin soups every year!

Thanks the professors who reviewed my thesis. They are: Prof. Dr. Markus Antonietti, Prof. Dr. Andreas Taubert and Prof. Dr. Eric Drockenmuller.

I would thank Dr. Bernhard V. K. J. Schmidt for guiding me in PIL nanoparticle self-assembly and Prof. Dr. Andreas Taubert for giving me the chance in teaching practical lab course.

Thanks Wuqi, Thomas, Jochen and Steffen for the efforts they made for my German abstract!

Without help of our lovely technicians, my thesis will not be possible. They are Ursula Lubahn, Silvia Pirok, Marlies Gräwert, Rona Pitschke, Heike Runke, Katharina Otte, Jürgen Hartmann, Regina Rothe, Ingrid Zenke, Olaf Niemeyer, Ingrid Zenke and Bodo Ryschka.

Thanks also go to those who shared lots of good memories with me in Germany: Jingsan, Xiaofei, Zhilong, Eddie, Chunxiang, Berti, Jochen, Huijun, Jie(Cao), Yaozu, Hefeng, Qinan, Afroditi, Max, Martin, Zhaoyong, Lina, Zhou, Xiaoqian, Ken, Kai and many more.

Thank my family for the love, patience and support!

H References

- [1] P. Walden, *Bulletin of the Russian Academy of Sciences* 1914, 405.
- [2] N. V. Plechkova, K. R. Seddon, *Chemical Society Reviews* 2008, 37, 123.
- [3] O. Wallach, *Berichte der deutschen chemischen Gesellschaft* 1883, 16, 534.
- [4] T. Welton, *Chemical Reviews* 1999, 99, 2071.
- [5] D. R. MacFarlane, N. Tachikawa, M. Forsyth, J. M. Pringle, P. C. Howlett, G. D. Elliott, J. H. Davis, M. Watanabe, P. Simon, C. A. Angell, *Energy & Environmental Science* 2014, 7, 232; R. D. Rogers, K. R. Seddon, *Science* 2003, 302, 792; T. L. Greaves, C. J. Drummond, *Chemical Reviews* 2008, 108, 206.
- [6] J. Yuan, M. Antonietti, *Polymer* 2011, 52, 1469.
- [7] J. Yuan, D. Mecerreyes, M. Antonietti, *Progress in Polymer Science* 2013, 38, 1009.
- [8] J. C. Salamone, S. C. Israel, P. Taylor, B. Snider, *Polymer* 1973, 14, 639.
- [9] O. Hiroyuki, I. Kaori, *Chemistry Letters* 1998, 27, 751.
- [10] J. Lu, F. Yan, J. Texter, *Progress in Polymer Science* 2009, 34, 431.
- [11] D. Mecerreyes, *Progress in Polymer Science* 2011, 36, 1629.
- [12] J. Tang, W. Sun, H. Tang, M. Radosz, Y. Shen, *Macromolecules* 2005, 38, 2037.
- [13] H. L. Ricks-Laskoski, A. W. Snow, *Journal of the American Chemical Society* 2006, 128, 12402.
- [14] S. Prescher, F. Polzer, Y. Yang, M. Siebenbürger, M. Ballauff, J. Yuan, *Journal of the American Chemical Society* 2014, 136, 12.
- [15] M. G. Cowan, D. L. Gin, R. D. Noble, *Accounts of Chemical Research* 2016, 49, 724.
- [16] O. Green, S. Grubjesic, S. Lee, M. A. Firestone, *Polymer Reviews* 2009, 49, 339.
- [17] B. Qiu, B. Lin, F. Yan, *Polymer International* 2013, 62, 335.
- [18] R. Marcilla, J. Alberto Blazquez, J. Rodriguez, J. A. Pomposo, D. Mecerreyes, *Journal of Polymer Science Part A: Polymer Chemistry* 2004, 42, 208.
- [19] K. Matyjaszewski, *Current Opinion in Solid State and Materials Science* 1996, 1, 769.
- [20] G. Moad, E. Rizzardo, S. H. Thang, *Polymer* 2008, 49, 1079.
- [21] K. Matyjaszewski, J. Xia, *Chemical Reviews* 2001, 101, 2921.
- [22] M. Ouchi, T. Terashima, M. Sawamoto, *Chemical Reviews* 2009, 109, 4963.
- [23] H. Ohno, *Electrochimica Acta* 2001, 46, 1407.
- [24] N. Nishimura, H. Ohno, *Polymer* 2014, 55, 3289.
- [25] K. Hoshino, M. Yoshio, T. Mukai, K. Kishimoto, H. Ohno, T. Kato, *Journal of Polymer Science Part A: Polymer Chemistry* 2003, 41, 3486; J. Huang, C.-a. Tao, Q. An, W. Zhang, Y. Wu, X. Li, D. Shen, G. Li, *Chemical Communications* 2010, 46, 967.
- [26] R. Guterman, E. R. Gillies, P. J. Ragona, *Langmuir* 2015, 31, 5181.
- [27] S. Grubjesic, S. Seifert, M. A. Firestone, *Macromolecules* 2009, 42, 5461.
- [28] J. Yuan, S. Soll, M. Drechsler, A. H. Muller, M. Antonietti, *J Am Chem Soc* 2011, 133, 17556.
- [29] J. Tang, M. Radosz, Y. Shen, *Macromolecules* 2008, 41, 493; J. Tang, H. Tang, W. Sun, M. Radosz, Y. Shen, *Journal of Polymer Science Part A: Polymer Chemistry* 2005, 43, 5477; J. E. Bara, E. S. Hatakeyama, D. L. Gin, R. D. Noble, *Polymers for Advanced Technologies* 2008, 19, 1415.
- [30] Q. Ye, T. Gao, F. Wan, B. Yu, X. Pei, F. Zhou, Q. Xue, *Journal of Materials Chemistry* 2012, 22, 13123.
- [31] B. P. Mudraboyina, M. M. Obadia, I. Abdelhedi-Miladi, I. Allaoua, E. Drockenmuller, *European Polymer Journal* 2015, 62, 331; I. Abdelhedi-Miladi, M. M. Obadia, I. Allaoua, A. Serghei, H. B. Romdhane, E. Drockenmuller, *Macromolecular Chemistry and Physics* 2014, 215, 2229.
- [32] A. T. De La Hoz, K. M. Miller, *Polymer* 2015, 72, 1.
- [33] H. He, D. Luebke, H. Nulwala, K. Matyjaszewski, *Macromolecules* 2014, 47, 6601.
- [34] D. Cordella, A. Debuigne, C. Jérôme, Z. Kochovski, D. Taton, C. Detrembleur, *Macromolecular Rapid Communications* 2016, 37, 1181.
- [35] D. Cordella, A. Kermagoret, A. Debuigne, C. Jérôme, D. Mecerreyes, M. Isik, D. Taton, C. Detrembleur, *Macromolecules* 2015, 48, 5230; Y. Men, M. Drechsler, J. Yuan, *Macromolecular Rapid Communications* 2013, 34, 1721.

- [36] M. Fevre, J. Pinaud, Y. Gnanou, J. Vignolle, D. Taton, *Chemical Society Reviews* 2013, 42, 2142.
- [37] J. Pinaud, J. Vignolle, Y. Gnanou, D. Taton, *Macromolecules* 2011, 44, 1900.
- [38] A. S. Shaplov, P. S. Vlasov, M. Armand, E. I. Lozinskaya, D. O. Ponkratov, I. A. Malyshkina, F. Vidal, O. V. Okatova, G. M. Pavlov, C. Wandrey, I. A. Godovikov, Y. S. Vygodskii, *Polymer Chemistry* 2011, 2, 2609.
- [39] S. Soll, P. Zhang, Q. Zhao, Y. Wang, J. Yuan, *Polymer Chemistry* 2013, 4, 5048; L. Zhang, J. Du, T. Ran, H. Gao, Y. Liao, *Journal of Materials Science* 2016, 51, 7186; R. Rajan, K. Matsumura, *Journal of Materials Chemistry B* 2015, 3, 5683.
- [40] J. Yuan, A. G. Marquez, J. Reinacher, C. Giordano, J. Janek, M. Antonietti, *Polymer Chemistry* 2011, 2, 1654.
- [41] in *Porous Polymers: Design, Synthesis and Applications*, The Royal Society of Chemistry, 2016, 249.
- [42] F. Yan, J. Texter, *Angewandte Chemie* 2007, 119, 2492.
- [43] J. S. Lee, H. Luo, G. A. Baker, S. Dai, *Chemistry of Materials* 2009, 21, 4756.
- [44] Q. Zhao, P. Zhang, M. Antonietti, J. Yuan, *Journal of the American Chemical Society* 2012, 134, 11852.
- [45] Q. Zhao, M. Yin, A. P. Zhang, S. Prescher, M. Antonietti, J. Yuan, *Journal of the American Chemical Society* 2013, 135, 5549.
- [46] Q. Zhao, J. Heyda, J. Dzubiella, K. Täuber, J. W. C. Dunlop, J. Yuan, *Advanced Materials* 2015, 27, 2913.
- [47] S. Zhang, K. Dokko, M. Watanabe, *Chemical Science* 2015, 6, 3684.
- [48] E. Lam, J. H. T. Luong, *ACS Catalysis* 2014, 4, 3393; L. Dai, D. W. Chang, J.-B. Baek, W. Lu, *Small* 2012, 8, 1130; S. Gupta, N.-H. Tai, *Journal of Materials Chemistry A* 2016, 4, 1550.
- [49] X. Wang, S. Dai, *Angewandte Chemie International Edition* 2010, 49, 6664; J. S. Lee, X. Wang, H. Luo, G. A. Baker, S. Dai, *Journal of the American Chemical Society* 2009, 131, 4596.
- [50] J. Yuan, C. Giordano, M. Antonietti, *Chemistry of Materials* 2010, 22, 5003.
- [51] P. Zhang, J. Yuan, T.-P. Fellingner, M. Antonietti, H. Li, Y. Wang, *Angewandte Chemie International Edition* 2013, 52, 6028.
- [52] D. Kuzmicz, S. Prescher, F. Polzer, S. Soll, C. Seitz, M. Antonietti, J. Yuan, *Angewandte Chemie* 2014, 126, 1080.
- [53] P. Zhang, Z.-A. Qiao, X. Jiang, G. M. Veith, S. Dai, *Nano Letters* 2015, 15, 823.
- [54] Y. Yang, M. Ambrogio, H. Kirmse, Y. Men, M. Antonietti, J. Yuan, *Chemistry of Materials* 2015, 27, 127.
- [55] G. M. Whitesides, B. Grzybowski, *Science* 2002, 295, 2418.
- [56] R. Hayes, G. G. Warr, R. Atkin, *Chemical Reviews* 2015, 115, 6357.
- [57] M. Yoshio, T. Mukai, H. Ohno, T. Kato, *Journal of the American Chemical Society* 2004, 126, 994.
- [58] Y. Zhou, J. H. Schattka, M. Antonietti, *Nano Letters* 2004, 4, 477.
- [59] R. L. Weber, Y. Ye, A. L. Schmitt, S. M. Banik, Y. A. Elabd, M. K. Mahanthappa, *Macromolecules* 2011, 44, 5727.
- [60] R. Tejero, A. Arbe, M. Fernández-García, D. López, *Macromolecules* 2015, 48, 7180.
- [61] J. Yuan, M. Antonietti, *Macromolecules* 2011, 44, 744.
- [62] J. H. Crandon, C. C. Lund, D. B. Dill *New England Journal of Medicine* 1940, 223, 353.
- [63] H. Kadin, M. Osadca, *Journal of Agricultural and Food Chemistry* 1959, 7, 358.
- [64] S. K. Gebauer, T. L. Psota, P. M. Kris-Etherton, *Lipids* 2007, 42, 787.
- [65] K. J. T. Noonan, K. M. Hugar, H. A. Kostalik, E. B. Lobkovsky, H. D. Abruña, G. W. Coates, *Journal of the American Chemical Society* 2012, 134, 18161.
- [66] H. Xue, H. Gao, J. n. M. Shreeve, *Journal of Polymer Science Part A: Polymer Chemistry* 2008, 46, 2414.
- [67] H. Chen, J.-H. Choi, D. Salas-de la Cruz, K. I. Winey, Y. A. Elabd, *Macromolecules* 2009, 42, 4809.

- [68] R. Marcilla, J. A. Blazquez, R. Fernandez, H. Grande, J. A. Pomposo, D. Mecerreyes, *Macromolecular Chemistry and Physics* 2005, 206, 299.
- [69] J. Tang, H. Tang, W. Sun, H. Plancher, M. Radosz, Y. Shen, *Chemical Communications* 2005, 3325; F. Yan, J. Texter, *Chemical Communications* 2006, 2696; M.-R. Gao, S.-H. Yu, J. Yuan, W. Zhang, M. Antonietti, *Angewandte Chemie* 2016, 128, 13004; Q. Zhao, J. W. C. Dunlop, X. Qiu, F. Huang, Z. Zhang, J. Heyda, J. Dzubiella, M. Antonietti, J. Yuan, *Nat Commun* 2014, 5.
- [70] Y. Jeong, J.-S. Ryu, *The Journal of Organic Chemistry* 2010, 75, 4183; M.-C. Tseng, H.-T. Cheng, M.-J. Shen, Y.-H. Chu, *Organic Letters* 2011, 13, 4434.
- [71] Y. R. Mirzaei, B. Twamley, J. n. M. Shreeve, *The Journal of Organic Chemistry* 2002, 67, 9340.
- [72] M. S. Kerr, J. Read de Alaniz, T. Rovis, *The Journal of Organic Chemistry* 2005, 70, 5725.
- [73] M. M. Obadia, G. Colliat-Dangus, A. Debuigne, A. Serghei, C. Detrembleur, E. Drockenmuller, *Chemical Communications* 2015, 51, 3332; M. M. Obadia, B. P. Mudraboyina, I. Allaoua, A. Haddane, D. Montarnal, A. Serghei, E. Drockenmuller, *Macromolecular Rapid Communications* 2014, 35, 794; M. M. Obadia, E. Drockenmuller, *Chemical Communications* 2016, 52, 2433.
- [74] H. W. Altland, E. L. Dedio, G. J. McSweeney, 1983.
- [75] U. G. Brauer, A. T. De La Hoz, K. M. Miller, *Journal of Molecular Liquids* 2015, 210, Part B, 286.
- [76] T. Buffeteau, J. Grondin, Y. Danten, J.-C. Lassègues, *The Journal of Physical Chemistry B* 2010, 114, 7587; O. Höfft, S. Bahr, V. Kempter, *Langmuir* 2008, 24, 11562; I. Rey, P. Johansson, J. Lindgren, J. C. Lassègues, J. Grondin, L. Servant, *The Journal of Physical Chemistry A* 1998, 102, 3249.
- [77] E. R. Talaty, S. Raja, V. J. Storhaug, A. Dölle, W. R. Carper, *The Journal of Physical Chemistry B* 2004, 108, 13177.
- [78] R. S. Massey, C. J. Collett, A. G. Lindsay, A. D. Smith, A. C. O'Donoghue, *Journal of the American Chemical Society* 2012, 134, 20421.
- [79] M. Ballauff, Y. Lu, *Polymer* 2007, 48, 1815; O. J. Cayre, N. Chagneux, S. Biggs, *Soft Matter* 2011, 7, 2211; J. Y. Cheng, A. M. Mayes, C. A. Ross, *Nat Mater* 2004, 3, 823; H. Cui, Z. Chen, S. Zhong, K. L. Wooley, D. J. Pochan, *Science* 2007, 317, 647.
- [80] Y. Bae, S. Fukushima, A. Harada, K. Kataoka, *Angewandte Chemie International Edition* 2003, 42, 4640; A. H. Gröschel, T. I. Löbbling, P. D. Petrov, M. Müllner, C. Kuttner, F. Wieberger, A. H. E. Müller, *Angewandte Chemie International Edition* 2013, 52, 3602.
- [81] A. H. Gröschel, A. Walther, T. I. Lobling, F. H. Schacher, H. Schmalz, A. H. E. Müller, *Nature* 2013, 503, 247; H. Qiu, Z. M. Hudson, M. A. Winnik, I. Manners, *Science* 2015, 347, 1329; S.-J. Jeon, G.-R. Yi, S.-M. Yang, *Advanced Materials* 2008, 20, 4103; T. Gadt, N. S. Jeong, G. Cambridge, M. A. Winnik, I. Manners, *Nat Mater* 2009, 8, 144; Z. Nie, D. Fava, E. Kumacheva, S. Zou, G. C. Walker, M. Rubinstein, *Nat Mater* 2007, 6, 609.
- [82] A. Hanisch, A. H. Gröschel, M. Förtsch, M. Drechsler, H. Jinnai, T. M. Ruhland, F. H. Schacher, A. H. E. Müller, *ACS Nano* 2013, 7, 4030.
- [83] D. Klinger, C. X. Wang, L. A. Connal, D. J. Audus, S. G. Jang, S. Kraemer, K. L. Killops, G. H. Fredrickson, E. J. Kramer, C. J. Hawker, *Angew Chem Int Ed Engl* 2014, 53, 7018; S. G. Jang, D. J. Audus, D. Klinger, D. V. Krogstad, B. J. Kim, A. Cameron, S. W. Kim, K. T. Delaney, S. M. Hur, K. L. Killops, G. H. Fredrickson, E. J. Kramer, C. J. Hawker, *J Am Chem Soc* 2013, 135, 6649.
- [84] Z. Lu, G. Liu, H. Phillips, J. M. Hill, J. Chang, R. A. Kydd, *Nano Letters* 2001, 1, 683; B.-S. Kim, T. A. Taton, *Langmuir* 2007, 23, 2198.
- [85] N. Doshi, S. Mitragotri, *Journal of The Royal Society Interface* 2010; J. Shim, H. Seok Kang, W.-S. Park, S.-H. Han, J. Kim, I.-S. Chang, *Journal of Controlled Release* 2004, 97, 477.
- [86] M. Antonietti, M. Maskos, *Macromolecules* 1996, 29, 4199; M. Ballauff, G. F. Schmidt, *Molecular Crystals and Liquid Crystals* 1987, 147, 163.
- [87] M. Ballauff, G. F. Schmidt, *Die Makromolekulare Chemie, Rapid Communications* 1987, 8, 93; A. F. Thünemann, *Progress in Polymer Science* 2002, 27, 1473.
- [88] D. S.-d. la Cruz, M. D. Green, Y. Ye, Y. A. Elabd, T. E. Long, K. I. Winey, *Journal of Polymer Science Part B: Polymer Physics* 2012, 50, 338.
- [89] P. Chi, Z. Wang, B. Li, A.-C. Shi, *Langmuir* 2011, 27, 11683; B. Yu, B. Li, Q. Jin, D. Ding, A.-C. Shi, *Macromolecules* 2007, 40, 9133.

- [90] N. J. Warren, S. P. Armes, *Journal of the American Chemical Society* 2014, 136, 10174.
- [91] C. Burger, M. A. Micha, S. Oestreich, S. Förster, M. Antonietti, *EPL (Europhysics Letters)* 1998, 42, 425.
- [92] W. Zhang, Z. Kochovski, Y. Lu, B. V. K. J. Schmidt, M. Antonietti, J. Yuan, *ACS Nano* 2016, 10, 7731.
- [93] R. K. O'Reilly, C. J. Hawker, K. L. Wooley, *Chemical Society Reviews* 2006, 35, 1068.
- [94] T. Rudolph, F. H. Schacher, *European Polymer Journal* 2016, 80, 317; M. Koebe, M. Drechsler, J. Weber, J. Yuan, *Macromolecular Rapid Communications* 2012, 33, 646.
- [95] K. Nakabayashi, A. Umeda, Y. Sato, H. Mori, *Polymer* 2016, 96, 81; W. Zhang, J. Yuan, *Macromolecular Rapid Communications* 2016, 37, 1124.
- [96] M. Koebe, M. Drechsler, J. Weber, J. Yuan, *Macromol Rapid Commun* 2012, 33, 646.
- [97] J. Yuan, S. Prescher, K. Sakaushi, M. Antonietti, *J. Mater. Chem. A* 2015, 3, 7229; P. Coupillaud, M. Fèvre, A.-L. Wirocius, K. Aissou, G. Fleury, A. Debuigne, C. Detrembleur, D. Mecerreyes, J. Vignolle, D. Taton, *Macromolecular Rapid Communications* 2014, 35, 422; C. Shi, L. Qiu, X. Chen, H. Zhang, L. Wang, F. Yan, *ACS Applied Materials & Interfaces* 2013, 5, 1453.
- [98] M. Döbbelin, I. Azcune, M. Bedu, A. Ruiz de Luzuriaga, A. Genua, V. Jovanovski, G. Cabañero, I. Odriozola, *Chemistry of Materials* 2012, 24, 1583; X. Chen, J. Zhao, J. Zhang, L. Qiu, D. Xu, H. Zhang, X. Han, B. Sun, G. Fu, Y. Zhang, F. Yan, *Journal of Materials Chemistry* 2012, 22, 18018; M. Díaz, A. Ortiz, I. Ortiz, *Journal of Membrane Science* 2014, 469, 379.
- [99] J. Wu, Z. Lan, J. Lin, M. Huang, Y. Huang, L. Fan, G. Luo, *Chemical Reviews* 2015, 115, 2136.
- [100] H. C. Zur Loye, B. J. Heyen, H. O. Marcy, D. C. DeGroot, C. R. Kannewurf, D. F. Shriver, *Chemistry of Materials* 1990, 2, 603.
- [101] L. C. Hardy, D. F. Shriver, *Journal of the American Chemical Society* 1986, 108, 2887.
- [102] A. F. Wells, *Structural inorganic chemistry*, Clarendon Press ; Oxford University Press, Oxford [Oxfordshire]; New York 1984.
- [103] P. H. Svensson, L. Kloo, *Chemical Reviews* 2003, 103, 1649.
- [104] P. Deplano, J. R. Ferraro, M. L. Mercuri, E. F. Trogu, *Coordination Chemistry Reviews* 1999, 188, 71; J. Wu, S. Hao, Z. Lan, J. Lin, M. Huang, Y. Huang, P. Li, S. Yin, T. Sato, *Journal of the American Chemical Society* 2008, 130, 11568.
- [105] C. C. Clark, A. Marton, R. Srinivasan, A. A. Narducci Sarjeant, G. J. Meyer, *Inorganic Chemistry* 2006, 45, 4728.
- [106] T. Sugano, K. Yamada, G. Saito, M. Kinoshita, *Solid State Communications* 1985, 55, 137; R. J. Webb, T. Y. Dong, C. G. Pierpont, S. R. Boone, R. K. Chadha, D. N. Hendrickson, *Journal of the American Chemical Society* 1991, 113, 4806.
- [107] M. E. Orazem, I. Frateur, B. Tribollet, V. Vivier, S. Marcelin, N. Pébère, A. L. Bunge, E. A. White, D. P. Riemer, M. Musiani, *Journal of The Electrochemical Society* 2013, 160, C215; V. F. Lvovich, in *Impedance Spectroscopy*, John Wiley & Sons, Inc., 2012, 49.
- [108] J. Yuan, M. Antonietti, in *Applications of Ionic Liquids in Polymer Science and Technology*, (Ed: D. Mecerreyes), Springer Berlin Heidelberg, Berlin, Heidelberg 2015, 47.
- [109] I. D. Raistrick, D. R. Franceschetti, J. R. Macdonald, in *Impedance Spectroscopy*, John Wiley & Sons, Inc., 2005, 27.
- [110] N. Bonanos, B. C. H. Steele, E. P. Butler, in *Impedance Spectroscopy*, John Wiley & Sons, Inc., 2005, 205.
- [111] Y. Lu, W. Chen, *Chemical Society Reviews* 2012, 41, 3594; Y. Tao, M. Li, J. Ren, X. Qu, *Chemical Society Reviews* 2015, 44, 8636.
- [112] C.-A. J. Lin, T.-Y. Yang, C.-H. Lee, S. H. Huang, R. A. Sperling, M. Zanella, J. K. Li, J.-L. Shen, H.-H. Wang, H.-I. Yeh, W. J. Parak, W. H. Chang, *ACS Nano* 2009, 3, 395; L. Zhang, E. Wang, *Nano Today* 2014, 9, 132; S. Wang, X. Meng, A. Das, T. Li, Y. Song, T. Cao, X. Zhu, M. Zhu, R. Jin, *Angewandte Chemie International Edition* 2014, 53, 2376.
- [113] X.-F. Yang, A. Wang, B. Qiao, J. Li, J. Liu, T. Zhang, *Accounts of Chemical Research* 2013, 46, 1740.

- [114] P. J. G. Goulet, R. B. Lennox, *Journal of the American Chemical Society* 2010, 132, 9582; R. M. Crooks, M. Zhao, L. Sun, V. Chechik, L. K. Yeung, *Accounts of Chemical Research* 2001, 34, 181.
- [115] M. E. Strayer, J. M. Binz, M. Tanase, S. M. Kamali Shahri, R. Sharma, R. M. Rioux, T. E. Mallouk, *Journal of the American Chemical Society* 2014, 136, 5687.
- [116] B. Wu, N. Zheng, *Nano Today* 2013, 8, 168; M. Soorholtz, L. C. Jones, D. Samuelis, C. Weidenthaler, R. J. White, M.-M. Titirici, D. A. Cullen, T. Zimmermann, M. Antonietti, J. Maier, R. Palkovits, B. F. Chmelka, F. Schüth, *ACS Catalysis* 2016, 6, 2332.
- [117] P. Lara, O. Rivada-Wheelaghan, S. Conejero, R. Poteau, K. Philippot, B. Chaudret, *Angewandte Chemie International Edition* 2011, 50, 12080; E. A. Baquero, S. Tricard, J. C. Flores, E. de Jesús, B. Chaudret, *Angewandte Chemie International Edition* 2014, 53, 13220.